## *Studies of energetic muons in cosmic ray showers*

Machin, A. C.

# Studies of Energetic Muons in Cosmic Ray Showers

by

A.C. Machin, B.Sc.

A Thesis submitted to the University of Durham in accordance with the Regulations for admittance to the Degree of Doctor of Philosophy.

Department of Physics
University of Durham

May 1972.

# C O N T E N T S

# ABSTRACT

A magnet spectrograph situated at the British Universities joint air shower array at Haverah Park, near Harrogate, has been used for studies of various aspects of the muon component of extensive air showers (EAS).

An introduction to EAS and the relevance of muon studies is given, and two momentum spectrographs are described, the second being an improvement over the first, yielding higher precision and momentum resolution.

A detailed survey of track-fitting methods applicable to neon flash tube data from muon spectrographs is made, and an accurate method is described. The results of track fitting data from both instruments are presented and discussed.

Theoretical model calculations on the muon component are described, and have been used to predict possible areas for further experiments. Comparisons are made between the prediction of model calculations and experimental data from the spectrograph in an attempt to determine several parameters governing the development of EAS.

Two methods of obtaining the mean production height of muons in EAS are described, and the results interpreted in terms of the development of EAS. Further experiments which may be relevant to measurements of the primary particle mass are described.

## Preface

This thesis contains an account of the work done in Durham and at Haverah Park during the period October, 1968 to August, 1971 by the author while under the supervision of Dr. K.E. Turver.

Extensive air showers are detected at Haverah Park by arrays of water Cerenkov detectors. These arrays are operated by workers from Leeds University, and detect showers due to particles in the primary energy range from about $10^{16}$eV to above $10^{19}$eV.

The original spectrograph was designed and constructed by Professor G.D. Rochester and Dr. K.E. Turver, in 1964, but was partially dismantled in April 1969. A modified version, designed and constructed by Dr. K.E. Turver, Mr. D.R. Pickersgill and the author, was completed in November 1969.

Together with his colleagues the author shared responsibility for operation of the spectrograph and treatment of the data, and is entirely responsible for the work presented in Chapter 3. The results of Chapter 5 is a continuation of work begun by Dr. K.J. Orford, and Chapter 6 is a complete recalculation amd improvement of the work of Dr. J.C. Earnshaw.

Recent reports of the work carried out by the group include Orford and Turver (1968), Machin et al (1969) and Earnshaw et al (1971a and 1971b).

# CHAPTER ONE

# INTRODUCTION

## 1.1. The Primary Cosmic Radiation.

Primary cosmic rays reaching the Earth's atmosphere comprise a wide range of particle types and energies. The majority of the particles are protons and light nuclei, with a smaller contribution from gamma rays, electrons and heavy nuclei. The range of energies extends from less than $10^9$eV to at least $10^{20}$eV, although the possibility of a high energy cut-off above about $10^{20}$ eV has been suggested. The primary energy spectrum shown in fig. 1.1 falls very steeply, and the rate of arrival of primaries possessing energies greater than $10^{18}$eV is about one per 3000 years per square metre, so that direct observation of such particles is impossible. However, several techniques have been used to make direct measurements on primaries of energy less than about $5.10^{14}$eV, notably the use of nuclear emulsion stacks flown in balloons and rockets (e.g. Fowler et al. (1967)) and large satellite experiments (Grigorov et al (1967)). Primary cosmic rays of energy greater than this figure are the only (present) source of ultra high energy particles, and the study of the nuclear interactions of these particles provides a rich source of information on the character of fundamental particles.

## 1.2. The Extensive Air Shower

### 1.2.1 General

Primary cosmic rays entering the atmosphere interact strongly with an air nucleus, producing a large number of secondary particles. Most of these secondaries are thought to be pions (both charged and uncharged), with a small proportion of strange particles and heavy mesons; it is also possible that isobars are produced. If the energy of the primary particle is great enough, the secondary particles may undergo interactions with further air nuclei, thus producing more particles. This successive production of particles results in the extensive air shower (EAS).

The majority of particles in an air shower are relativistic electrons, and they move through the atmosphere in substantially the same directions as the primary particle. When a shower reaches sea level, it may cover an area of tens of square kilometres, so that the chance of detecting the arrival of the high energy primary in the atmosphere is much magnified by the composition and effect of the atmosphere itself.

1.2.2 The Electron-Photon Component

The electron-photon component of an air shower arises from the decay of uncharged pions, and subsequent pair production and bremsstrahlung. It is subject to wide statistical fluctuations, but the average number of particles in a shower at a given observation level (the "size") is generally used to determine the energy of the particle initiating the shower. An approximate relation given by Clark et al (1958) shows $E(\text{primary}) = 2.10^9 . N_{max}$ GeV, where $N_{max}$ is the number of particles in the shower at the point of maximum development. However, accurate measurements of the shower size are difficult because of the large detector area required. It is more usual to measure some parameter which is dependent on shower size, and to use this to estimate the primary particle energy (e.g. Hillas et al (1971)).

1.2.3 The Muon Component

Muons in air showers arise from the decay of charged pions produced in the nuclear interactions. The highly relativistic pions produced high in the atmosphere are time dilated; further, because of the low atmospheric density at such heights, the probability of their interaction is decreased. The result of these competing processes is that muons (particularly those of energies greater than 50 GeV) tend to originate in the early region of the cascade. Further, the low interaction cross-section and the relatively long lifetime (also dilated because of the energies in question) of the muon means that a very large proportion of muons, even those originating very high in the atmosphere, survive to reach sea level. The effects of coulomb scattering and geomagnetic deflection on the muon trajectories are relatively

small, so that the muon component on the whole retains far more information about the region of the production of the parent pions than the electron-photon component.

1.3. Experimental Work on Extensive Air Showers

The most straightforward experimental measurement on EAS is that of the lateral density distribution of all charged particles above a fixed detector threshhold. Many such measurements have been made, and all are consistent over a large range of shower size and measurement altitude (and therefore state of shower development). The results also agree closely with the form computed for a pure electromagnetic cascade (Nishimura and Kamata (1950, 1951, 1952)):

$$\rho = \frac{N}{r_1^2} \cdot f(s, r/r_1) \qquad \ldots\ldots\ldots\ldots 1.1$$

where N is the number of electrons, r the perpendicular distance from the shower axis, and $r_1$ the Moliere unit. The function $f(s, r/r_1)$ has been derived by Kamata and Nishimura (1958) and shown to be a close fit to many experimental results (Greisen (1960)). Many simpler approximations have been made to the lateral distribution function to facilitate the analysis of showers at certain restricted core distances, e.g:

$$\rho(N,r) = \frac{aN}{r} \exp\left\{\frac{-r}{b}\right\} \qquad \ldots\ldots\ldots\ldots 1.2$$

fits well for $1 < r < 200$ m.

Several experimenters have also measured the energy spectrum of the electromagnetic component, using cloud chambers or ionisation chambers below lead absorbers. Such experiments showed the lack of high energy electrons in EAS, and suggested that the proportion of the total energy carried by the electron-photon component is by no means as large as the relative abundance of electrons in the shower (about 20% of the total energy carried by some 90% of shower particles).

Experiments performed on the nuclear-active component of EAS ( e.g. Dovzenko et al (1960)) indicate that the lateral distribution of these particles is much steeper than that of electrons, so that almost all NAPs -

are found very close to the core. This makes precise conclusions about their energy spectrum very difficult because of the high level of electron-photon accompaniment (Hook et al (1969)). In the energy range 3 to 100 GeV, it has been shown that the majority of NAPs in air showers are protons and neutrons, with a smaller contribution from $\pi$ (or K) mesons (Greisen (1960)). The total energy carried by the nuclear-active component is roughly the same as that carried by the electron-photon component.

It was suggested by Galbraith and Jelley (1952) that most of the electrons in EAS are sufficiently energetic to cause emission of Cerenkov light during their passage through the atmosphere. Chudakov et al (1960) and Jelley et al (1965) have shown that the radiation produced carries much information on the development of the shower, and the technique may be a useful one for comparison with the predicted longitudinal development of the shower. The experimental difficulties are enormous, and the overall detecting efficiency of a Cerenkov system is only of the order of 10%.

Porter et al (1970) have reported the detection of scintillation light from the atmosphere, using electronic techniques similar to those of Jelley. Scintillation light is emitted isotropically (unlike Cerenkov light, which is emitted in a rather narrow cone about the shower axis), and this means that an air shower could be detected at a distance of several kilometers from the core. The efficiency is again low (5-15%), but the technique has possibilities considering the larger acceptance area covered by one fairly small detecting station. Both this and the Cerenkov light technique could best be investigated by the operation of detectors in conjunction with a large EAS array, in order to obtain precise information on individual events.

The detection of radio pulses associated with EAS was first reported by Jelley et al (1965) and Porter et al (1965), although suggestions concerning their existence were made several years earlier. Theoretical work by Askaryan (1965) and Kahn and Lerche (1965) succeeded in predicting the general form of the pulses, and also the frequency dependence, but

experimental work has been difficult because of the very low signal levels. Clay (1970) and Allan (1971) report efficient detection of pulses at frequencies ~ 30 MHz, and the technique is now well established. The progression from observing radio pulses in showers to the logical extreme, that of detecting large showers, still appears remote, but the advances made in the last six years indicate that the prospects may be promising as a means of estimating the primary particle mass.

Experimental work on the muon component of EAS is far more straightforward than all the methods mentioned above. The early work of Barrett et al (1952), Clark et al (1958) and Dovzenko (1957) established the broad characteristics of muon energy and lateral distribution, but the first reliable muon energy spectrum was that obtained by Bennett and Greisen (1961). They used a small air-gap magnet spectrograph (with Geiger-Muller counters as muon detectors) in an array of plastic scintillators. Coincidences were recorded between the spectrograph and any scintillator, so that the core position and size of individual showers were not accurately determined. However, their results have been shown to be substantially correct by later experiments. In view of the comments above about the necessity in all measurements of a detailed knowledge of shower parameters (e.g. size, core distance, arrival direction), a magnet spectrograph, to be described later, was constructed for use in conjunction with the Haverah Park Air Shower array. The detailed results obtained from this experiment make possible the subdivision of the data on the basis of both muon and EAS parameters, and enable the maximum amount of information to be drawn from each measurement. Early results from this experiment have been published, Earnshaw et al (1967), Machin et al (1969).

## 1.4. Current Topics of Interest in Cosmic Rays

### 1.4.1 The Primary Energy Spectrum at High Energies

The difficulties in determining the shape of the primary energy spectrum at high energies ($>10^{17}$eV) have been outlined earlier. Basically, the problem is one of converting an experimentally measured shower parameter (e.g. size, energy flux) into an appropriate value of primary particle energy. This requires some form of theoretical treatment and Hillas et al

(1971) report on the basis of model simulations that, for an array such as Haverah Park the detector signal amplitude at a distance of some 500m from the core is almost linearly related to primary energy, and is almost independent of the structure function exponent used in the analysis of the shower. Andrews et al (1971), using this form of conversion, report an integral primary spectrum of slope $-2.24 \pm 0.04$ for the energy range $3.10^{17}$ eV to $10^{19}$ eV. Linsley (1963) had earlier suggested that a change of shape takes place at about $10^{18}$eV. However, Andrews et al. point out that the weakness of the previous methods of converting measurement to primary particle energy may cause an apparent reduction in the spectral exponent at the highest energies. Fig. 1.1 shows the latest results available on the primary spectrum. The Sydney group (Brownlee et al (1969)) suggested a possible change in slope at about $10^{19}$eV although more recent data support the Haverah Park conclusions. The very wide detector spacing of the Sydney array may cause systematic errors in the conversion from muon size to primary energy, but the small number of showers from primaries $>10^{19}$eV detected at Sydney and Haverah Park (31 for the data shown here) does not allow firm conclusions to be drawn about the existence of a change in slope at such high energies.

1.4.2 The Mass Composition of the Primary Radiation

The mass composition of the primary cosmic radiation is well known up to energies of about $10^{15}$eV from emulsion data. The results as summarised by Ginzberg and Syrovatsky (1964) are shown in Table 1.1. The end-point of direct measurement is slightly below the "knee" ((i) in fig. 1.1) in the energy spectrum, and this change in slope has been widely interpreted as the beginning of a change in the mass composition of primary particles. The argument in favour of this interpretation is that the magnetic cut-off rigidity of the galaxy progressively excludes protons, light nuclei etc. from arriving at the Earth. Alternatively, the change in slope could be due to a fundamental change in the characteristics of high energy nuclear interactions taking place in EAS (Glencross (1962)). The former view implies that the primaries at about $10^{17}$eV should be predominantly heavy

Figure 1.1 The Primary Energy Spectrum

The experimental points are the highest energy points quoted by Brownlee et al (1969) and Andrews et al (1971) for the Sydney and Haverah Park arrays respectively.

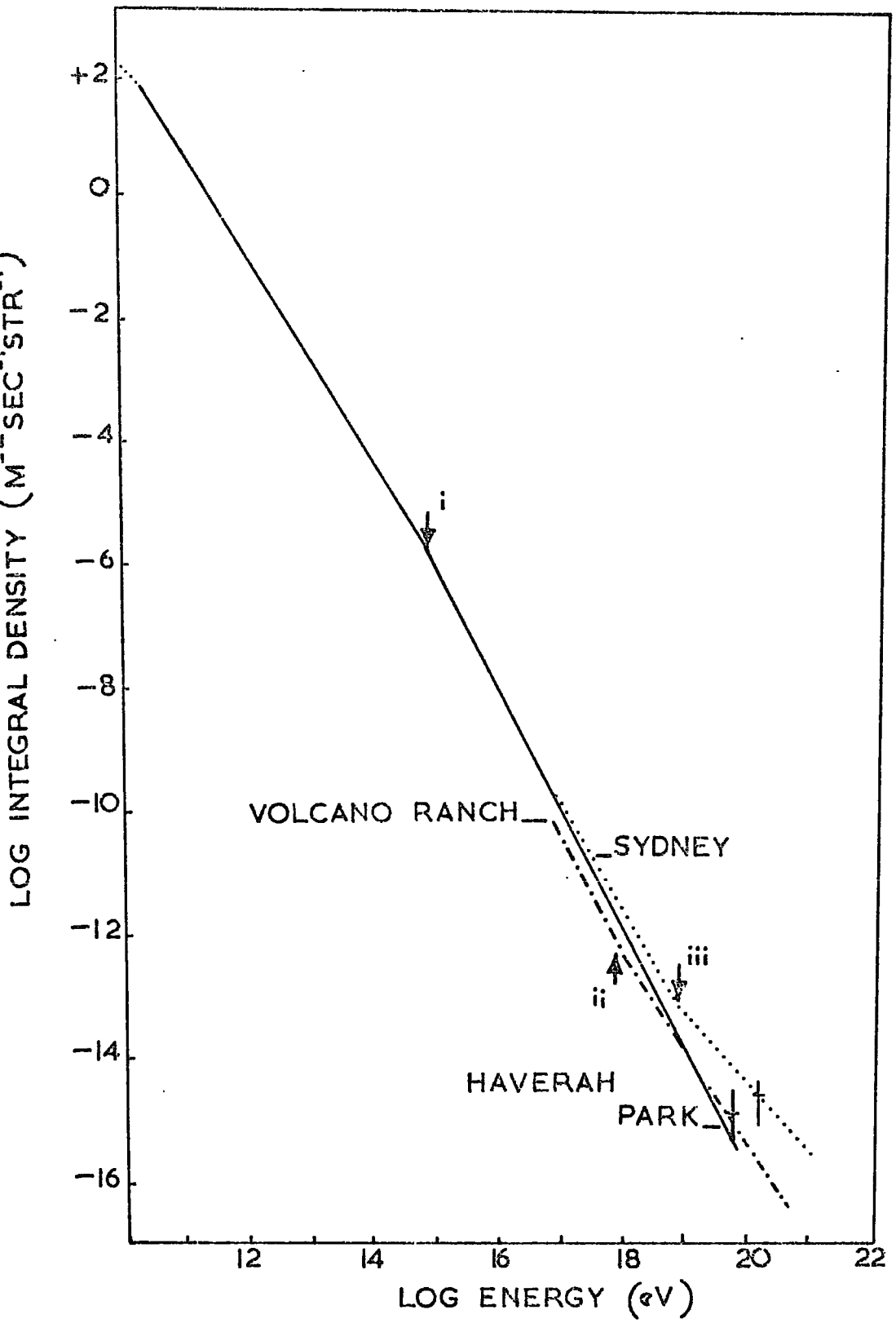
LOG INTEGRAL DENSITY ($M^{-2}SEC^{-1}STR^{-1}$)
+2
0
-2
-4
-6
-8
-10
-12
-14
-16
12
14
16
18
20
22
LOG ENERGY (eV)
i
ii
iii
VOLCANO RANCH
SYDNEY
HAVERAH
PARK

Table 1.1

Composition of Primary Cosmic Rays

| Nucleus | Z | $\bar{A}$ | % of flux |
|---|---|---|---|
| Proton | 1 | 1 | 93 |
| Helium | 2 | 4 | 6.3 |
| Light | 3-5 | 10 | 0.14 |
| Medium | 6-9 | 14 | 0.41 |
| Heavy | 10-20 | 25 | 0.10 |
| Very Heavy | > 20 | 51 | 0.04 |

while the latter suggests that the composition should be basically the same as that below $10^{15}$eV and be mainly protonic. Linsley (1963) reported the existence of a further "kink" ((ii) in fig. 1.1), and interpreted this as a total failure of containment within the magnetic field of the galaxy, so that primaries above about $10^{18}$eV should be extragalactic in origin, and presumably protons. The existence of the second "kink" now seems unlikely.

Experimental evidence on the mass composition lags behind the various containment and propagation theories proposed above. Zatsepin et al. (1963) concluded that from observations of Cerenkov light at mountain altitudes the composition below $10^{15}$eV was similar to that measured directly. Several workers have studied the core structure of EAS, and have reported the existence of multiple cores (e.g. Bray et al (1965), Matano et al (1967), Shibata et al (1965), Thielheim and Karius (1965)). Multiple cores may arise on a simple model when heavy primary particles fragment in the atmosphere, releasing energetic nucleons giving sub-cores. McCusker et al (1968) reports a change-over from equal numbers of single and multiple-cored events below $10^{15}$ eV, to predominantly multiple core events at energies greater than about $3.10^{15}$eV. This is interpreted as a change-over to predominantly heavy primaries at these energies. However, the Kiel group (Samorski et al (1969)) do not find a large proportion of multiple-cored events at

energies around $10^{15}$eV. Hasegawa et al (1962) conclude from fluctuation studies that an appreciable number of primaries greater than $10^{16}$eV must be heavier than protons. Linsley and Scarsi (1962a) and Toyoda et al (1966) conclude that for energies greater than $10^{17}$eV, the composition of table 1.1 is incompatible with observed fluctuations, and that either pure protons or heavy nuclei are required. Linsley further concludes from the narrow band of fluctuations of muon numbers in showers that the primaries are probably protons. One of many problems in interpreting any experimental results is the lack of detailed knowledge about the interaction characteristics of heavy nuclei at high energies. Most workers consider that a shower resulting from a mass A primary of energy E is equal to the superposition of A proton-initiated showers each of energy E/A and this rather crude approximation may be misleading for some aspects of EAS.

1.4.3 The Existence of a High-Energy Cut-off to the Primary Radiation

The discovery of an isotropic microwave background radiation corresponding to a black-body temperature of about $3^{o}$K (Penzias and Wilson (1965), Roll and Wilkinson (1966)) led Greisen (1966) to consider the possibility of energy loss by high energy primary protons (by photo-pion production) in interactions with the low energy photons of the $3^{o}$K background. Greisen suggested that the upper limit for the primary energy should be less than $10^{20}$eV, because energies higher than this required long path lengths and containment times, so that the probability of energy loss was increased. Hillas (1967) suggests that the removal of protons will occur at about $3.10^{19}$eV, that of heavy nuclei (by photo-disintegration) at lower energies. However, several events ($\sim$17) of primary energy greater than $10^{19}$eV have been detected at Haverah Park, including two showers $> 5.10^{19}$eV, and Brownlee et al (1969) report 41 showers $> 10^{19}$eV, with 4 showers $> 10^{20}$eV, so that the possibility of a real cut-off is at present in doubt. Konstantinov et al (1968) point out that the shape of the spectrum above $10^{19}$eV should give information on the containment time of cosmic ray primaries, and therefore on the evolution of the universe.

## 1.5 Scope of the Present Work

The results presented in this thesis relate to the muon component of EAS of primary energy confined to a narrow band centred on $2.10^{17}$eV. The experimental results have been compared with model predictions in an effort to determine the approximate mass composition at these primary energies. Early results (Earnshaw (1968), Orford (1968)) and model calculations (Orford (1968), Orford and Turver (1968), Orford and Turver (1969)) indicated that a primary mass of $A \sim 10$, together with a change in the nuclear interaction characteristics were required to agree with experiment. However, with improved model calculations and completely re-analysed air shower data, some of the discrepancies have been removed. Certain regions of interest still exist, and an improved experiment designed to investigate these regions has been constructed and put into operation. The results from both experiments are compared, and predictions of primary particle mass-sensitive quantities for further experiments are also made.

# CHAPTER TWO

# EXPERIMENTAL EQUIPMENT

## 2.1 The Haverah Park EAS Arrays

### 2.1.1 Introduction

The Haverah Park EAS array is situated some 3 miles NW of Harrogate, Yorkshire at a latitude of $53^{\circ}$ 58.2' N., longitude $1^{\circ}$ 38.1' W., and is at a mean altitude of 220m above sea level, corresponding to an atmospheric depth of 1016 gm $cm^{-2}$. A plan of the arrays is shown in fig. 2.1, and the arrays which are operated by scientists from the University of Leeds are best described in three sections. The 500m., or main array, consists of four detecting stations, each of area $34m^2$ and provides all triggering requirements. The 150m. array (section 2.1.3) provides additional density samples close to the core of showers, and so improves the EAS analysis. The 2Km array (section 2.1.5) is used for accurate analysis of very large showers, where the core can fall well outside the bounds of the main 500m. array.

### 2.1.2 The Individual Detectors

Each detector unit consits of a galvanised steel tank 1.85 x 1.24 x 1.29m. filled to a depth of 120 cm. with clear water. The internal surfaces of the tank are lined with white plastic, giving a diffuse reflection of the Cerenkov light produced in the water by the passage of a relativistic shower particle. A fraction of the light produced is detected by a single 5" photomultiplier, situated at the top of the tank, with its photocathode immersed in the water to provide optical coupling. The design and operation of these detectors is described by Lillicrap (1963) and Turver (1963).

### 2.1.3 The 500 m Array

Each station consists of fifteen of the above detector units; the pulses from each unit are added electronically and combine to give a "station" pulse. The four "station" pulses so obtained are recorded photographically on a four-beam oscilloscope, so that the relative times of arrival and the pulse heights corresponding to each station may be determined from the film record. A full account of the electronics and test procedures employed in the recording system is given by Hollows (1968).

Figure 2.1 The Haverah Park Arrays

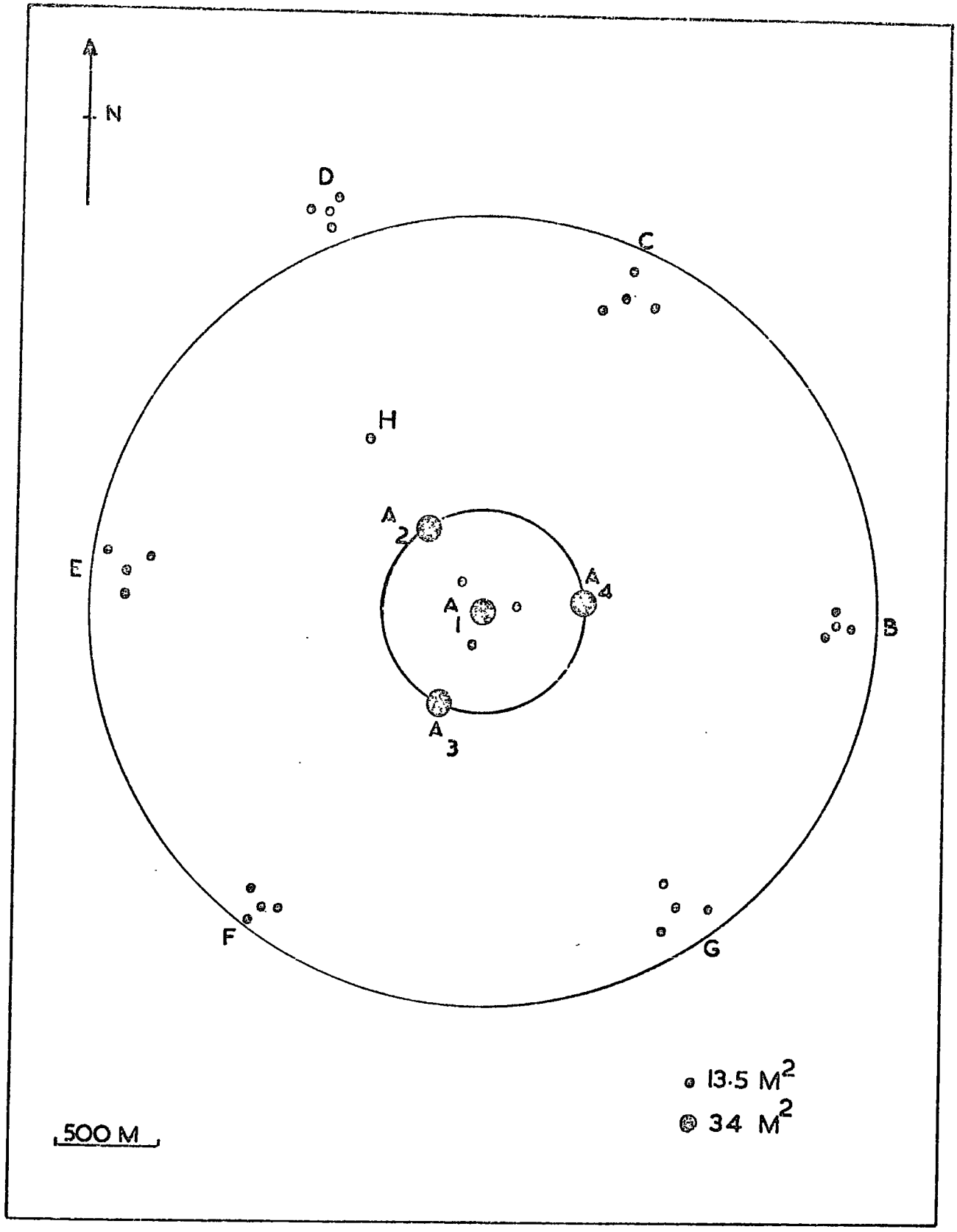
A
N
D
C
H
A2
E
A4
A1
B
A3
F
G
• 13.5 M2
⊛ 34 M2
500 M

2.1.4 The 150m. Array

The geometry of this array is similar to that of the 500m. array, but the individual stations comprise four detector units of total area 13.5$m^2$, and the station spacing is 150 m. Whenever the 500m. array detects a shower, the pulse heights from the 150m. array are recorded (as in 2.1.3) for use in shower analysis. The short baseline of the array prohibits any significant contribution towards timing accuracy, but the extra density samples provide data for more accurate core location than the 500m. array alone. The extra samples have been available from May 1971, so that none of the EAS data associated with the muon events reported in this thesis have benefited from this improvement in shower data. In place of the normal central detector in this array (since it is coincident with the 500m. array detector), two units are run with a low photomultiplier EHT, thus making the pulse heights for a given particle density much lower than from a conventional unit. This allows an estimate of very high particle densities, when the conventional units have reached the limits of their dynamic range. This array is described further by Andrews (1970).

2.1.5 The 2KM Array

This array consists of six sites, each one a small array of either 50m. or 150m. spacing, situated approximately on the circumference of a circle, radius 2Km, centred on the 500m. array. The low rate of the large showers detected by this array, together with the large mean distance from the spectrograph, and the relatively small acceptance area of the spectrograph, mean that the rate of useful muon events from 2Km showers is extremely low, and no useable data sample has yet been accumulated.

2.1.6 The Measurement of Arrival Directions from the 500m. Array

After detection of a shower by the 500m. array, the station pulses are delayed electronically to allow each of them to appear fully on the timebase of the recording oscilloscope. The relative times of arrival of the four pulses can then be measured by reference to time markers (which appear simultaneously on all four channels). Only three "times" are required in order to fit a plane

front to the shower and obtain the arrival direction. It is usual to select the three longest time intervals from the four available, in the interests of accuracy. These generally correspond to the three outer stations, and the symmetry of the array permits the four times to be reduced to three, by quoting them as relative to the central detector. The arrival directions $(\theta,\phi)$ derived from these times correspond to a shower possessing a plane front. Dennis (1964) gives a set of corrections to be applied to the plane-front angles to allow for the effect of shower front curvature. Although these transformations are ill-conditioned in certain areas of $\theta,\phi$ and core position, there is a distinct overall improvement in accuracy (see Ch. 6).

From measurements of simulated shower pulses recorded via each channel, it has been found that the width of the distribution in time measurement corresponds to a standard deviation in time of 0.08 $\mu$sec. This figure may be used to predict the overall uncertainties in $(\theta,\phi)$ by differentiating the appropriate equations and the results of such calculations are given by Hollows (1968). Typical figures are $2.5^{\circ}$ in $\theta$ and $7^{\circ}$ in $\phi$. The overall error in $\theta$ and $\phi$ is important for the studies of the height of production of muons to be described in Chapter 6.

2.1.7 Errors in Core Location

Hollows (1968) gives an account of the methods used to estimate the core location accuracy by means of simulated showers. Pickersgill (1971) gives an alternative method, which relies upon a knowledge of the lateral distribution of muons of known energies (as determined by Earnshaw (1968)). Briefly, the method consists of investigating the change in muon density predicted for different energies by small movements in core distance, from the lateral distribution. Both methods yield an accuracy of about 30m. and it is unlikely that such errors will have any significant effect on the muon momentum spectra described in section 4.1. The inclusion of the 150m. array data, for the period since May 1971, has shown one interesting feature with regard to core location. Core positions determined from the 500m. data alone are generally substantiated when the (500m. +150m) data are analysed, and any movements in core position tend to be transverse rather than radial. This adds confidence to the rather small overall effect on measurements made

at the centre of the array expected from errors in core location.

## 2.2. The Mark I Spectrograph

### 2.2.1 Dimensions and Statistics

A full description of this instrument has been given by Walton (1966), but a brief account is included to show the improvements made in the updated version (section 2.3). Figure 2.2 is a scale drawing of the spectrograph. The neon flash tubes used for track delineation were 17mm. external diameter, and half were accurately located in milled duralumin supports, while the remainder rest on top of the accurately positioned layers. The small trays (A2,B2) played no part in deflection measurements, but were included in an attempt to resolve parallel muon tracks. The magnet is of the "picture-frame" type, 60cm. total thickness, comprising 45 low-carbon-content steel plates. The energising current of some 13.5 amperes (power dissipation 2KW) is passed through 325 turns of enamelled, double cotton covered 14 gauge copper wire on each arm. The resulting induction is found to be $14.6 \pm 0.3$ K gauss, uniform over the useable magnet volume.

### 2.2.2 The Use of the Instrument as a Muon Detector

Apart from mechanical considerations, three main factors govern the choice of magnet and detectors for use in EAS muon spectrograph work. Firstly, the minimum momentum acceptable in the instrument, depends on the angular acceptance and the amount of matter traversed, and this is roughly fixed by the overall dimensions and thickness of the component parts. Secondly, the signal to noise ratio (taken here as the ratio of magnetic deflection of a particle trajectory to the root mean square angle of Coulomb scattering) is not momentum dependent, since, to a first approximation, both magnetic deflection and scattering angle vary as the reciprocal of the muon momentum (Rossi (1952)). Finally, the maximum detectable momentum (hereafter called the m.d.m), which depends upon the overall deflection of the muon (i.e. on the value of $\int Hdl$ in the magnet), and upon the resolution of the visual detectors. These three factors are not independent, and a design of a useable instrument usually involves some compromise usually in terms

Figure 2.2 A scale diagram of the Mk.I Haverah Park Magnet Spectrograph

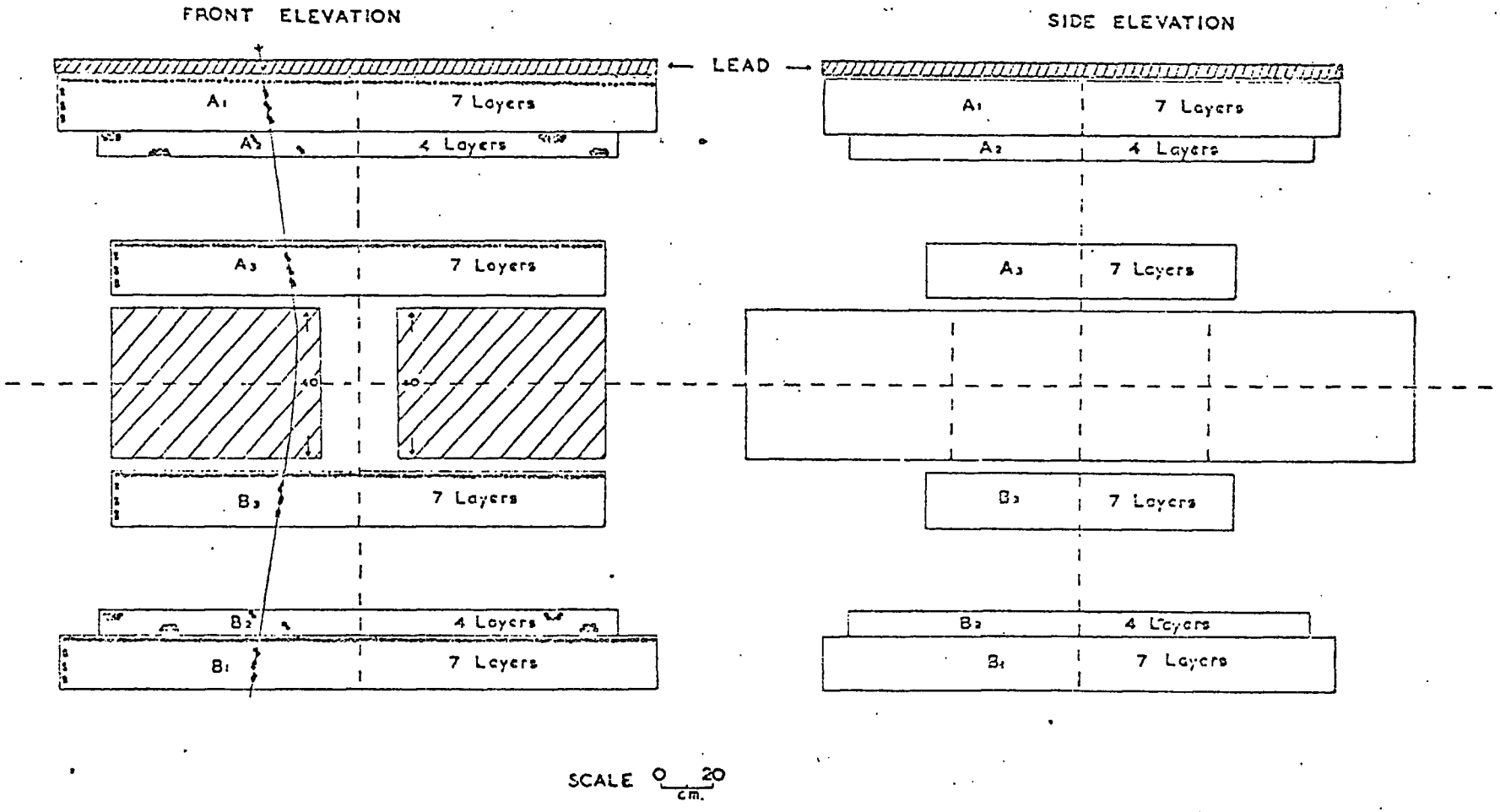
FRONT ELEVATION
SIDE ELEVATION
LEAD
A1
7 Layers
A2
4 Layers
A3
7 Layers
40
40
B3
7 Layers
B2
4 Layers
B1
7 Layers
A1
7 Layers
A2
4 Layers
A3
7 Layers
B3
7 Layers
B2
4 Layers
B1
7 Layers

SCALE 0 20 cm.

of overall size, and therefore in terms of event rate. The Mark I instrument described above covers the range 1-60 GeV/c with a signal to noise ratio of 3:1. It is important that the three quantities are accurately defined, in order that the necessary corrections may be applied during the derivation of spectra (see Chapter 4). The first quantity is relatively straight forward to determine (basic trigonometry and computation of the overall thickness in gm $cm^{-2}$ is required), and the signal to noise ratio is similarly straight forward. However, the m.d.m is a rather more difficult quantity to measure. Orford (1968) quotes four different methods which have been used to obtain the overall angular error, and hence the m.d.m.

1. The deflection distribution of single unassociated cosmic ray muons traversing the magnet before the energising current was switched on.
2. The distribution in angular deflection of a track simulated by hand repeatedly over a period of time.
3. The distribution in lateral separation of the intersection points of the two half-tracks with the mid-plane of the magnet.
4. The deflection distribution of muons traversing the central hole of the magnet and thus not undergoing Coulomb scattering in the magnet iron.

The first method suffers from the relatively large amount of angular scattering undergone by unassociated muons (since their mean energy is low), and the measurement is difficult to make with accuracy. The second method gives a good estimate of the simulation and operator errors, but does not give an accurate estimate of the overall error in track location because of systematic errors in constructing the simulator. The third method requires some mathematical treatment to remove the effects of lateral scattering in the magnet, and is not as direct as the fourth method. The overall error deduced from these methods is closely gaussian in form, with a standard derivation of $0.3 \pm 0.03^{\circ}$. The m.d.m is then the momentum corresponding to this value of angular deflection, namely $58 \pm 5$ GeV/c.

## 2.3. The Mark II Spectrograph

### 2.3.1 Design Considerations

The data gathered during the operating period of the Mk I spectrograph led to interest in regions of momentum which were close to the m.d.m. of the instrument (e.g. densities of muons greater than 50 GeV/c). Accordingly, it was decided to rebuild the spectrograph, in order to increase the momentum resolution, and also to extend the useful operating range to include smaller values of core distance than were previously possible. An improvement in m.d.m. of about 3 times was chosen as the target for the new instrument, so that information on muons of momentum $> 100$ GeV/c could be quoted with confidence. There are two basic methods by which such an m.d.m can be obtained: firstly, the magnitude of the deflection in the magnet for a given momentum can be increased (i.e. increase the value of $\int Hdl$), or secondly, increase the precision of track location by the use of small, accurately located detectors.

There are two avenues of approach to the first of these methods. Either the magnetic induction over the useable magnet volume must be increased (either by the use of high permeability metal or by increasing the energising current), or the total path length in the magnet may be increased at a constant induction. The steel plates used in the Mk I spectrograph combined the advantages of relatively low cost, ready availability and fairly high permeability, so a change in magnet material from iron was not considered. The method of increasing the induction by an increase in energising current is very dependent on the closeness of the magnet plates to saturation; in the case of the Mk I spectrograph magnet, a 100% increase in current would only increase the induction by some 5%, and the power dissipation entailed (about 4KW) would increase the likelihood of mechanical failure due to overheating. It was therefore thought impractical to consider increasing the total induction integral in the magnet, other than by thickening the magnet.

The advantages of increasing the total path length in the magnet are much more apparent in practical terms. The magnitude of the deflection of a muon depends linearly (to a first approximation) on the magnet thickness, while

Figure 2.3 A scale diagram of the Mk. II Haverah Park Magnet Spectrograph

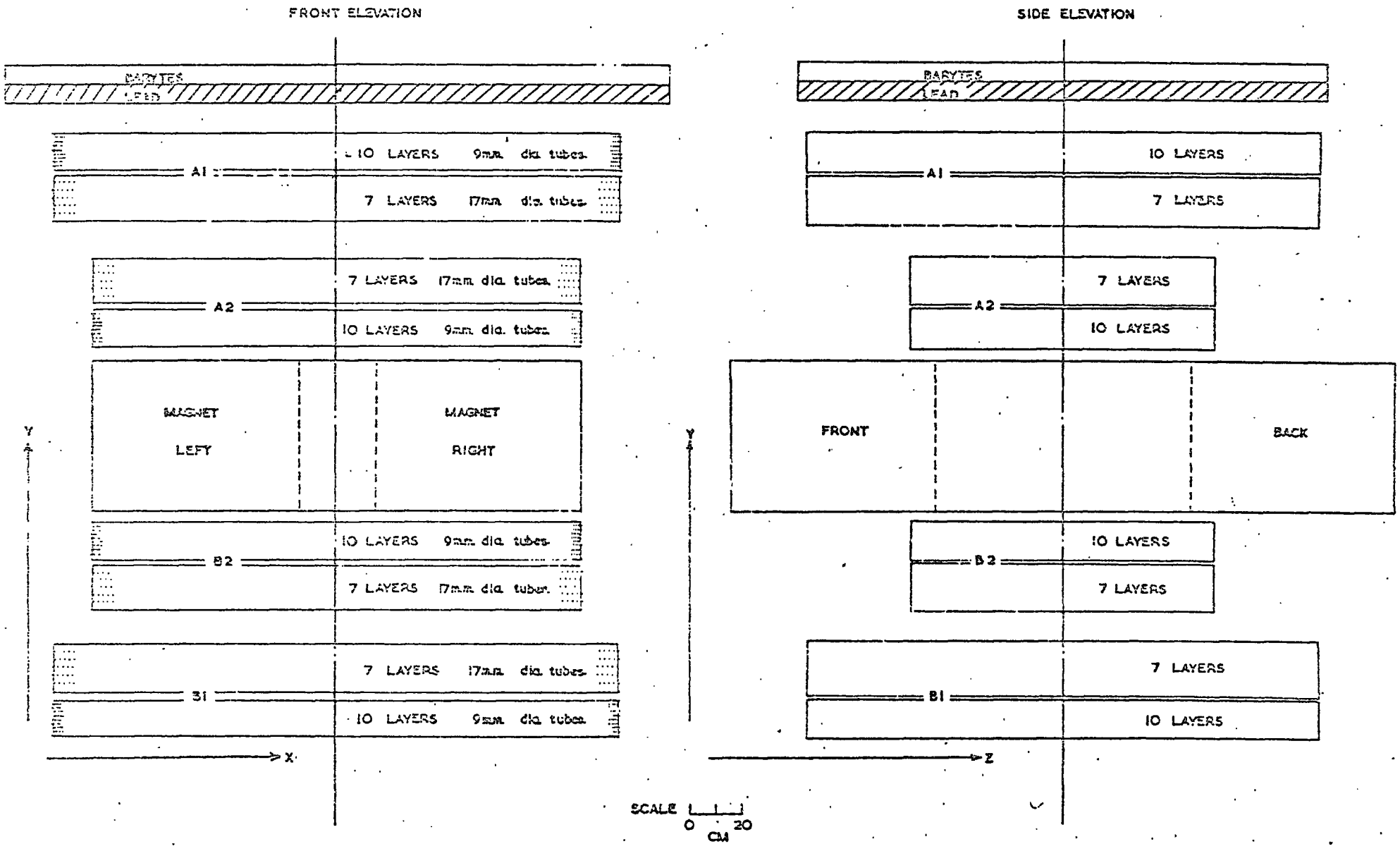
FRONT ELEVATION
SIDE ELEVATION
BARYTES
LEAD
10 LAYERS 9mm dia. tubes
7 LAYERS 17mm dia. tubes
A1
A2
B1
B2
MAGNET
LEFT
MAGNET
RIGHT
FRONT
BACK
Y
X
Z
SCALE
0
20
CM

the apparent r.m.s angular deflection due to Coulomb scattering rises as the square root of the thickness. However, this basic fact cannot be fully exploited if the measurement noise is much greater than that due to scattering (as the overall noise is computed quadratically), and the major mechanical reconstruction necessary to increase the overall height of the instrument ruled out this course of action.

The remarks above concerning the comparison of measurement noise and Coulomb scattering noise provide the basis of the improvements carried out in the spectrograph construction. It was decided to achieve the improved m.d.m by decreasing the effective noise from $0.3^{o}$ to $0.1^{o}$ by the use of small diameter, accurately located neon flash tubes. The use of tubes of diameter 0.7 cm. (internal), 1.0 cm (external), filled to a pressure of 2.4 atmospheres individually located in dural supports to an accuracy of 0.1 mm, gave an estimated noise of the desired value of $0.1^{o}$, and the rest of the mechanical design was made to meet the above requirements.

2.3.2 Mechanical Design

A full description of the mechanical design of the Mark II instrument is given by Pickersgill (1971) and fig. 2.3 is a scale drawing of the spectrograph. The 7mm. flash tubes are used as the track locators, and the 17mm. tubes (removed from the Mark I spectrograph) are used only to resolve close muon tracks and provide information useful for the selection of tracks for analysis. The overall location accuracy would not be significantly improved by also using the larger tubes for location purposes. The spectrograph acceptance function is shown in fig. 2.4.

2.3.3 The Small (7mm.) Flash Tubes

2.3.3 (i) Location of tubes

The high accuracy of track location specified for the Mk II spectrograph necessitates individually mounted flash tubes. This is accomplished by supporting the front and rear of each tube in milled slots in duralumin bar of 1.27 x 0.63 cm section for the 7 mm tubes, and in hollow tubing of 1.52 x 1.52 cm. box section for the 17mm. tubes. Production of these supports on the scale necessary required a large number of cutting strokes, and it has

Figure 2.4 The spectrograph acceptance function

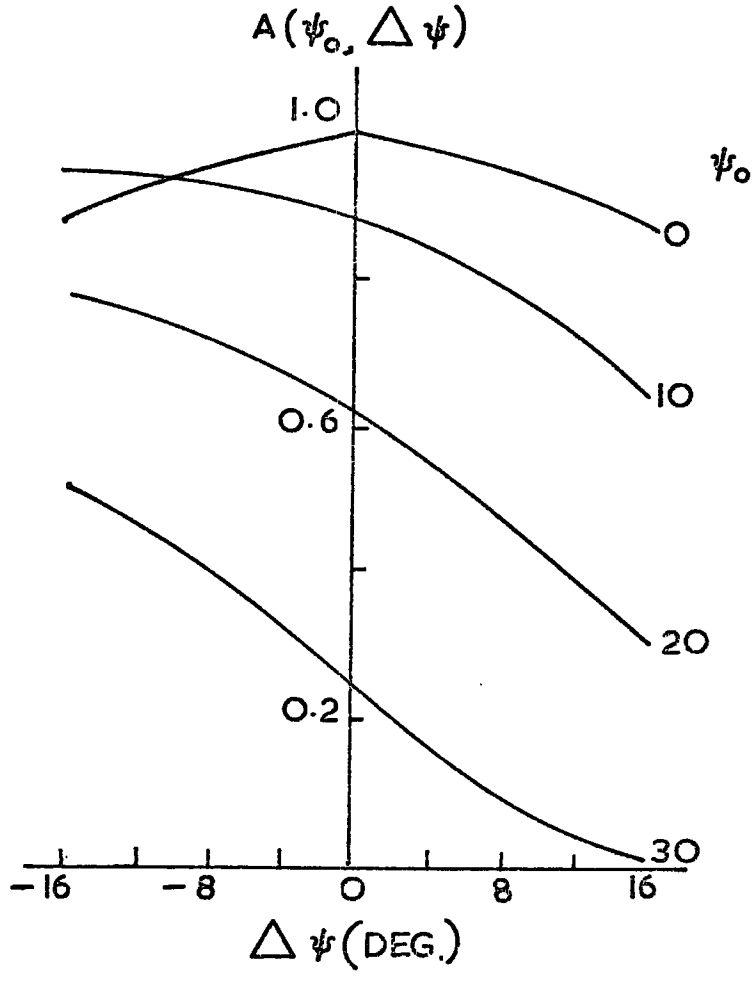
A(ψ₀, △ψ)
1.0
0.6
0.2
ψ₀
0
10
20
30
−16
−8
0
8
16
△ψ (DEG.)

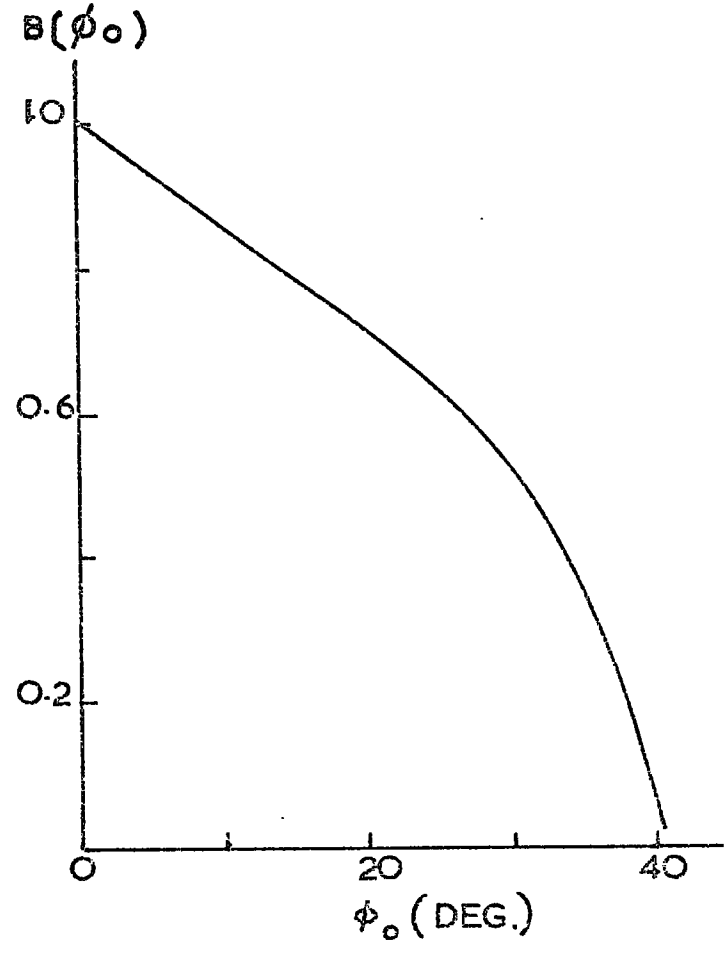
B(φ₀)
1.0
0.6
0.2
0
20
40
φ₀ (DEG.)

been noted that the shape of the slot in the solid duralumin supports for the 7mm. tubes is not constant. This does not imply inaccurate tube location (the pitch of the slots is still constant), since the effect of slight errors in location in a vertical direction imparted by a change in slot shape is small when converted into a net lateral error (because of the limited range of incident particle angles considered, $0^{\circ}$ -$30^{\circ}$). The main problem caused by the variation in shape occurs during measurement, as it is impossible to define "Universal" key points for all slots (see section 2.3.3 (ii)). During initial testing of the small tubes, it was found that the sag at the centre of the 2m. long tubes was too great to be tolerated (about 1.5cm), but the 1.2m. tubes were self-supporting. Accordingly, the design for the trays for the longer tubes is slightly different - each layer of small tubes is supported at the centre by strips of insulating material over the whole width of the tray. However, this form of support allows the tube centre to move laterally away from the plane joining the mid-points of the supporting slots, so that further insulating mid-tray restraints are also included, and these are adjusted during measurement of the spectrograph to ensure that each tube remains straight.

2.3.3 (ii) Measurement of position of flash tubes

The purpose of this measurement is to provide a knowledge of the coordinates of each tube centre. During manufacture, the tube supports were milled to a constant pitch, so that the problem reduces to measuring at least one tube in each layer (hence check measurements are simple to carry out). Dummy tubes are used to indicate the tube centres - these are short perspex rods (1.0cm. diameter), marked with a cross, and are checked for eccentricity by rotating about the "tube" axis whilst viewing the cross through a travelling microscope. First of all a plane, defined by three thin nylon plumb lines, is set parallel to the edge of the magnet in a position such that all four trays contain small tubes close to the position of the plane. The necessary tubes are removed, and the front and back tube supports adjusted as required to make the line joining the mid-points of each pair of slots parallel to the defined plane. In the case of the 2 metre tubes, the central supports are also adjusted to coincide with the plane. Repeated measurements are then taken of the lateral

separation of the $n^{th}$ tube (in a given layer) from the plane. The vertical coordinates of the tube centres are obtained using a cathetometer and engineer's scale, the latter being fixed close to the tube fronts as a check on the cathetometer readings. Check measurements were performed at the other side of the spectrograph to investigate the constancy of the tube pitch; such measurements showed that, in the case of the Mk II instrument the pitch is constant within the measuring error. The measurements obtained using the above procedure may be reduced to any suitable arbitrary zero point- that chosen for the Mk. II instrument is the centre of the $(zero)^{th}$ tube in the bottom layer of tray A1. The overall noise figure on the location of any small flash tube centre is estimated to be $\pm$ 0.2mm., which is slightly larger than the design figure. It is difficult to see how this figure could be reduced, as the effects of variation in tube diameter and shape are only slightly smaller than the quoted figure (implying little scope for improvement in the measurements).

2.3.4 Flash Tube Operating Conditions - Preliminary Tests

A small section of one tray was set up in Durham before the reconstruction of the spectrograph in an attempt to define the operating conditions necessary for the 7mm. flash tubes. In order to minimise the costs, the specification of the Mk.II instrument provided for only half the 7mm. tubes to be painted fully, the other half being clear glass. When the two types are placed alternately, spurious flashing caused by photo-ionisation should be a small effect, but experimental verification of this suggestion was required. Aluminium electrodes were placed between every three layers of tubes, and the whole stack was driven by a pulsing system similar to that used in the Mark. I spectrograph. Triggering was provided by a simple three fold Geiger-Muller telescope. Two camera positions were used, the first, close-up to the tray front, was used for efficiency counts, while the second, at a path length of 30 feet containing two reflections, duplicated the likely operating conditions at Haverah Park. These results indicated that an EHT field of about 8kV $cm^{-1}$ gives an internal flashing efficiency close to 100% at zero time delay, falling to about 90%

at 15 μsec delay in agreement with the theory of Lloyd (1960). The visibility tests suggested that acceptable film records could be obtained for tubes at the centre and edges of trays. The spurious flashing rate of the small tubes was extremely low.

2.3.5 Operating Conditions of the 7mm Flash Tubes in situ

2.3.5 (i) Introduction

In spite of the indications of the preliminary tests, very low flash tube efficiencies were found when the complete Mk. II spectrograph was first tested. Because of the nature of the pulsing system (section 2.3.5(ii)), alternate electrodes are "live" (i.e. the EHT pulse is applied directly to them), while the remainder are earthed. The low flash tube efficiencies apparently occurred because tubes adjacent to an "earth" electrode fired very infrequently while those adjacent to a "live" electrode performed normally. A likely explanation for this effect is distortion of the electric field caused by the tubes themselves. Whenever a tube flashes, it causes a local short-circuit (i.e. a very low resistance compared with the steady state), and the high-voltage field is grossly distorted. The field gradient across a tube close to a "live" electrode will be slightly greater than for the corresponding case near an "earth" electrode, because of the effect of the glass tubing, so that tubes near a "live" electrode will tend to fire slightly before any other tube. The resulting field distortion is sufficient to prevent "earthy" tubes from firing at all, thus yielding low overall efficiencies. Slight mismatching of the pulser and tray will tend to reduce the efficiency even more, and this mismatching is very difficult to avoid. However, the major part of the problem was solved by inserting extra electrodes, so that each layer was contained within a "live-earth" electrode pair, and this solution removed the uneven efficiency entirely.

2.3.5 (ii) The High Voltage Pulsing System

The system used in the Mk. I spectrograph, and also for initial tests of the improved instrument, is shown in fig. 2.5.(i). When triggered, the thyratron earths one end of the capacitor, which discharges through the

Figure 2.5 (i) The Mk. I Pulsing system

(ii) The Mk. II Pulsing system

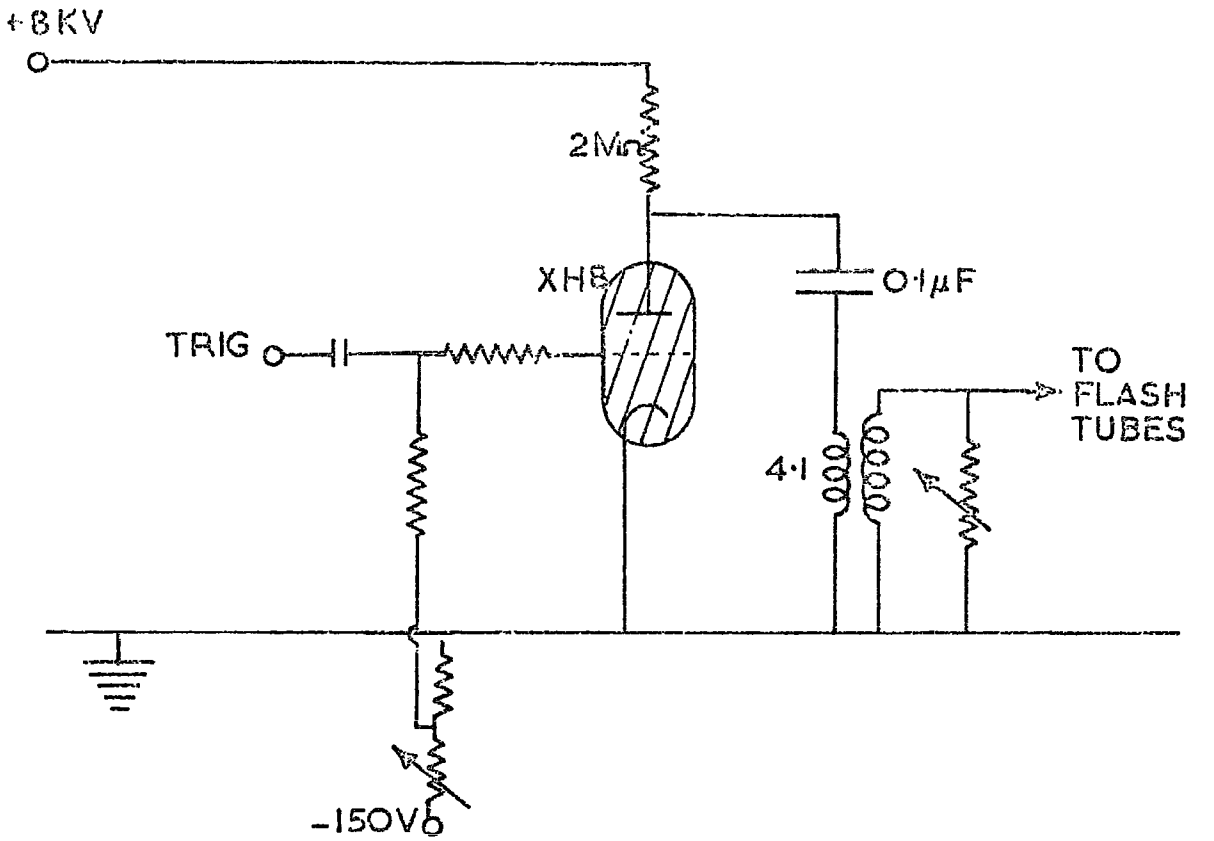
+8KV
2MΩ
XH8
0·1μF
TRIG
TO
FLASH
TUBES
4·1
-150V

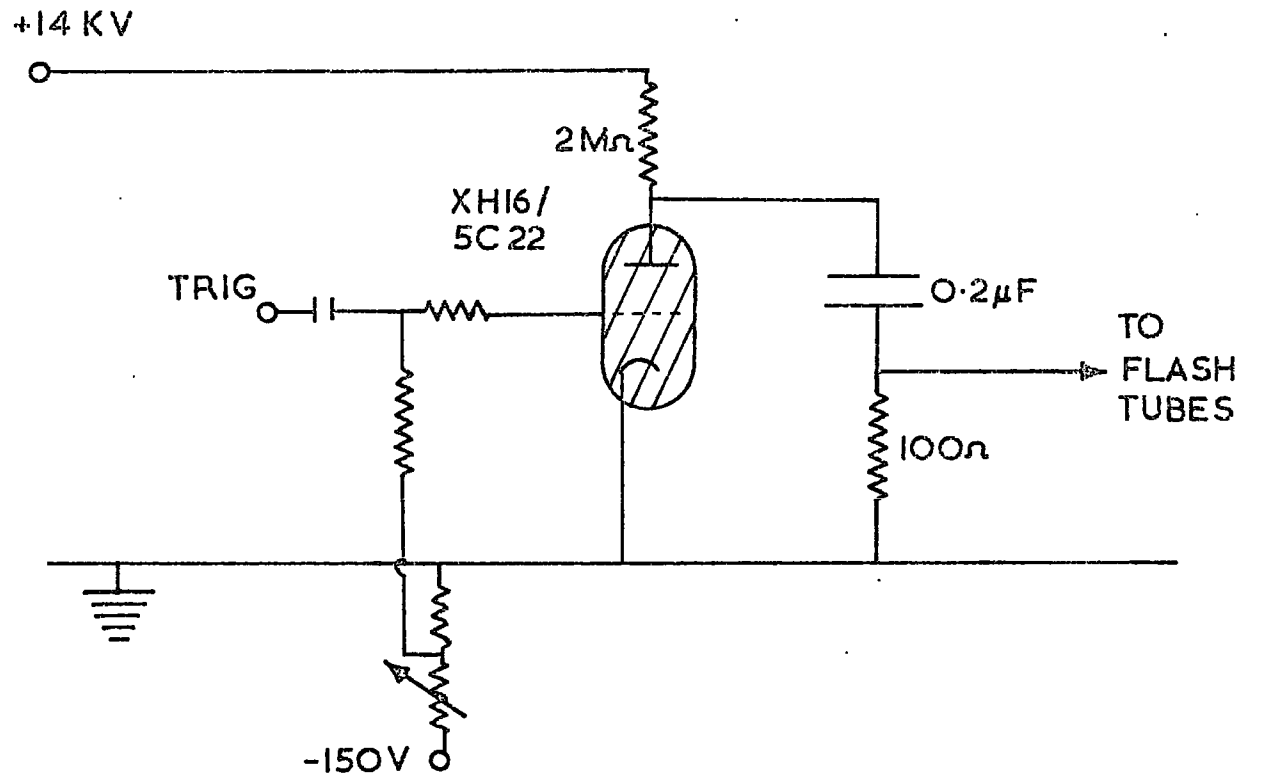
+14 KV
2MΩ
XH16/
5C22
TRIG
0·2μF
TO
FLASH
TUBES
100Ω
-150V

primary of the pulse transformer. The output of the transformer is approximately matched and fed to the electrodes. This system worked well for the 17mm. tubes, but gave low efficiencies and a high spurious rate when used with the 7mm. tubes. The effect of the pulse transformer is to step up the high voltage pulse (about 4:1), but also to slow the pulse risetime due to the inherent inductances present in the transformer. The straight forward RC pulsing system of fig. 2.5(ii) works satisfactorily with the 7mm. tubes, although it is necessary to work at a higher voltage in order to obtain the necessary EHT field at the electrodes. The applied EHT pulse to the 7mm. tubes is now ~ 14kV, lasting for some 20 $\mu$sec (3 $\tau$), and the peak electric field is about 9 kV $cm^{-1}$. The tube brightness under these conditions is adequate for normal photography (see section 2.3.6), and the internal efficiency at zero time delay is 95%.

2.3.5 (iii) The Control Electronics

The control electronics, shown in fig. 2.6, is concerned mainly with the correct sequencing of applied EHT pulse, fiducial lights and camera operation. There is one additional feature not found in the Mk. I spectrograph system, namely, the provision of Geiger-Muller counters, situated in the central hole of the magnet. These counters are included to give positive identification of an (EAS) muon traversing the hole of the magnet, and such muons may be used for noise estimation (see Chapter 4). There are eleven counters in all, close-packed in two layers, and each counter is 60 cm. long, 3 cm. diameter. The cathodes are grounded at the magnet end, and the anodes are fed individually to allow separate "plateau" settings to be made (and also to allow full readout if necessary). It has been found satisfactory to operate the hole detector in two "commoned" layers, rather than eleven separate counters. On detection of a coincidence between the two layers of counters, a 4 $\mu$sec gate pulse is generated (to allow for the variable arrival time of the air shower trigger), and, if a shower trigger pulse arrives during the gate, an indicator lamp on the spectrograph is flashed. Subsequent scanning of the film shows if the event is due to a (useful) single muon track in the region of the hole, or whether it is due to a high electron

Figure 2.6 Block diagram of control electronics.

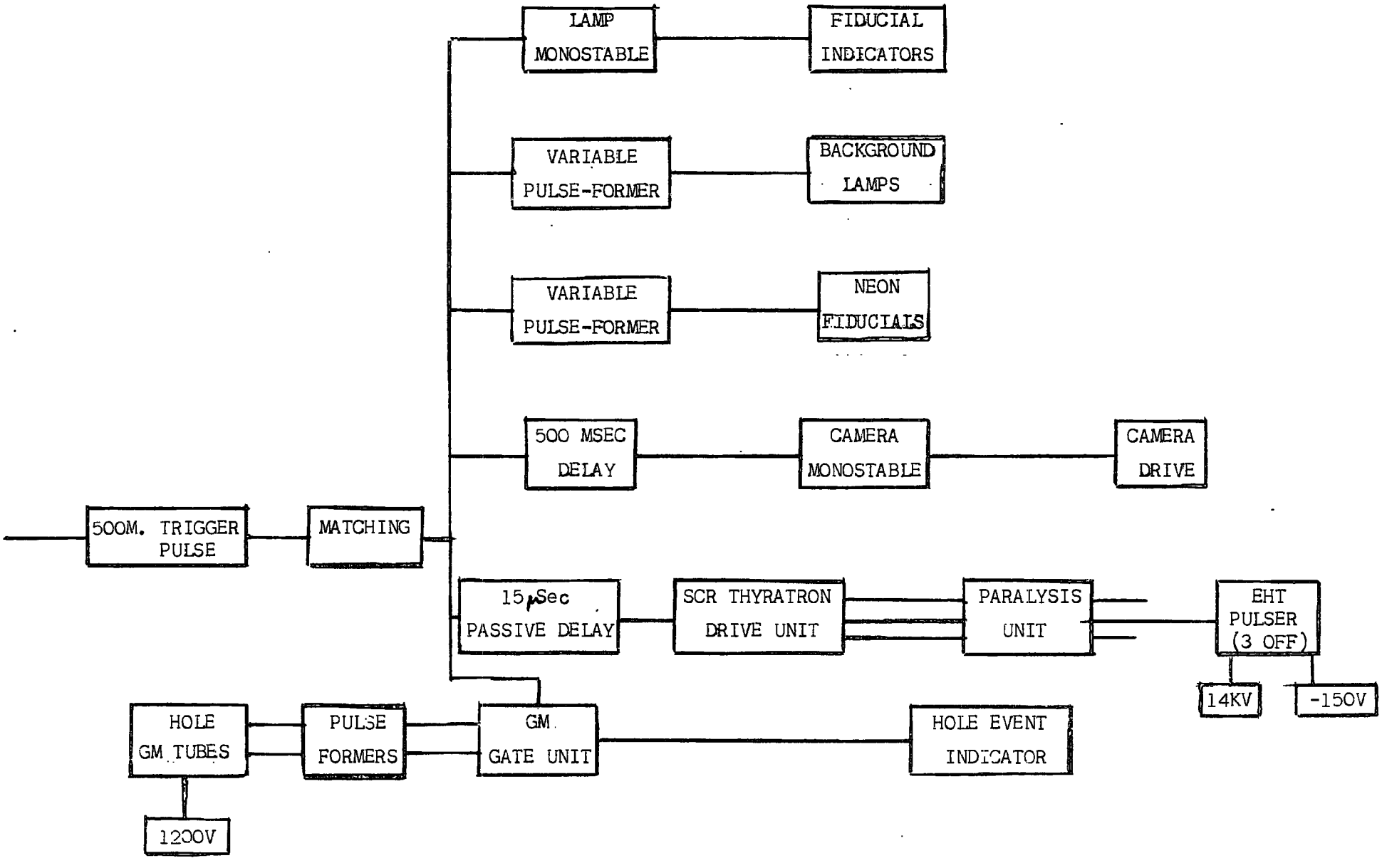
LAMP MONOSTABLE
FIDUCIAL INDICATORS
VARIABLE PULSE-FORMER
BACKGROUND LAMPS
VARIABLE PULSE-FORMER
NEON FIDUCIALS
500 MSEC DELAY
CAMERA MONOSTABLE
CAMERA DRIVE
500M. TRIGGER PULSE
MATCHING
15 μSec PASSIVE DELAY
SCR THYRATRON DRIVE UNIT
PARALYSIS UNIT
EHT PULSER (3 OFF)
14KV
-150V
HOLE GM TUBES
PULSE FORMERS
GM GATE UNIT
HOLE EVENT INDICATOR
1200V

photon density which does not provide useful information.

2.3.5 (iv) The Attainment of Stable Running Conditions

Because of the electronic pickup generated by the EHT pulsing system, and by other experiments at Haverah Park, it is desirable to reduce the possibility of spurious triggering of the spectrograph as much as possible. This has been accomplished in two ways. Firstly, the thyratron grids are maintained at a steady DC level of -50V. A level of about +100V is required to "fire" the valve, and this is provided by AC-coupling the thyristor drive unit into the thyratron grid. This simple precaution makes spurious triggering of the thyratrons (due to mechanical vibration, etc). very rare. Secondly, a paralysis unit, which isolates the pulser inputs for some ten seconds after each event, prevents any possible multiple triggering from any external source. These two precautions have reduced spurious effects (apart from electrical failures) to a negligible level.

2.3.6 Optics and Photography

In order to reduce the loss of data due to faulty camera operation, it is desirable to photograph the entire spectrograph on one frame, if possible. In the Mk. I instruments, this was accomplished by reflecting the images between the trays and placing the camera at the rear, so that the optical path was long enough. The design of the Mk II spectrograph prohibits this solution, so small mirrors are situated on the front of the magnet, and the trays are viewed from the frontal direction. This system gives an overall (central) path length of 28 feet, as opposed to 34 feet in the Mk I version, but requires only two reflections instead of three. However, the angle subtended by the edges of the trays at the camera is rather larger than could be desired (about $20^{\circ}$), but this "polar angle" effect is shown later (section 4.2.3) to be relatively unimportant. The chosen camera position has the advantage of filling a 35mm. frame fully, so that the largest possible image size is obtained. The diameter of the image of a 7mm. tube at the focal plane of the camera is approximately 0.09 mm., and adjacent tubes in the same layer have an apparent separation of 0.13 mm. between centres. A compromise between high film speed (necessary because of the

20 μsec. light pulse from the tubes) and resolution (limited by the grain size of the film) has to be found, and Ilford HP4 has been found to satisfy both criteria adequately. In fact, the resolving power of HP4 is about 40 lines/mm., corresponding to about one quarter of a tube image. Working close to the limit of resolution of the film means that cleanliness in handling is essential, and the mode of processing must be standardised. A simple form of continuous agitation during development (to prevent local exhaustion of developer) has been provided, and has yielded consistently good results.

## 2.4. The Track Reconstruction System

### 2.4.1 General Requirements

The two main requisites of any data reconstruction system are that it should be capable of exploiting the accuracy of the original instrument fully, and that the routine required should be as simple as possible (in order to avoid systematic and operator errors respectively). A complete spectrograph record of an air shower event is desirable, so that possible obliteration and confusion of muon tracks can be reduced to a minimum. It is possible to achieve the first condition by projecting the film record and drawing out all the flashed tube images, as in the Mk. I system, but this method is laborious and prone to error. It was therefore decided to print all useful events photographically, and to locate the flashed tubes by means of a transparent overlay.

### 2.4.2. Overall Description

Preliminary track selection and classification is carried out by direct inspection of the film negative . Useful events are printed to 15" x 12" with a good quality 35mm. enlarger. The exposed print is developed and stabilised in about ten seconds using a print processor, enabling large numbers of events to be handled in a short time. Each frame is checked against the overlay during printing, and the lens-paper distance altered to preserve constant magnification. The great advantages of this system are the ease with which a full copy of each event is produced, and the simplicity of producing further copies at any time.

2.4.3 Errors in Reconstruction and the Effect on Track Location

Some evidence of non-uniform shrinking of the prints during drying has been found - this makes it impossible to locate the overlay on all eight fiducial marks simultaneously. However, the provision of background illumination of the trays (section 2.3.5 (iii)) enables distinctive portions of the tube supports to be used for precise location of the overlay in the region of the muon track. The most common error caused by shrinkage is mis-location of a track by one tube spacing, either in a tray or in a half-track. This problem has been generated artificially, and is included in the checks on the track fitting programme (Chapter 3). Since all events are checked, particularly those exhibiting small angular deflections, the problem should only occur very rarely, and if any doubt remains, a further copy of the event may be made. A modification has been made to install some 50 small neon tubes at a regular spacing at four levels on the spectrograph - this should allow unambiguous location of the overlay close to a track in any section of the instrument.

2.4.4 The Overlay

The overlay used in tube location is a sheet of clear plastic film, marked out by hand from a master print of the spectrograph. The film used for the production of the master was slow, fine grain material with a resolution of about five times that of HP4 ( 200 lines/mm.), and the spectrograph was illuminated with flood lights in order to produce shadow - free lighting over the entire recording area.

# CHAPTER THREE

# COMPUTER ANALYSIS OF FLASH TUBE DATA

## 3.1. Introduction

Neon flash tubes have been used in cosmic ray experiments in two main applications: firstly, as a means of indicating the presence of a charged particle (e.g. for density determinations in lateral distribution experiments), and secondly, as a means of delineating the trajectory of a particle (e.g. the deflection of a charged particle in a magnetic field). In the former application, the tubes are used only to indicate the presence of particles, although the general direction of the track may be used as a check on instrumental acceptance, so that accurately located tubes and well defined tracks are not required. In the second use, an accurate reconstruction of the particle trajectory is essential and to optimise the precision of measurements accurately located flash tubes are required. Some possible methods of achieving an accurate analysis of the data are discussed in this chapter.

## 3.2. General Principles in the Fitting of Particle Tracks

The fitting of a track to an observed particle trajectory (ie. a series of flashed and non-flashed tubes) is very similar to the mathematical problem of producing a "best fit" line to a series of data points. Hence, the best estimate (however derived) is an approximation to the "true" track, and the mean deviation of the estimate from the "true" track should be as small as possible. Preferably, the distribution of the deviations of best estimate from "true" should be gaussian, so that this form of "noise" is readily combined with errors arising from other sources. The number of data points in this case is limited by experimental design considerations, and the range of possible tracks is limited by the physical size of the flash tubes (broadly, a track should not pass outside a flashed tube, except under special circumstances). A comparision may be made with a spark chamber where the range of possible tracks is limited by the spark width. In either case, it is necessary to consider all possible tracks that lie within the experimental bounds defined by detector size - this, of course, is very

relevant to the overall time required to process each track. Finally, some means of defining the "best estimate" must be found, and this is one of the most difficult criteria to define. Several methods have been tried, and the overall results are in fair agreement. However, there is a significant population of tracks which yield widely differing "best estimates" depending on the method used - this problem is discussed later in connection with the mean error expected on a fitted track.

## 3.3 The Mark I Spectrograph Track Fitting Programmes

### 3.3.1 General Method

The method used in this computer programme followed the suggestion by Bull et al (1962) (see section 3.7) that the tube flashing probability, as a function of lateral position of the track within the tube, may be determined experimentally, and then used in order to find the "most probable" track. The probability functions was not determined during the course of the experiment, instead the form given by Bull et al. suitably modified for the different tube size and efficiency, was used.

### 3.3.2 Internal Working of the Programme

The input data for the programme consisted of the tube numbers of the flashed tubes belonging to a muon track (one tube per layer only) in all 28 layers in the spectrograph. The data for layers not containing a flashed tube was initally set to zero. The horizontal and vertical coordinates of the reference tubes in each layer were stored internally, so that the coordinates of the flashed tube centres (assuming a constant support pitch) were readily determined. From this point, the two arms of the spectrograph were treated alike, and the upper half-track was processed first. A trial half-track was found by taking the extreme upper and lower flashed tubes. This track was used to predict the nearest "gap" centre for those layers not containing a flashed tube, since it is most likely (but not certain) that a layer will give no flashed tubes only if the muon does not traverse any tube in that layer. Each of the fourteen layers in a "half track" then had a position coordinate associated with it ( either a tube centre or a gap centre). A "best fit" line was then found by Gauss' method, to

give the mathematically most probable fit to the observed data. This line was then taken as the starting point for further processing. Trial lines were predicted, ranging from $-0.5^{o}$ to $+0.5^{o}$ difference in angle from the initial line, and also $\pm$ 0.5 cm. in lateral position of the centre of gravity of the initial line. For each trial line, the overall probability found by multiplying the probability determined for each layer in turn, was compared with the previous largest value, and when the complete set of trial lines had been attempted, the best track taken was that exhibiting the largest overall probability. This process was then repeated for the lower half-track. The two best half-tracks so found were then checked to ascertain whether their intersection point fell within the magnet. This intersection test gave much invaluable information about each muon event, and further mention will be made of the use of this part of the programme when dealing with that version adopted for use with the Mk. II spectrograph data.

3.3.3 Performance of the Programme

Although the overall results of the programme agreed fairly well with those determined by hand simulation, a population of events was found which contained marked differences in angular deviation between the two methods. In many of these cases, no simple explanation (e.g. incorrect input data) could be found for the deviation of the computer fit from a reasonable simulated result. Indications of this drawback led Earnshaw (1968) and Orford (1968) to conclude that the then available computer fitting method was not reliable for high energy EAS muon work. Refinements in the procedure have confirmed the reliability of the methods and such methods are now considered acceptable although, to insure against large deviations, all muons exhibiting angular deflections less than $2^{o}$, according to the computer fit, were checked exhaustively by hand simulation. The results of the checks on the data presented by Machin et al (1969), indicated that the major limitation in this method of fitting lay in the form of probability function used, and an alternative method was proposed for the analysis of the data from the modified spectrograph.

## 3.4. The Mk. II Spectrograph Track-Fitting Programme

### 3.4.1 Introduction.

In order that the high precision of the angular measurements from the Mk. II instrument may be fully exploited, a fitting programme of greater reliability than the previous version is required. In view of the difficulties discussed in section 3.3, it was decided to abandon the "probability function" method, and to use the geometric path length in a tube as a measure of the flashing probability. There is no definite experimental evidence that, for all possible tracks, this function represents the true case less accurately than any other proposed shape.

### 3.4.2 General Description of the Method

As in the earlier programme, the input data consists of the numbers of the flashed tubes in each of the 40 layers of the spectrograph, and these numbers are converted into horizontal position coordinates. The associated vertical coordinates are known from the stored measurement data, and from the ordering of the input data. A trial line is fitted to the flashed tube centres by a least-squares minimisation method. In this way only the "active" information is used in determining the slope and position of the trial line. The lines used from now on are simply of the form : $y = mx+c$, and the initial values for m (or $\tan\psi$) and c are given by the least-squares solution. Small changes of a fixed step size are made in both m and c (angular change $0.025^{\circ}$, position change 0.25 mm.) so that a matrix of combinations of gradient and constant is covered fully. For each combination (total 41 x 41 = 1681 attempts) a check is performed to ascertain whether the line passes through all the flashed tubes. If not, then a null entry is made in the matrix corresponding to that combination. Evidently, the provision of such extreme values of $\pm 0.5^{\circ}$, $\pm 0.5$ cm. means that many of the tracks will not be acceptable, and this preliminary check saves at least a factor of ten in the computing time for each event. For all acceptable tracks, further investigation is then carried out in which the trial line is used (as before) to predict the nearest "gap" centres in layers containing non-flashed tubes. For each attempt having a non-zero entry in the matrix

the geometric path length of the line in the gas of each tube is calculated, and the value stored. If the line passes through a non-flashed tube, the path length is assigned with a negative value. A quantity termed the "efficiency" may then be calculated by dividing the total path length in all the flashed tubes by the overall total path length (including non-flashed tubes). The line possessing the highest value of "efficiency" satisfies two criteria: it chooses the longest path length in the flashed tubes, and the shortest in non-flashed tubes, which is the closest possible reconstruction of the "true" track. If no non-flashed tubes are found, the longest overall path length is taken. Conversely, if no track passing through all the flashed tubes is found (ie. no acceptable track exists), the least-squares information is displayed and the input data checked.

When the two best estimate tracks for the arms of the spectrograph have been found, an intersection test is carried out to ascertain whether the combination of the two half-tracks is acceptable. The test consists basically of finding the intersection point of two lines of the form $y=mx+c$, together with the associated errors (assuming an angular error of $0.15^{o}$ on each half-track). Several extra tests are also performed, in connection with the position of the tracks relative to the magnetic volume, and these are of great help in subsequent classification of the event since they provide a firm criterion for rejection or acceptance of data.

3.4.3 Performance of the Programme on Spectrograph Events

The variation of the best track efficiency value with the number of flashed tubes on the track (taken from events at core distances $150 < r < 250$ m) is shown in fig. 3.1. The mean number of flashed tubes in a half-track (i.e. out of a total of 20 tubes) is 10.44, corresponding to a flash tube internal efficiency of 81.5%. This means that there are, on average, 2.6 non-flashed tubes per track (since the maximum layer efficiency is less than 70%, the mean number of tubes traversed is slightly greater than 13). The treatment of non-flashed tubes is therefore important in the present experiment if gross errors are to be avoided. The method of section 3.4.2 shows that the non-flashed tubes are treated in almost exactly the same

Figure 3.1

(i) The mean number of flashed tubes as a function of the track efficiency found by the fitting programme.

(ii) The mean efficiency as a function of the number of flashed tubes.

Both the above results are taken from 150-250m. Mk.II Spectrograph events.

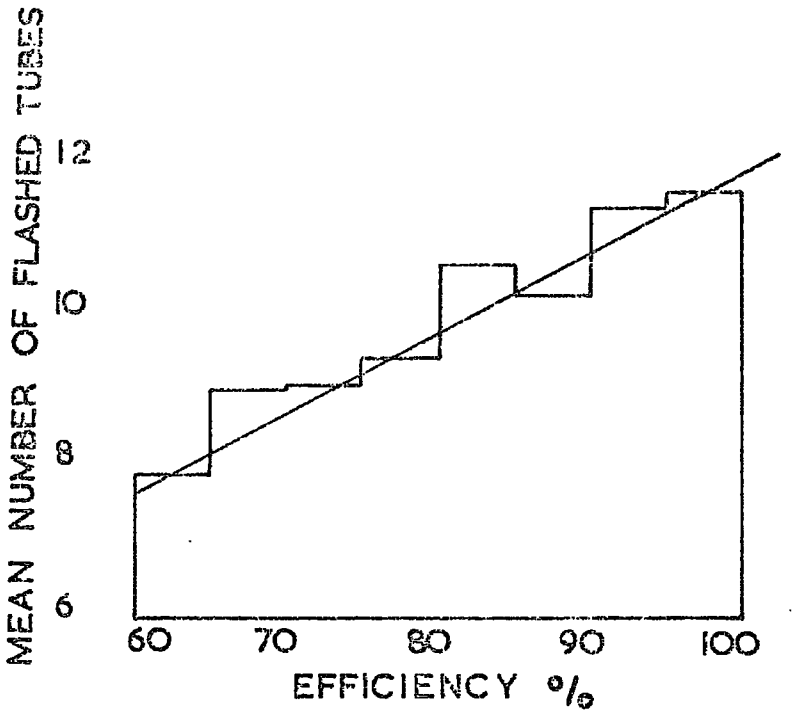
MEAN NUMBER OF FLASHED TUBES
12
10
8
6
60
70
80
90
100
EFFICIENCY %

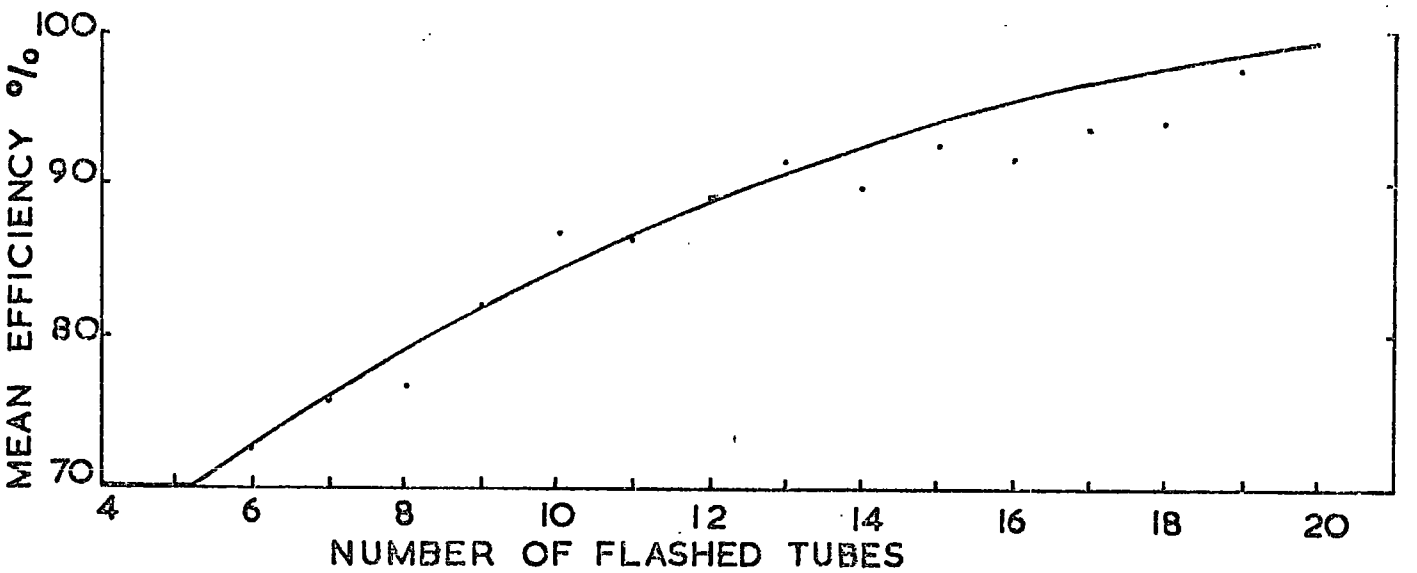
MEAN EFFICIENCY %
100
90
80
70
4
6
8
10
12
14
16
18
20
NUMBER OF FLASHED TUBES

manner as flashed tubes (unlike the earlier version of the programme), and it appears that this form of treatment reduces the possibility of very large deviations markedly. The data have also been checked for any momentum bias: a sample of events with deflections less than $2^{o}$ (corresponding to momenta $>8$ GeV/c) had a mean efficiency value of $83.2 \pm 1\%$, while a sample of events with deflections greater than $6^{o}$ (momentum $< 3$ GeV/c) had a mean of $83.5 \pm 1\%$. It is concluded that there is no apparent momentum bias in the value of efficiency predicted by the programme - the slight discrepancy between the overall mean predicted efficiency value and the measured value (some 2%) probably arises from slight deviations in the form of the path length function from the "truth", and also in cumulative errors in tube location and measurement.

### 3.5. Tests of the Track-Fitting Programme

#### 3.5.1 Introduction

In view of the discussion of section 3.2 concerning the difference between the "true" track and the "best estimate" track, it is essential to devise a thorough checking procedure to determine the overall track-fitting error. Since the error was expected to be in the region of $0.1^{o}$ or less, an analogue device (such as a hand simulator) would be impossible to use, in terms of physical size alone, irrespective of the possible resolution and setting limitations. It was decided to approach the problem using computer-generated artificial tracks, so that no manual operations are necessary in assessing the accuracy of track fitting.

#### 3.5.2 The Production of Artificial Tracks ("Hole" Events)

The method uses computer-generated pseudo-random numbers to select incident angles and positions, and to "decide" whether a tube traversed by the chosen "track" has flashed or not. The procedure adopted is as follows:-

i) the random-number generator is started with a tabulated random number (further details are given in Appendix 1). The output is a uniformly distributed number in the range 0.0 to 1.0, so that this range must be transformed to suit each measure of the track.

ii) an incident angle is chosen (the initial tests covered the range $-10^{o}$ to $+10^{o}$, but some runs out to $30^{o}$ have been performed).

iii) the sign of the angle is found by calling a new random number; if the value is less than 0.5, the sign of the angle is negative.

iv) the lateral position of the track (constrained to make the track fall within the acceptance limits of the spectrograph hole) is found from a further random number.

v) the position of the track with respect to each of the 20 layers in the top half of the spectrograph is evaluated - if the track falls within a "gap" then the "tube number" for that layer is automatically zero. If the track falls within a tube at a perpendicular distance Z from its centre, the value of $P(Z) = 1 - (Z/R)^4$ when the internal radius of the tube is evaluated, (the justification of this is discussed in 3.5.3). If on calling a new random number, the value is $\leqslant P(Z)$, the tube is said to have flashed (and its tube number is calculated). If the value is $> P(Z)$, the tube number is set to zero (ie a non-flashed tube).

vi) the upper half-track is complete, and the lateral position of the intersection of the track with the mid-plane of the magnet is calculated.

vii) it is shown in section 4.2 that the standard deviation of the difference in lateral position of upper and lower half-tracks at the mid-plane of the magnet is 3.8 mm. for "hole" events, so that a random lateral position for the lower half track is chosen by the second generator (see Appendix 1 ) which ensures that the difference between the two lateral positions conforms to a normal distribution with the correct mean and standard deviation. Since the aim is to generate "hole" events the above figure of 3.8mm. is appropriate and is used. Similarly, the standard deviation in deflection for "hole" events is $0.16^{o}$, so that the lower half track is so generated as to be distributed normally in angle and position about the upper (selected) half-track.

viii) the routine of (v) is used to determine the flashed tube numbers for the lower half-track.

Figure 3.2

(i) Various forms of flashing probability with the associated value of internal efficiency. The curve $1-AL^{\gamma}$ is that used in the Mk.I programme with $A = 0.95$, $\gamma = 6.5$.

(ii) The probability function determined by Bull et al (1962), showing the contribution to the overall flashing efficiency due to muons traversing the glass wall of the tube.

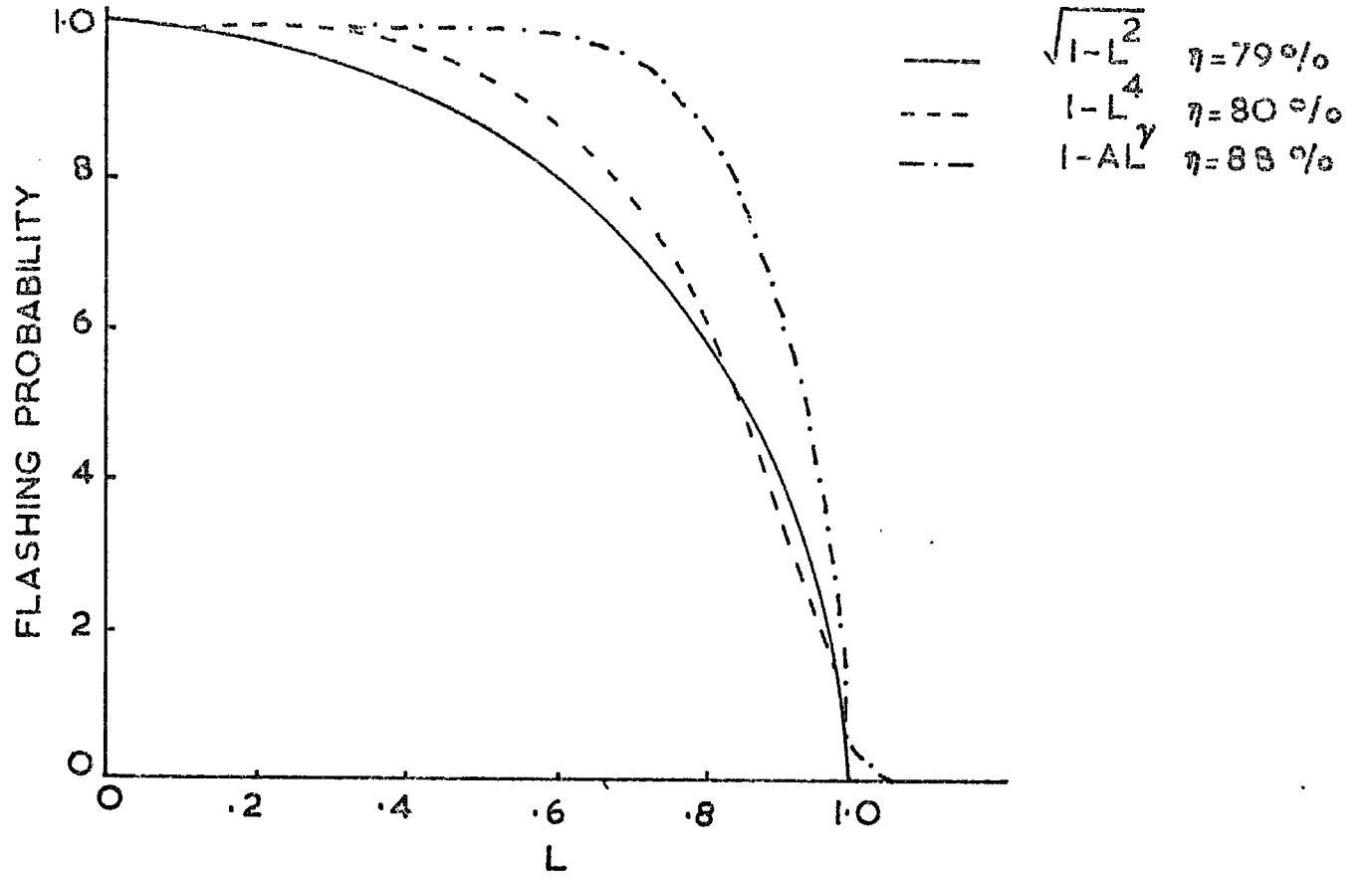
FLASHING PROBABILITY
1·0
·8
·6
·4
·2
0
0
·2
·4
·6
·8
1·0
L
$\sqrt{1-L^2}$ η=79 %
$1-L^4$ η=80 %
$1-AL^\gamma$ η=88 %

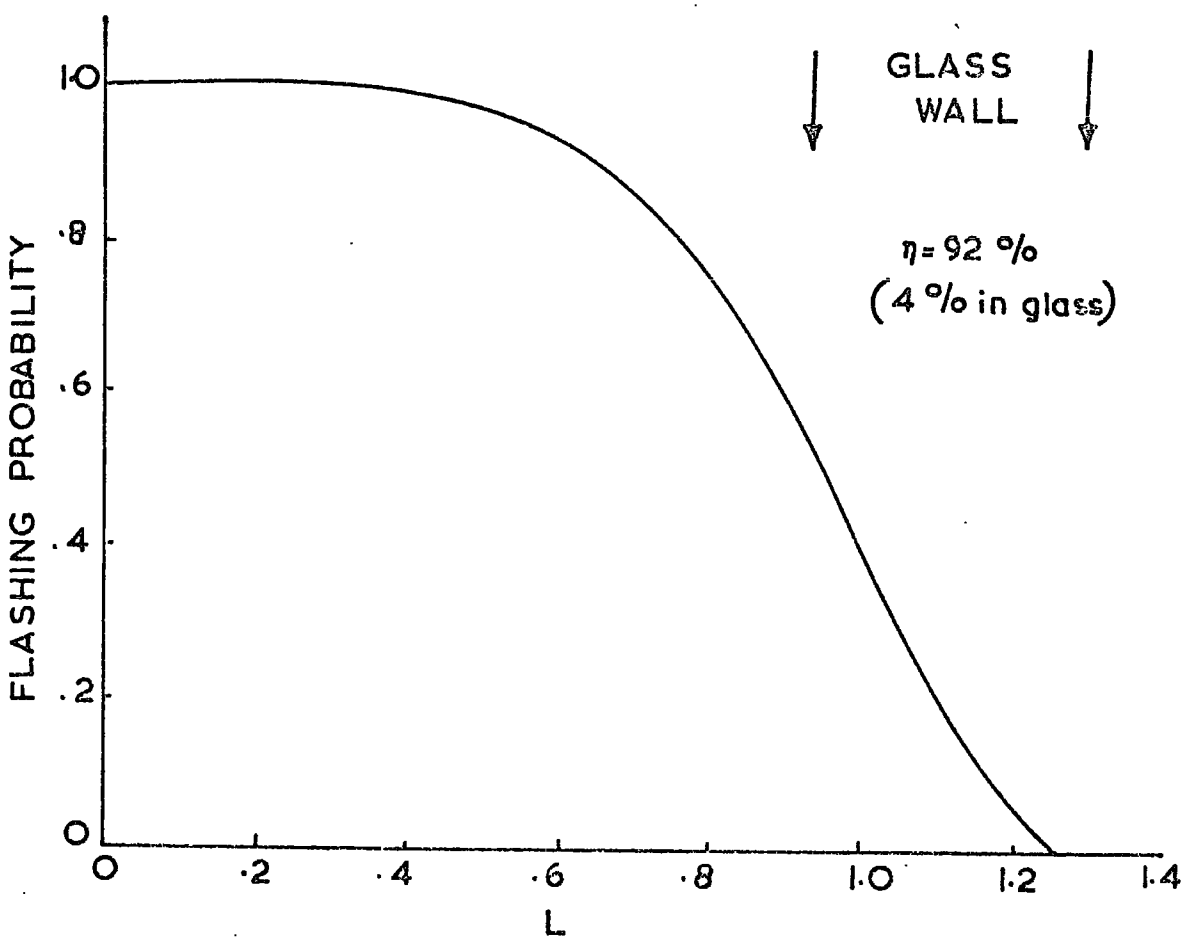
FLASHING PROBABILITY
1·0
·8
·6
·4
·2
0
0
·2
·4
·6
·8
1·0
1·2
1·4
L
GLASS
WALL
η = 92 %
(4 % in glass)

ix) the entire event is output on cards in a format suitable for the track-fitting programme. Also, the total number of flashed tubes in the track is stored, to be output as end-of-run accounting information.

This programme generates 85 complete events in ten seconds, so that the limiting factor in this analysis is the time taken to track-fit each generated or real event (at present some seven seconds).

3.5.3 Usefulness of Artificial Tracks

It is important that the artificial tracks should be as similar as possible to real tracks when direct comparisions are to be made. For this reason, several forms of the function P(Z) have been investigated, and fig 3.2 summarises those which fit the experimental data best. If P(Z) is regarded as a probability of flashing (as inferred from the use of the random number method), then $\int_0^R P(Z)\, dR = \eta_{int}$, the internal flashing efficiency of the tube, (not the efficiency value given by the programme). The closest form of P(Z) is therefore that which yields $\eta_{int} = 81.5\%$. A form of $(1-L^4)$, where L is defined as (Z/R), gives 80%, and $(1-L^5)$ gives 83.3%. The two forms are in fact very similar, and the former has been chosen so that any error is made rather on the side of too many non-flashed tubes per track.

The genuine particle tracks described in the previous section passed through the "hole" of the magnet, that is, they did not undergo any magnetic deflection. This simulation of such events was chosen because of its simplicity; any attempt to simulate real magnetic deflection means that the appropriate degree of Coulomb scattering must be introduced, and this would only make the task of comparison more difficult. However, the results of this work give a good estimate of the overall noise, both instrumental and track-fitting, and there is no reason why the simulation should not be extended to cover tracks with magnetic deflection and scattering included.

3.5.4 Results Obtained by Fitting a Generated Track

The difference between the angular deflection of a generated track and the deflection found for that event by the track-fitting programme has been recorded for 489 artificial events, and the distributions is shown in fig. 3.3. The fact that the distribution is closely gaussian indicates

Figure 3.3

(i) The difference in lateral separation of half-tracks in the mid-plane of the magnetic ($\Delta x_m$) between the "true" track and that determined by the fitting programme.

(ii) As above but showing the difference in angular deviation ($\Delta\psi$).

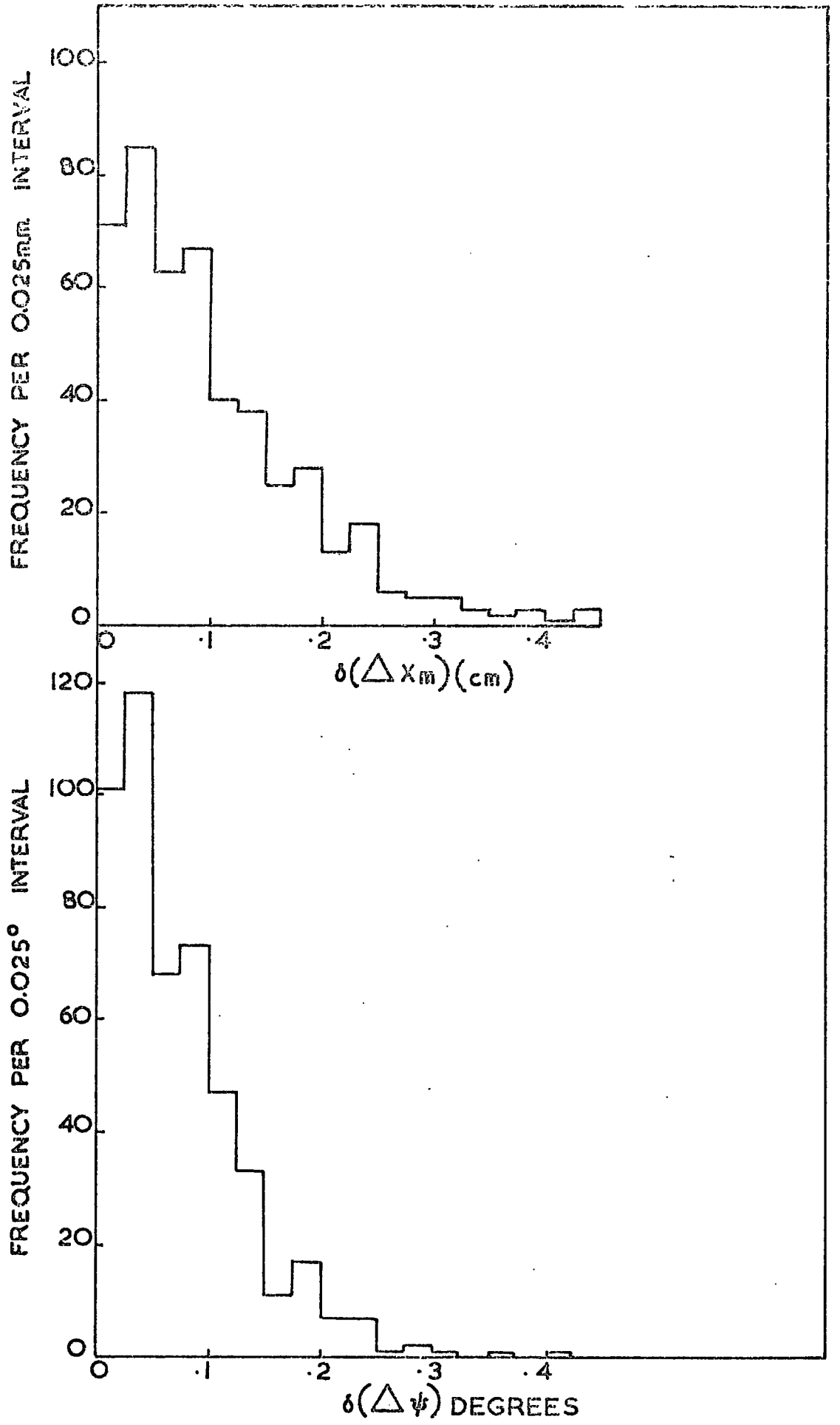
FREQUENCY PER 0.025mm. INTERVAL
100
80
60
40
20
0
0
·1
·2
·3
·4
δ(Δ Xm)(cm)
FREQUENCY PER 0.025° INTERVAL
120
100
80
60
40
20
0
0
·1
·2
·3
·4
δ(Δ ψ) DEGREES

Figure 3.4 The difference between the "true" angular deviation and that determined by a least-squares fit to the centres of the flashed tubes.

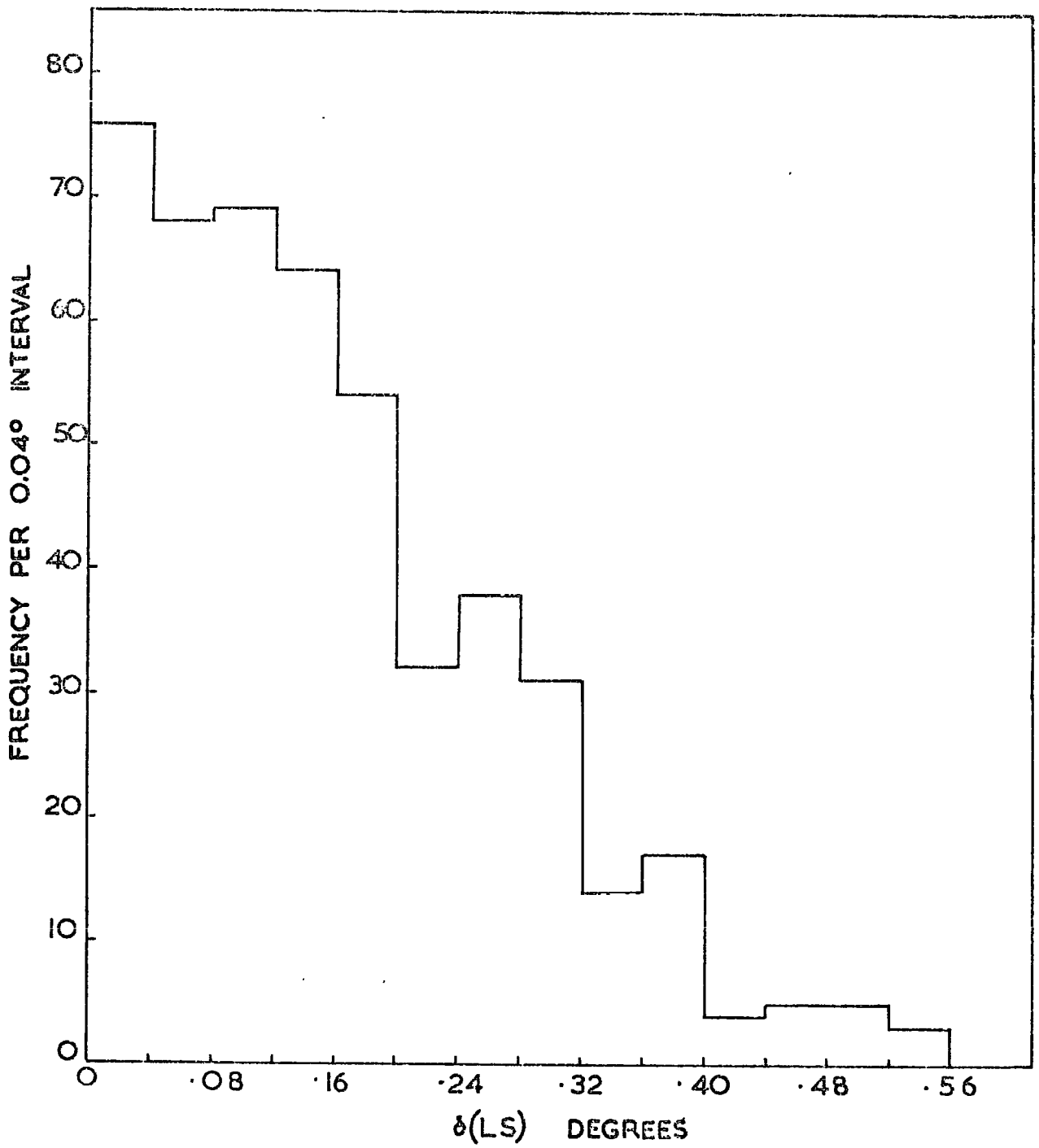
80
70
60
50
40
30
20
10
0
FREQUENCY PER 0.04° INTERVAL
0
·08
·16
·24
·32
·40
·48
·56
δ(LS) DEGREES

that the fitting programme is in fact giving a value distributed uniformly about the true value with a standard deviation of $0.06^{\circ}$ ( the mean absolute error is $0.064^{\circ}$). If the experimental value for the overall noise of $0.16^{\circ}$ is assumed to be compounded only of track-fitting noise and tube location errors, then, since $\sigma^2_{n} = \sigma^2_{tf} + \sigma^2_{L}$ , this gives $\sigma_L = 0.13^{\circ}$. Hence the track-fitting error is considerably smaller than that introduced by the tube location (and the location error is very close to the design figure of $0.10^{\circ}$).

Fig. 3.3 also shows the difference in the lateral separation of tracks at the mid-plane of the magnet ($\Delta x_m$). The standard deviation of this distribution is some 1.2mm, which is considerably smaller than the overall figure of 3.8mm found experimentally. The fitting programme appears therefore to give a very good estimate of the $\Delta x_m$ value - which is essential for the proper classification of events.

Fig. 3.4 shows the difference in angular deflection between the true value and that given by the least-squares fit value. The standard deviation is $0.20^{\circ}$, indicating that the improvement in accuracy using the path-length optimisation is slightly greater than a factor of two. However, the total noise on a least-squares deflection will be about $0.24^{\circ}$ (using $\sigma_L = 0.13^{\circ}$), so that this method is quite acceptable if a less precise measure of the deflection is required (the time taken to least-square analyse an event is only about one second).

It should be noted that, while the function $P(Z) = 1-(Z/R)^4$ was used for generating tracks, the path length (analogous to the use of $P(Z) = 1-(Z/R)^2$ ) was used to fit the tracks. This was done mainly to introduce a slight difference in the functions used (a form $P(Z) = 1-(Z/R)^2$ predicts $\eta_{int} = 78.5\%$, or only 1.5% lower than a function of form $P(Z) = 1-(Z/R)^4$). However, as a check on the method of fitting, a standard track-fitting programme was modified to use the relation $P(Z) = 1-(Z/R)^4$.

The results on generated tracks were very similar to those using the path length optimisation, so the conclusion drawn from this test is that the true form of function is either relatively insensitive (which seems unlikely in view of previous indications) or that it is very similar to the two

forms used here. Certainly, it appears that the geometric path length representation is sufficiently accurate for the small flash tubes, and little advantage is gained by using a more complex function.

3.6 Comparision with Other Work

Bull et al (1962) described the method used to fit tracks from the Nottingham spectrograph, and suggested the use of a probability function of the form shown in fig. 3.2. From an analysis of 30 particles, they claimed an error of $0.045^{o}$ on a track, corresponding to an error of $0.065^{o}$ on a deflection measurement, for only twenty layers of tubes. The flash tubes had an internal efficiency of almost 100%, so that there was on average less than one non-flashed tube per track. The flashing probability function was determined experimentally, using ten layers of tubes to define the track, while observing the "intercept" on the remaining ten layers. 580 layer transits were observed from the passage of 58 particles. The authors did not quote the method used to fit the track for this part of the experiment; but it is to be expected that the form of the resulting probability function must depend strongly upon the method of fitting the track, as the frequency of observation of a given "intercept" on a test layer depends upon the probability assigned to the associated positions on the fitting layers. The small errors quoted by the authors probably result from the high efficiency of the tubes (ie. the treatment of non-flashed tubes arises only rarely), and from the carefully selected sample of tracks used. It is essential that a representative sample of tracks should be used for such testing preferably of a similar size to the data sample.

3.7 Discussion

This chapter has described two different methods of fitting tracks to flash tube data. For highly efficient tubes, the differences between the two are probably small. However, when the internal efficiency of the tubes is considerably different from 100% (as is unavoidable then the Mk II spectrograph because of the 15 $\mu$sec delay in applying the EHT pulse), the treatment of non-flashed tubes is critical, and a very sharply changing probability function can lead to large deviations from the "truth" in certain cases. In view

of the lack of precise knowledge about the probability function, it appears that the geometric path length method (basically saying that the ionisation is proportional to track length) is more likely to give a better overall fit. Accurate experimental information about the behaviour of flash tubes may be possible using spark chambers to define muon tracks, and observing the flashing frequency at various intercepts. However, spark widths of the order of 0.5 mm. are necessary for the critical region near the tube edge, where the change in shape is very rapid. It is likely that tube mislocation and variations in tube diameter would render such an experiment difficult to interpret.

The form of the present programme allows simple examination of "strange" events. Many track parameters are calculated and output, and difficulties caused by spurious tubes (usually from knock-on electrons and materialising $\gamma$-rays) are readily resolved. Two improvements are at present in progress; firstly, a modification to the input format to allow two tubes in a layer to be read (to allow the computer to reject spurious tubes automatically), and secondly, an investigation of the effect on flashing of the glass wall of the tube. It is apparent that a track passing very close to the gas but within the glass wall must have a finite probability of causing the tube to flash. Initial trials assigned a flat 5% chance to these events, and had some success in resolving some "strange" tracks. Further investigation of this effect may lead to an improvement in the accuracy obtainable, but the gain is only likely to be marginal.

# CHAPTER FOUR

## RESULTS FROM Mk. I and Mk. II SPECTROGRAPHS

### 4.1. The Mk. I Spectrograph

#### 4.1.1 Introduction

The Mk. I spectrograph was in operation in conjunction with the 500 m. array for a total of 4.38 years, and an overall efficiency of 70.7% was obtained, while the 500m. array during a similar period yielded some 91% (Andrews et al (1969)). The loss of a further 20% of data over the main array figure was mainly due to faulty operation of the camera and high voltage systems. The number of acceptable showers recorded during this period was 2497, yielding a total of 3187 muons in the energy range 1-100 GeV, at core distances ranging from 150m. to 600m. Data accumulated for showers falling outside these limits have been considered separately (Earnshaw (1968)), but are subject to limitations in the accuracy of the analysed shower parameters.

#### 4.1.2 The Momentum Spectra Derived from the Mk. I Spectrograph Data

When deriving momentum spectra from the data on the angular deflections of muons recorded with a spectrograph, it is essential to determine several basic parameters concerned with the geometry and design of the instrument. The most important factors are the geometrical acceptance ( as a function of momentum), the relation of momentum to magnetic deflection, correct inclusion of the effects of scattering, both in the flash tube trays and the magnet iron, and allowance for the uncertainties in measurement of angles arising from the mislocation of flash tubes and measurement errors. The geometrical acceptance was evaluated by Orford (1968), using an analogue method, and a computer simulation of the problem gave substantially the same results (D.R. Pickersgill, private communication). The typical acceptance function is shown in fig. 2.4. The relation between momentum and magnetic deflection which has been used is due to Rastin (1964), and takes account of energy loss in the magnet:

Figure 4.1 The deflection spectrum derived from the Mk. I spectrograph for core distances between 150 and 250 metres.

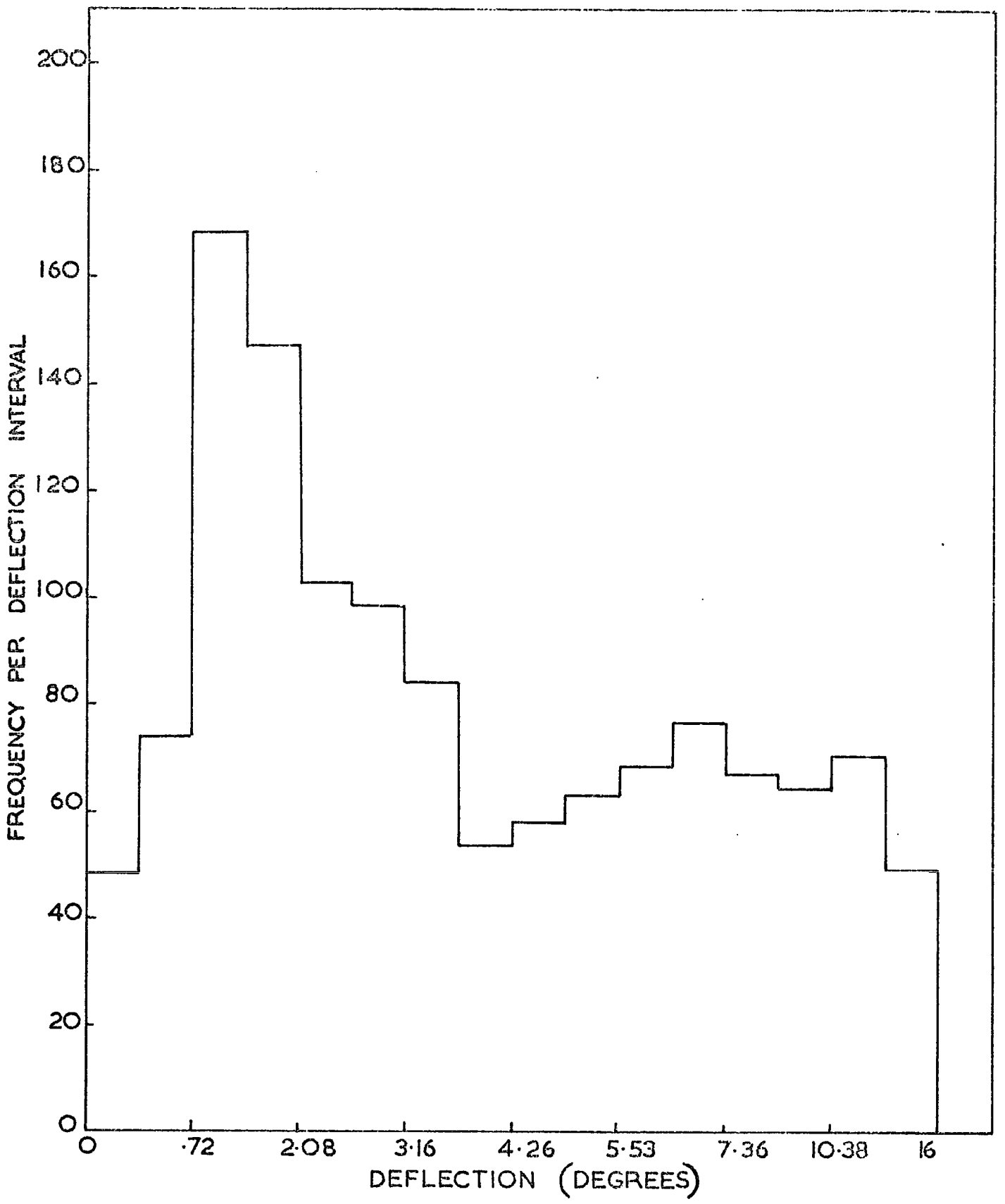
200
180
160
140
120
100
80
60
40
20
0
FREQUENCY PER DEFLECTION INTERVAL
0
·72
2·08
3·16
4·26
5·53
7·36
10·38
16
DEFLECTION (DEGREES)

$$P = \frac{\ell_k \left(1 + \epsilon^2/k^2\right)}{\left(\exp\left\{\frac{\Sigma}{k}\left(\psi_1 - \psi_2\right)\right\}\left(\cos\psi_2 + \frac{\Sigma}{k}\sin\psi_2\right)\right) - \left(\cos\psi_1 + \frac{\Sigma}{k}\sin\psi_1\right)} \quad ..4.1$$

where $k = 300B$, $\Sigma$ = energy loss in MeV $cm^{-1}$, $\ell$ = magnet thickness in cm. $\psi_1$ = incident direction, $\psi_2$ = emergent direction of particle.

Coulomb scattering in the magnet iron was evaluated using the equation given by Rossi (1952), but scattering in the flash tube trays was not included in this calculation (being some 30 times smaller). However, the effects of scattering in the trays were included in the noise estimates of Walton (1966)) and Orford (1968) (see Chapter 2).

The deductive method of spectral derivation is described by Pickersgill (1971) and follows that outlined by Orford (1968). The expected deflection distribution is predicted from a trial momentum spectrum (taking account of all the above factors), compared with the experimental data, and the differences are used to produce an improved trial momentum spectrum. The method is therefore iterative and the procedure is normally followed until a close fit (1% - 5%) is obtained by the data. Several other criteria have also been used, and yield very similar results. The effect of a fairly large number of iterations ($\gtrsim$20) is to cause the momentum spectrum to "follow" the data, that is, the resulting spectrum shows peaks and troughs corresponding to the statistical fluctuations in the deflection data. This lends confidence to the method, and involves little loss of accuracy due to the small momentum intervals employed. Numerical processing of the final momentum spectrum yields acceptably smooth integral and differential momentum spectra. Errors on the spectra are obtained by causing the cell populations corresponding to the largest and smallest deflection intervals to increase and decrease by one standard deviation ($\sqrt{n}$), and interpolating between these extreme movements across all other cells (basically "pivoting" the deflection data about its centre). A typical deflection spectrum is shown in fig. 4.1, and the final Mk I momentum spectra are shown in fig. 4.2 with representative errors.

Figure 4.2 The Mk.I integral muon spectra for four core distance intervals in showers with $\rho_{500} = 0.33$

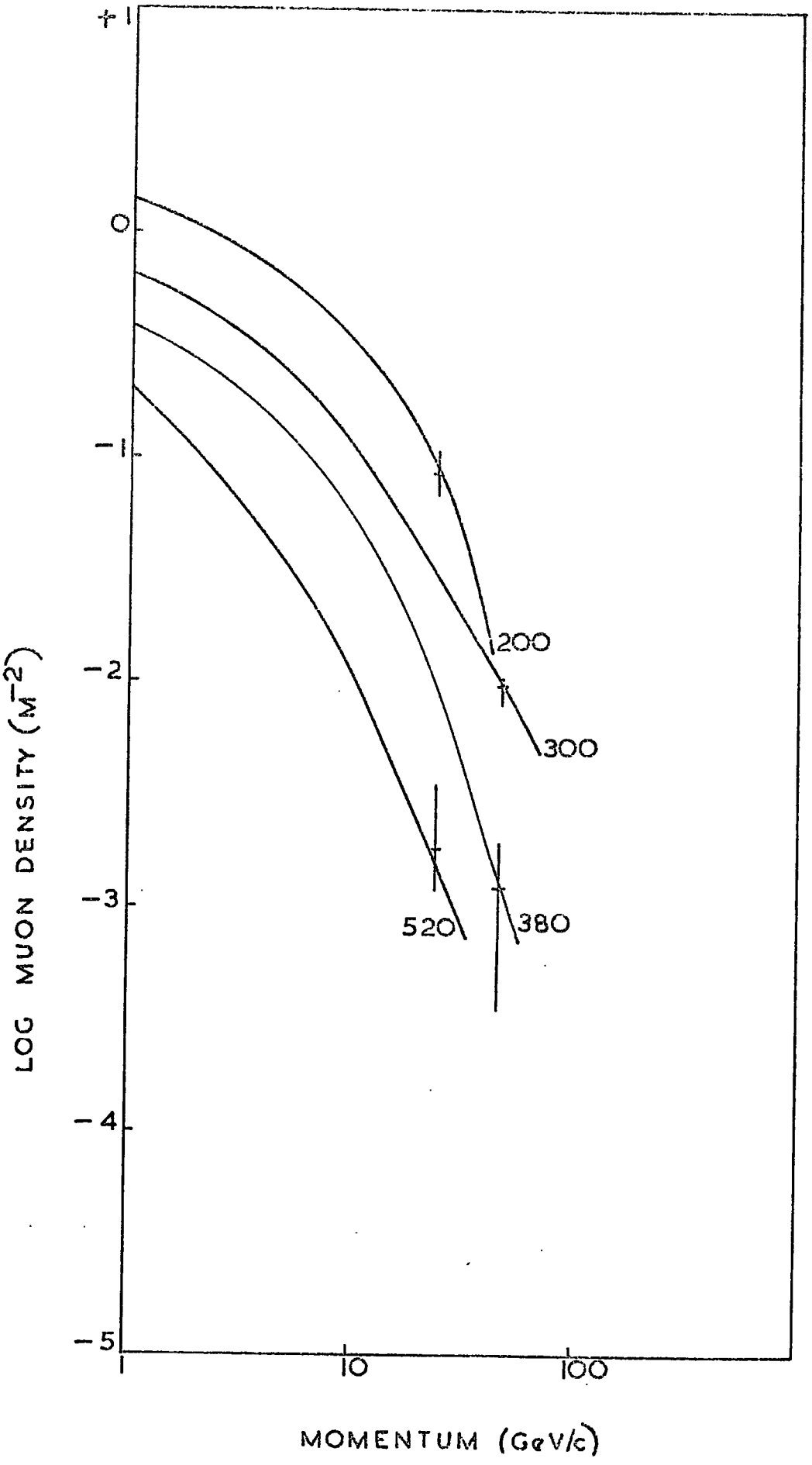
+1
0
-1
-2
-3
-4
-5
LOG MUON DENSITY ($M^{-2}$)
200
300
520
380
1
10
100
MOMENTUM (GeV/c)

The "inductive" method of Walton (1966) has not been used for the derivation of spectra, but has been employed in determinations of mean momentum of muon populations for the work described in Chapter 6.

4.1.3 Checks on the Experimental Data

4.3.3(i) The Muon Data

About half the muon tracks in the Mk.I data were analysed by computer the remainder being hand simulated (Walton (1966)). However, all particles exhibiting small angular deflections ($\leq 2^{\circ}$) were checked by hand simulation for possible large fitting errors, and those with deflections less than $0.36^{\circ}$ (corresponding to momenta in excess of 50 GeV/c) were checked exhaustively by several operators. The initial drawing sheet of the event was also rechecked against the film, to obviate mistakes and omissions. Random triggering of the spectrograph has shown (Earnshaw (1968)) that the probability of chance inclusion of an unassociated muon is very small, particularly when the tracks are subject to the criteria that the muon must possess the same general incident direction as all other shower particles. These safeguards preclude acceptance of uncorrelated half-tracks, spurious events, and unassociated events. Since the overall measurement noise is $0.3^{\circ} \pm 0.03^{\circ}$, it is to be expected that only 55% of particles with deflection less than $0.36^{\circ}$ are true high energy particles, the remainder being particles of lower energy which effectively (due to scattering and noise) appear as high energy particles (Machin et al (1969)). However, if the noise is known with adequate precision, this effect can be accounted for in the spectral derivation. The distribution in the lateral separation of half-tracks at the mid-plane of the magnet ($\Delta x_m$) for particles with deflection less than $0.36^{\circ}$ has a high $\Delta x_m$ "tail" due to the "false" particles; true high energy particles can be selected with confidence by requiring that $\Delta x_m \leq 10$ mm, and exist in the proportions expected from the derived momentum spectra.

4.1.3 (ii) The EAS Data

All data described in this chapter were collected using the 500 m. array as a trigger, and a full analysis was available for all showers (The "Durham" analysed showers of Earnshaw (1968) and Orford (1968) have been omitted).

Figure 4.3 The deflection spectrum of events containing a single acceptable muon in the spectrograph (solid line), compared with the (normalised) deflection spectrum of "multiple" muon events (dotted line).

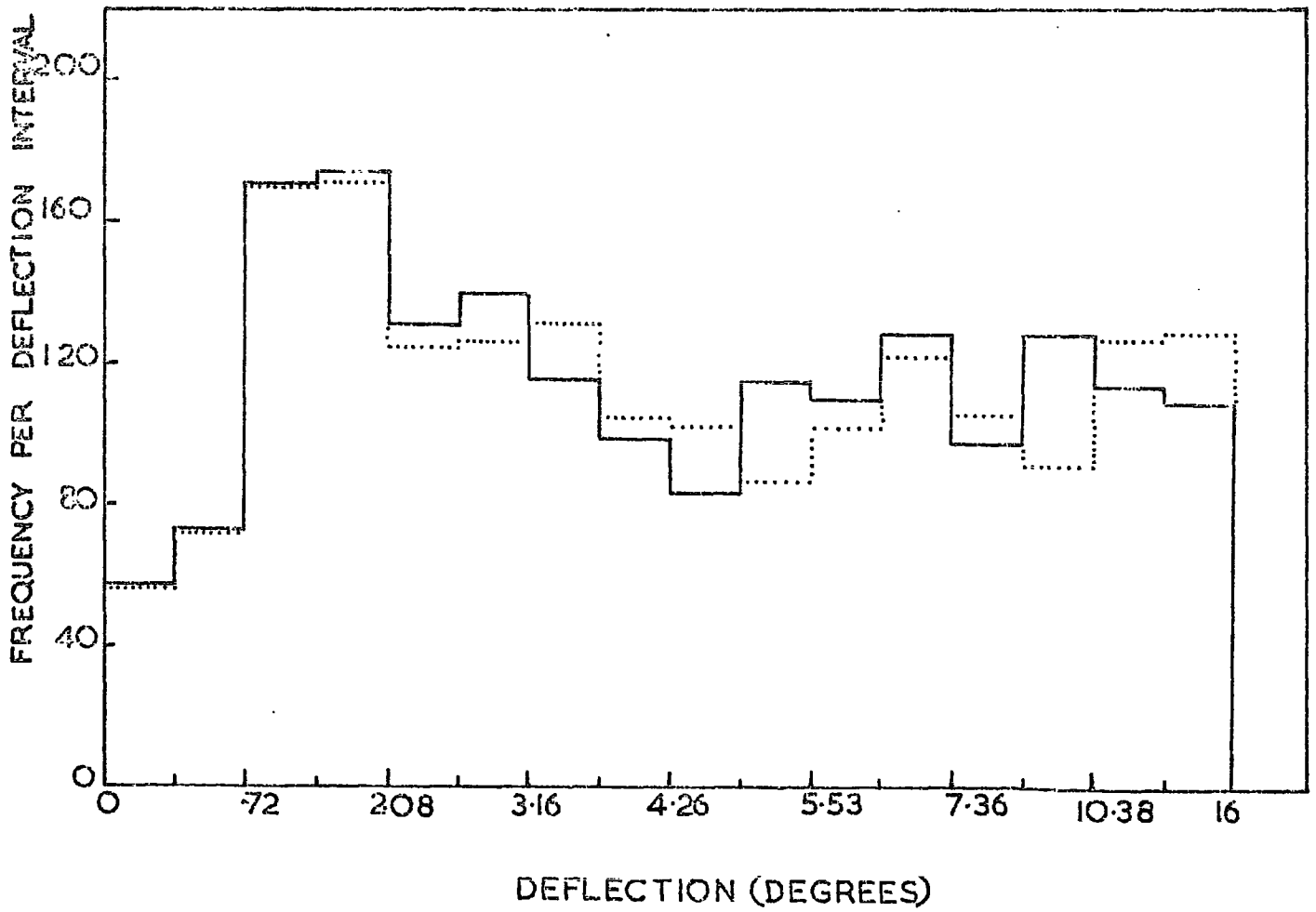
FREQUENCY PER DEFLECTION INTERVAL
200
160
120
80
40
0
0
·72
2·08
3·16
4·26
5·53
7·36
10·38
16
DEFLECTION (DEGREES)

However, the data used in the analysis of Machin et al (1969) were not of a uniform standard, as the EAS data had been accumulated over a period of years, during which the shower analysis programmes had undergone several improvements. Because of the apparent need to check the EAS arrival directions (see Chapter 6) it was decided to update the EAS data for the entire Mk I period by employing the results of the latest analysis programme. Hence all the data presented here result from the latest version of the Leeds University shower analysis programme, and are subject to strict rejection criteria. As a result of the improved data a few large changes in core distances have been noted, but the effect on the spectra has been very small, probably because of the relatively large sorting intervals used. The changes in arrival directions are however very significant, and are reported in Chapter 6.

4.1.4 The Momentum Spectra of Multiple Muons

The data comprising the Mk I sample have been divided into two sets; those events producing a single acceptable muon recorded in the spectrograph, and those containing more than one muon. The reason for this check was to ascertain whether the muon density on the spectrograph caused any overall momentum bias during analysis. The "acceptable muon" criterion means that occasionally very dense events will only yield one muon, so that some dilution of any real effect is inevitable using this method. The frequency of very dense events of core distances greater than 150m. is acceptably low, and the deflection spectra of the two sets of data have been compared in figure 4.3. The data are similar and show no appreciable differences, particularly regarding the percentage population of the smallest deflection interval. It is concluded that any momentum bias arising from this effect is small. In particular, a shower of $2.10^7$ particles at a core distance of 300m. (an example of the interesting portion of the data apparently showing a high proportion of energetic muons) gives a muon density of 0.68 $m^{-2}$, so that on average the spectrograph will record only one muon. Hence the "density" effect is expected to be very small in the region of interest.

Figure 4.4 The distribution in the number of acceptable muons in 25m. bins of core distance. The dotted line refers to muons possessing angular deflections less than $0.36^{\circ}$ (momenta greater than 45 GeV/c), and is plotted on a 10 x scale.

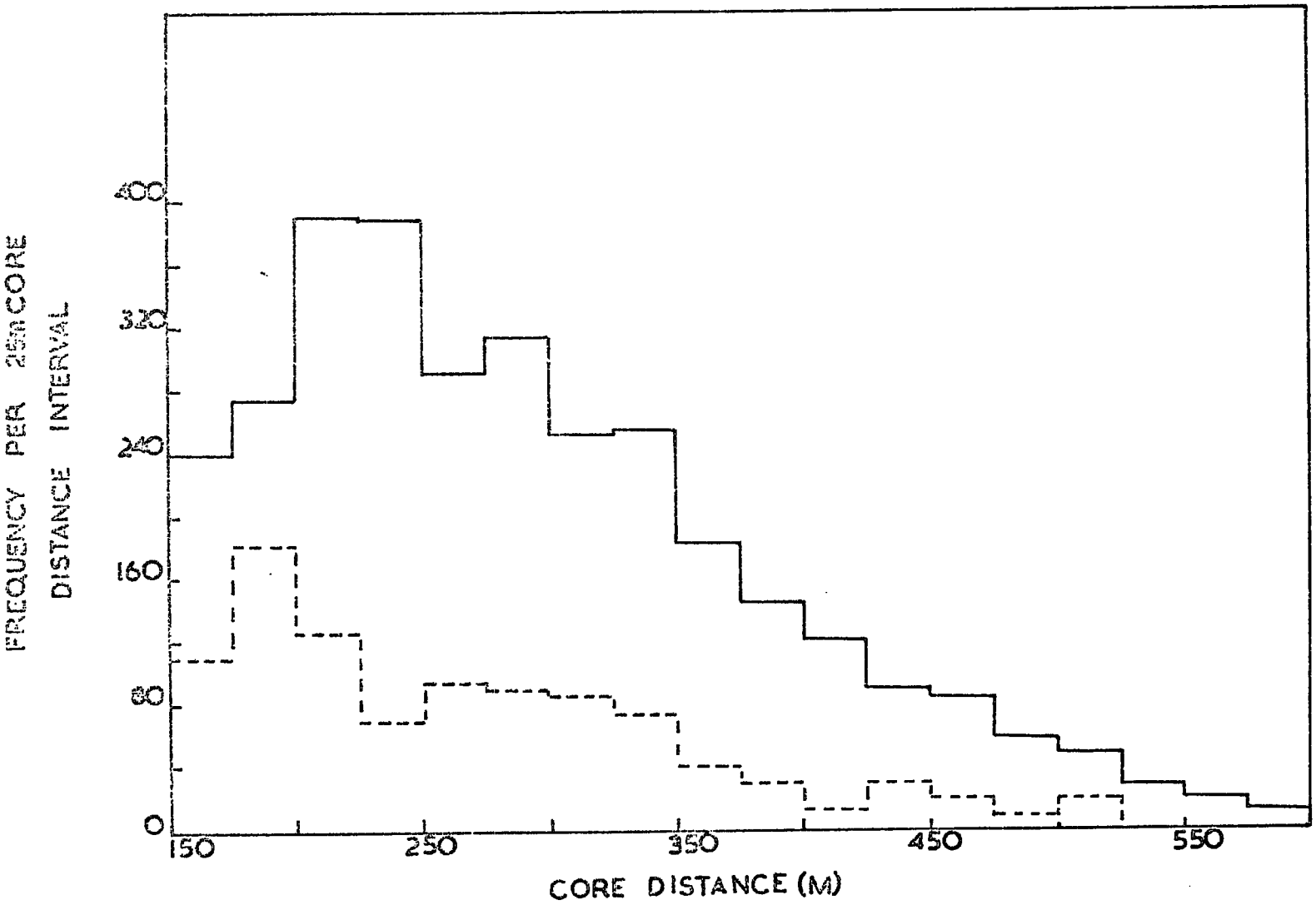
FREQUENCY PER 25m CORE
DISTANCE INTERVAL
40
32
24
16
8
0
150
250
350
450
550
CORE DISTANCE (M)

Figs. 4.4 and 4.5 show the distribution of acceptable events in 25m. intervals of core distance, and also the ratio of the numbers of multiple events to single events. It may be observed that the relative number of events below 200m. core distance falls sharply, while the ratio of multiple/single is still rising. This effect is caused by the density of particles in the spectrograph becoming so high that the muon tracks are obscured and it appears (section 4.2) that the extra shielding used in the Mk. II instrument has alleviated the problem. The effects of this alteration in operating conditions are treated fully later.

4.1.5 The Charge Ratio of Muons in EAS

The charge ratio of muons recorded by the spectrograph has been investigated as a function of momentum (p) and core distance (r) and the result is shown in Table 4.1. There is no significant deviation from a figure of unity for the regions of core distance and momentum considered. A knowledge of the overall charge ratio of all muons is important for use in geomagnetic calculations (Chapter 6). The charge ratio at large (p x r) products may also be expected to reflect the nature of the secondaries produced in the initial interactions of the primary particle, particularly if a large proportion of the secondaries are charged (predominantly positive) kaons. This has been considered by Orford (1968), and no significant conclusions about the $k/\pi$ ratio at production can be drawn from the present sample, which is approximately twice as large as that available earlier.

4.1.6 The Distribution of Arrival Directions

4.1.6 (i) Introduction

A major aim of many EAS experiments has been the search for possible anisotropies in celestial arrival directions, because of their astrophysical implications. It is usually necessary with events of high primary energy to collect data over periods of years in order to obtain a sufficiently large data sample to allow subdivision into small angular intervals, and it is particularly important to investigate any experimental bias which may lead to apparent anisotropies. The aim of the present work was to investigate

Figure 4.5 The ratio of the number of muons contained in "multiple" muon events to "single" muon events in 25m. bins of core distance.

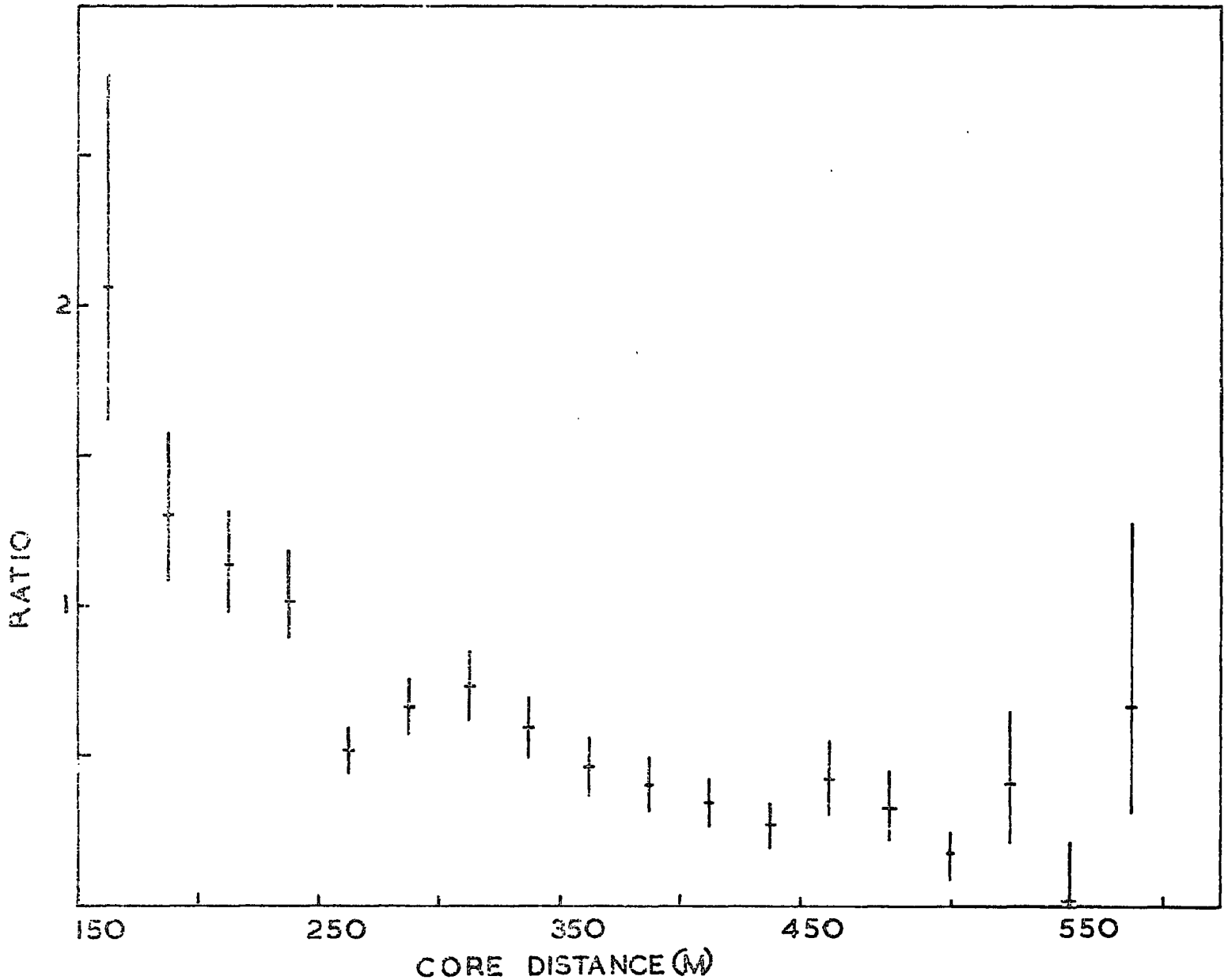
RATIO
2
1
150
250
350
450
550
CORE DISTANCE (M)

TABLE 4.1

| r metres / $\Delta\psi$ deg. | 200 | | 300 | | 380 | | 520 | | TOTAL | |
|---|---|---|---|---|---|---|---|---|---|---|
| | $N^+$ | $N^-$ | $N^+$ | $N^-$ | $N^+$ | $N^-$ | $N^+$ | $N^-$ | $N^+$ | $N^-$ |
| 0 - 0.36 | 24.5 | 22 | 19.5 | 10 | 5 | 5 | 3 | 2 | 52 | 39 |
| 0.36 - 0.72 | 41 | 33 | 20 | 20.5 | 7 | 8 | 1 | 2 | 69 | 63.5 |
| 0.72 - 1.42 | 83 | 85 | 51 | 49.5 | 18 | 16.5 | 8 | 7 | 160 | 158 |
| 1.42 - 2.62 | 149.5 | 98 | 80.5 | 95 | 41 | 40.5 | 20 | 20 | 291 | 253.5 |
| 2.62 - 4.26 | 107.5 | 128.5 | 114 | 127 | 54 | 37 | 26 | 20 | 301.5 | 312.5 |
| 4.26 - 6.33 | 83 | 106.5 | 78 | 102 | 52 | 49 | 27 | 24 | 240 | 281.5 |
| 6.33 - 16.0 | 168.5 | 157 | 165 | 159 | 109 | 98 | 51 | 50 | 493.5 | 464 |
| Total | 2 zero deflection 1289 | | 5 zero deflection 1096 | | 1 zero deflection 541 | | 261 | | 1607 | 1572 |
| Charge Ratio | $1.04 \pm 0.08$ | | $0.94 \pm 0.08$ | | $1.13 \pm 0.14$ | | $1.09 \pm 0.19$ | | $1.02 \pm 0.05$ | |

the distribution in celestial angle of arrival of muon-containing showers, as recorded in the spectrograph, with a view to subdivision by muon momentum and core distance. This immediately causes a problem of classification in the case of "multiple muon" events, and for the results presented here, only those events containing a single acceptable muon have been included. This causes some 50% of the total data to be lost, and further investigations of the philosophy of classification is warranted.

4.1.6 (ii) The Distribution of Events in Zenith and Azimuth

The distributions of the arrival directions of showers selected using the "single" muon criterion have been inspected for any dependance on zenith angle ( $\theta$) and azimuth angle ( $\phi$). A fairly strong dependence on $\theta$ is expected from the form of the spectrograph acceptance, and thedistribution in $\theta$ of the showers yielding "single" muons is markedly different (at large $\theta$) from a typical sample from the 500m. array alone (D.R. Pickersgill, private communication). However, the value of right ascension ascribed to a particular value of $(\theta,\phi)$ depends only weakly on $\theta$ for the ranges of $\theta$ and $\phi$ within which the majority of the events fall, and the check on the $\theta$ distribution shows that the general form is similar to that predicted by the acceptance function of both the spectrograph and the main array. Hence it was concluded that any bias in $\theta$ for these showers was accountable in terms of known functions, and that the overall effect would be slight. The dependence of the acceptance on $\phi$ is more complex, and varies with muon momentum. An approximation to the overall effect, using the acceptance data of Orford (1968) for deflections of $0^{\circ}$ and $16^{\circ}$, gives a form similar to the observed distribution. It is therefore assumed that the $\phi$ distribution is also explicable in terms of a fairly well-known function, so that any variation in right ascension can be traced reasonably simply to the component parts (i.e. $\theta$, $\phi$ and sidereal time).

4.1.6 (iii) Check of the Spectrograph On-Time

Any systematic sidereal variation of sensitive time could cause spurious variations in the form of the distribution in right ascension of the shower sample. All the film records used in the Mk.I spectrograph data sample have

been scanned, and three particulars noted:

(i) the time of commencement and termination of the film,

(ii) whether there were any interruptions during the course of the film, and for how long these lasted,

(iii) whether full shower analyses were available for the duration of the film.

These data were then converted into a sidereal on-time plot (see Fig. 4.6), corresponding to the time for which the spectrograph was sensitive in each interval ($1/100^{ths}$) of the sidereal day. The r.m.s variation is 2.3%, so that any effect of this sensitive time will be very small indeed.

4.1.6 (iv) The Determination of Celestial Arrival Directions

The relations connecting $\theta$, $\phi$ and sidereal time to right ascension and declination are given by Suri (1966). In view of the differences between values obtained from the shower analysis for $(\theta,\phi)$ corrected and $(\theta, \phi)$ uncorrected explained in Chapter 6, the values of right ascension derived from both values of $(\theta,\phi)$ have been investigated. Little change has been found, due almost entirely to the large sorting intervals necessary ($40^{o}$ bins in right ascension) in the present analysis.

4.1.6 (v) Results

The distribution in right ascension for all the showers containing single recorded muons is almost completely flat. Similarly, a check on the declination distribution showed this to be similar to that found by the Leeds group for all showers. However, it was decided to subdivide the showers according to muon momentum and core distance, since the (pxr) product of the muon represents a further shower characteristic - a measure of height of origin of the muon - not included in the other analyses. In particular, high (pxr) products may relate to very early muon production, and therefore may provide an indication of the mass of the primary particles. Accordingly, the data were divided into core distances and momentum intervals, and the data from the (pxr) interval with the greatest "anisotropy" is shown in fig. 4.2. These data are from the $250 < r < 350$ m., muon momentum $\geq 11$ GeV/c interval. Also shown in fig. 4.7 are the distributions in $\phi$ (with the form expected from the spectrograph acceptance shown by the broken line) and

Figure 4.6 The distribution in on-time of the Mk. I Spectrograph as a function of the sidereal day.

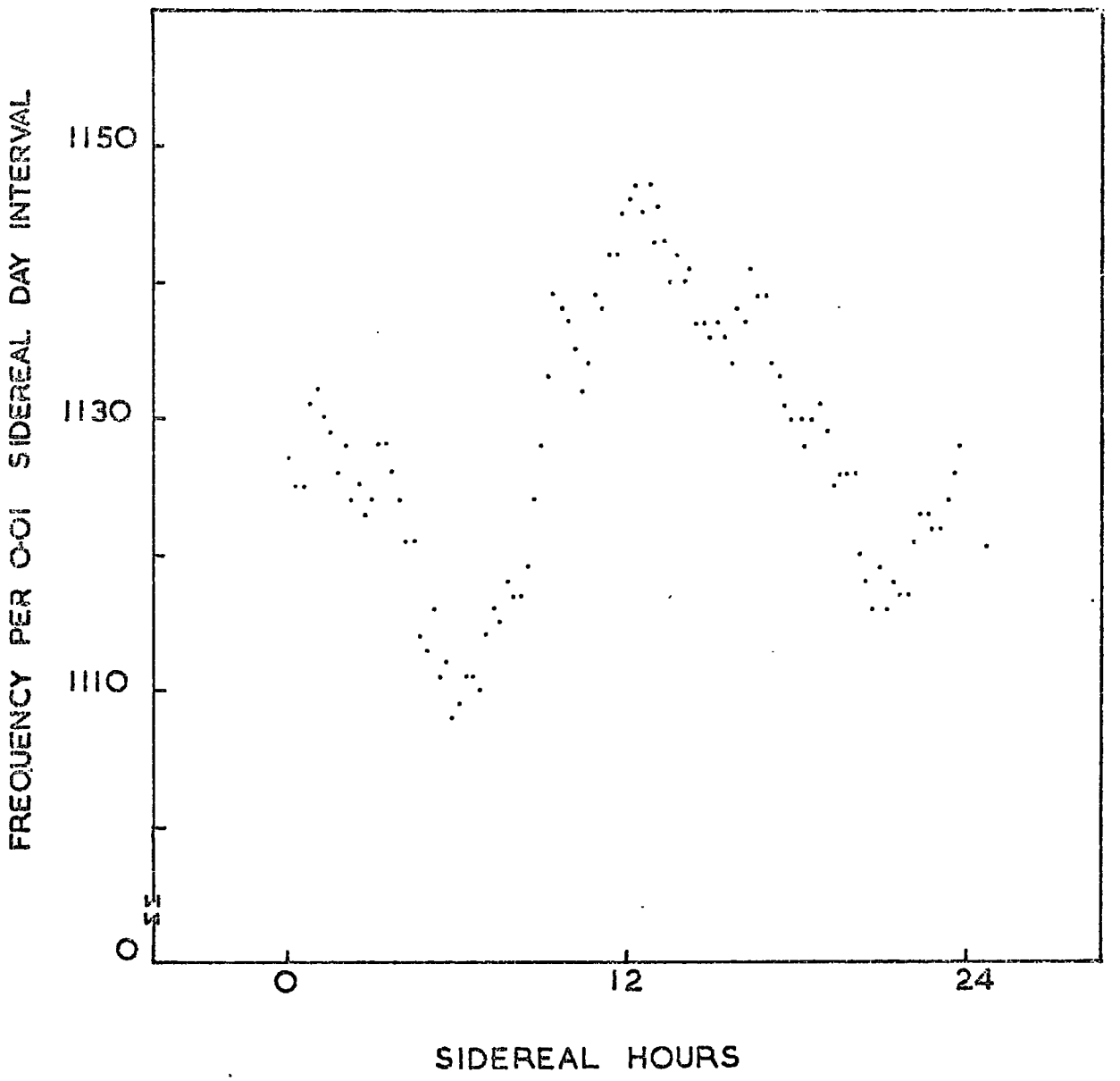
FREQUENCY PER 0·01 SIDEREAL DAY INTERVAL
1150
1130
1110
0
0
12
24
SIDEREAL HOURS

Figure 4.7 The distribution of single muon events possessing angular deflections of less than $1.42^{\circ}$, in the core distance interval 250-350m.

(i) as a function of sidereal time

(ii) as a function of $\phi$, the azimuth angle (the spectrograph acceptance is shown dotted)

(iii) as a function of right ascension.

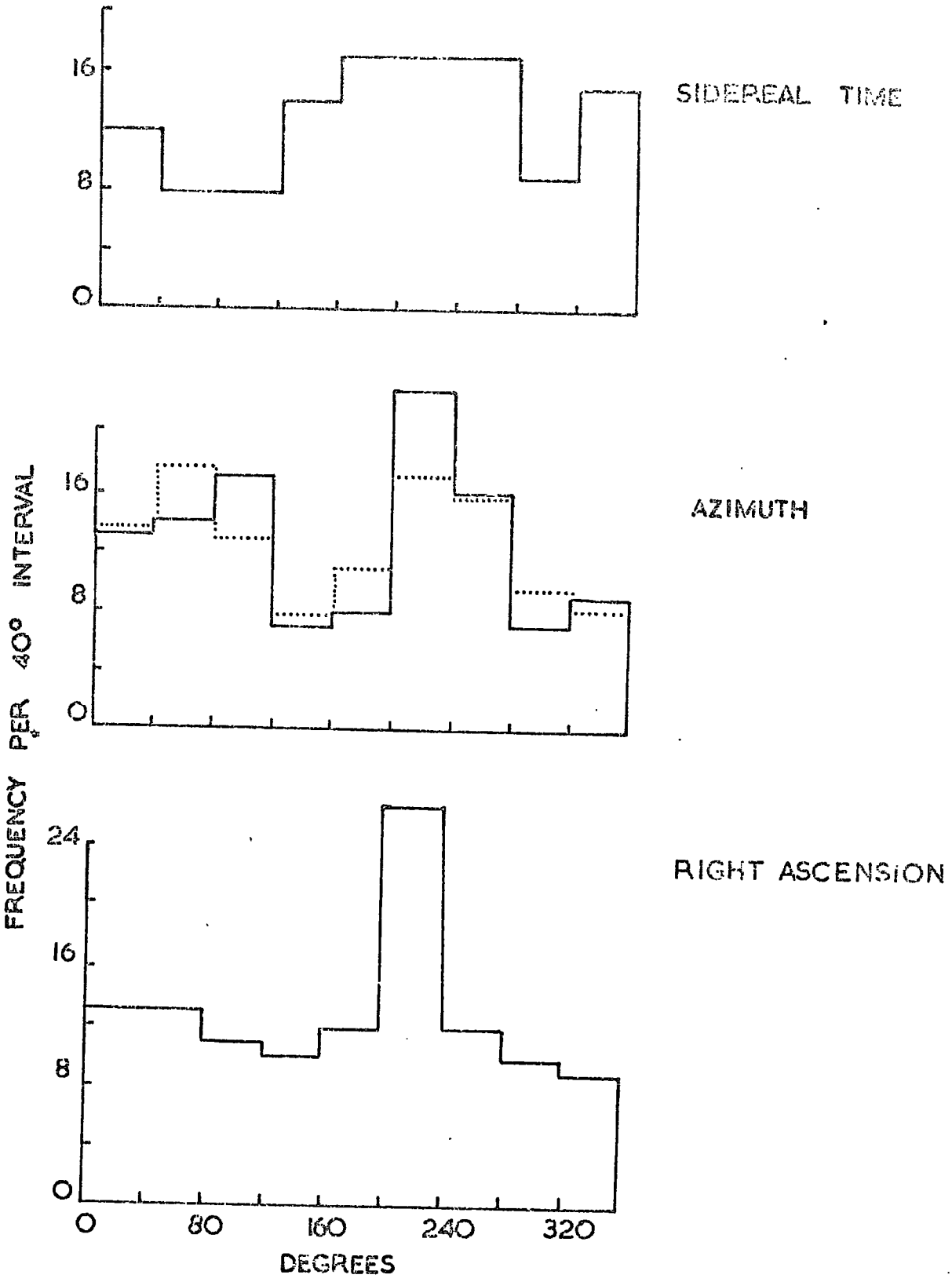
16
8
0
SIDEREAL TIME
16
8
0
AZIMUTH
FREQUENCY PER 40° INTERVAL
24
16
8
0
RIGHT ASCENSION
0
80
160
240
320
DEGREES

the distribution in sidereal arrival time (in degrees). It may be seen that, while the peak at 200 - 240° right ascension has a probability (Poissonian) of occurance of about 0.001, there is a upward trend in $\emptyset$ over and above the expected level, and an upward trend in sidereal time. It is not claimed that the very limited statistics shown here could support a hypothesis of a true anisotropy, but it is suggested that the Mk. II data sample should be inspected carefully for similar trends in this sorting interval. Any experimental biases in this sample will be far less important, as not only is the Mk. II instrument of far higher precision and reliability, but the 500m. array, supported by the 150 m. array, will yield more accurate density sampling and better overall shower analyses. However, it is to be expected that at least three years' running time will be required before definite conclusions can be drawn. It is noted that the Leeds group (Lapikens et al (1970)) find no significant anisotropies in right ascension for all the showers triggering the 500m. array.

## 4.2 Results from the Mk. II Spectrograph

### 4.2.1 Introduction

The improved instrument was put into routine operation on August 1st, 1970, and the present data sample covers some eight months running. The aim in the analysis of these results is twofold - firstly, to derive a noise estimate, hence a value for the momentum resolution, for comparision with the earlier value, and secondly, to use this figure in the spectral analysis of the MK.II data as a check on the momentum spectra derived from the Mk I data sample.

### 4.2.2 The Overall Track Location Error

Four methods of obtaining the track location error were described in Chapter 2, in connection with the Mk. I spectrograph, of these, the zero field run was discounted, because of the difficulty in removing the residual magnetisation, and also in allowing correctly for the relatively large amount of Coulomb scattering. The method of repeated simulation is impossible, because the high angular accuracy required of such an analogue

device means that its physical size would render it useless. The method using the lateral separation of half-tracks again requires the removal of Coulomb scattering, so that the most attractive method is that of obtaining the deflection distribution of "hole" particles, especially in view of the selection device comprising the G-M counters described in Chapter 2. The deflection distribution of acceptable "hole" events using EAS muons is shown in fig. 4.8. Within the limits of the statistics, the sample appears to be of gaussian form, with a standard deviation of $0.16^{o} \pm 0.02^{o}$.

The distribution in deflection for unassociated cosmic ray muons passing through the spectrograph hole is also shown in fig. 4.8. The data for this was obtained by placing a further tray of Geiger-Muller counters above the spectrograph and obtaining 3-fold coincidences with the "hole" counters. The distribution has a standard deviation of $0.24^{o}$, and is broader than that for EAS muons because of the lower mean energy, and hence greater mean scattering angle, of unassociated muons. The relation yielding the r.m.s scattering angle is given by Eyges (1948):

$$\sigma^2 = \frac{E\,s}{2p(p-qs)} \qquad \ldots\ldots\ldots\ 4.2$$

where $E = 21.10^{6}$eV, $s$ is the thickness of the material in radiation lengths, p the momentum in GeV/c and q the energy loss in eV/radiation length.

For the small amount of matter in the flash tube trays, the energy loss is small, and the equation 4.2 reduces to the form $\sigma = K/p$. If the total width of the deflection distribution $\sigma_T$ is composed of a "location" term, $\sigma_L$, and a scattering term, $\sigma_p$, then

$$\sigma_T^2 = \sigma_L^2 + \sigma_p^2 \qquad \ldots\ldots\ldots\ 4.3$$

Now, the value of $\sigma_T$ has been determined for two mean momenta, ~5 GeV/c for EAS muons, and ~1 GeV/c for unassociated muons (Earnshaw (1968)). Hence

$$\sigma_T^2 = \sigma_L^2 + \left(\frac{K}{p}\right)^2 \qquad \ldots\ldots\ldots\ 4.4$$

which yields two equations with K and $\sigma_L$ unknown. Hence the value of $\sigma_L$, the overall track location error, with Coulomb scattering in the trays removed, is $0.15^{o} \pm 0.01^{o}$.

Figure 4.8 The distribution in angular deviation of muons traversing the central hole of the Mk. II spectrograph (i.e. the overall noise distribution)

(i) for muons in EAS events

(ii) for unassociated cosmic ray muons.

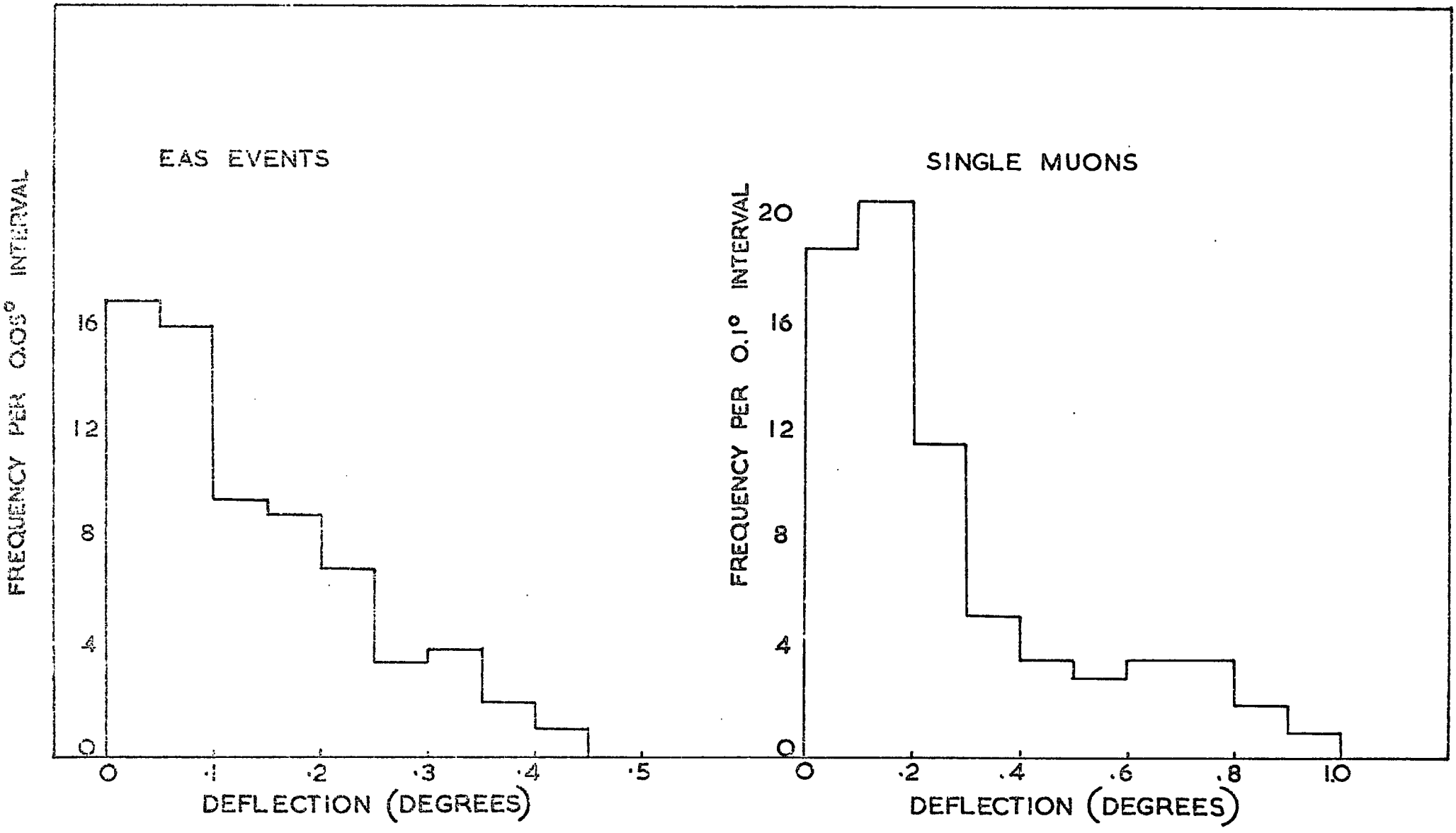
EAS EVENTS
FREQUENCY PER 0.05° INTERVAL
0
4
8
12
16
0
·1
·2
·3
·4
·5
DEFLECTION (DEGREES)
SINGLE MUONS
FREQUENCY PER 0.1° INTERVAL
0
4
8
12
16
20
0
·2
·4
·6
·8
1.0
DEFLECTION (DEGREES)

However, it must be stressed that the overall noise figure used in the spectral derivation must be the original one of $0.16^{o}$, since no allowance is is made for scattering in the trays in the above treatment. The above calculation shows that, for particles of momenta above 5 GeV/c, the effect on the angular deflection due to scattering in the trays is negligible compared with the overall location noise.

4.2.3 Checks on Muon Data

All events were analysed using the track fitting programme described in Chapter 3; the classification of events was much simplified by the output of the programme, particularly in the case of uncorrelated upper and lower half-tracks. The enumeration of all tracks was checked, after evidence of some initial poor overlay-print location was found (Chapter 2) - in bad cases the error was often apparent on the programme output. Any problem events (crossing close tracks, spurious tubes and tubes discharge by knock-on electrons) were referred to a simple photographically-made simulator, and it became apparent that, once a fault was shown up by the track-fitting programme, it could be readily identified and remedied in most cases, on the simulator.

4.2.4 Comparison of the Results of the Mk.I and Mk.II Instruments.

In view of the limited number of muons in the Mk.II sample ($\sim$450 in the range of core distance $150 < r < 350$ m.), the derivation of a momentum spectrum is not reliable, and it is preferable to produce a predicted angular deflection spectrum for 450 events in the Mk. II spectrograph from the Mk. I momentum spectra, and to compare this with the experimental data derived from the new instrument. The method consists of using that part of the spectral analysis programme which converts a momentum spectrum into an angular deflection spectrum, taking account of the slightly modified acceptance function and the new noise figure.

Fig. 4.9 shows the results obtained by converting a Mk I $150 < r < 350$ m. momentum spectrum into a predicted deflection distribution for the Mk. II spectrograph. The data have been normalised to the total number in the Mk.II sample, and corrected for core distance distribution in 25 metre intervals (using the

Figure 4.9 The deflection spectrum obtained from the Mk. II spectrograph for events with core distance between 150 and 350m., ~~compared with that predicted from the~~ data observed with the Mk. I spectrograph.

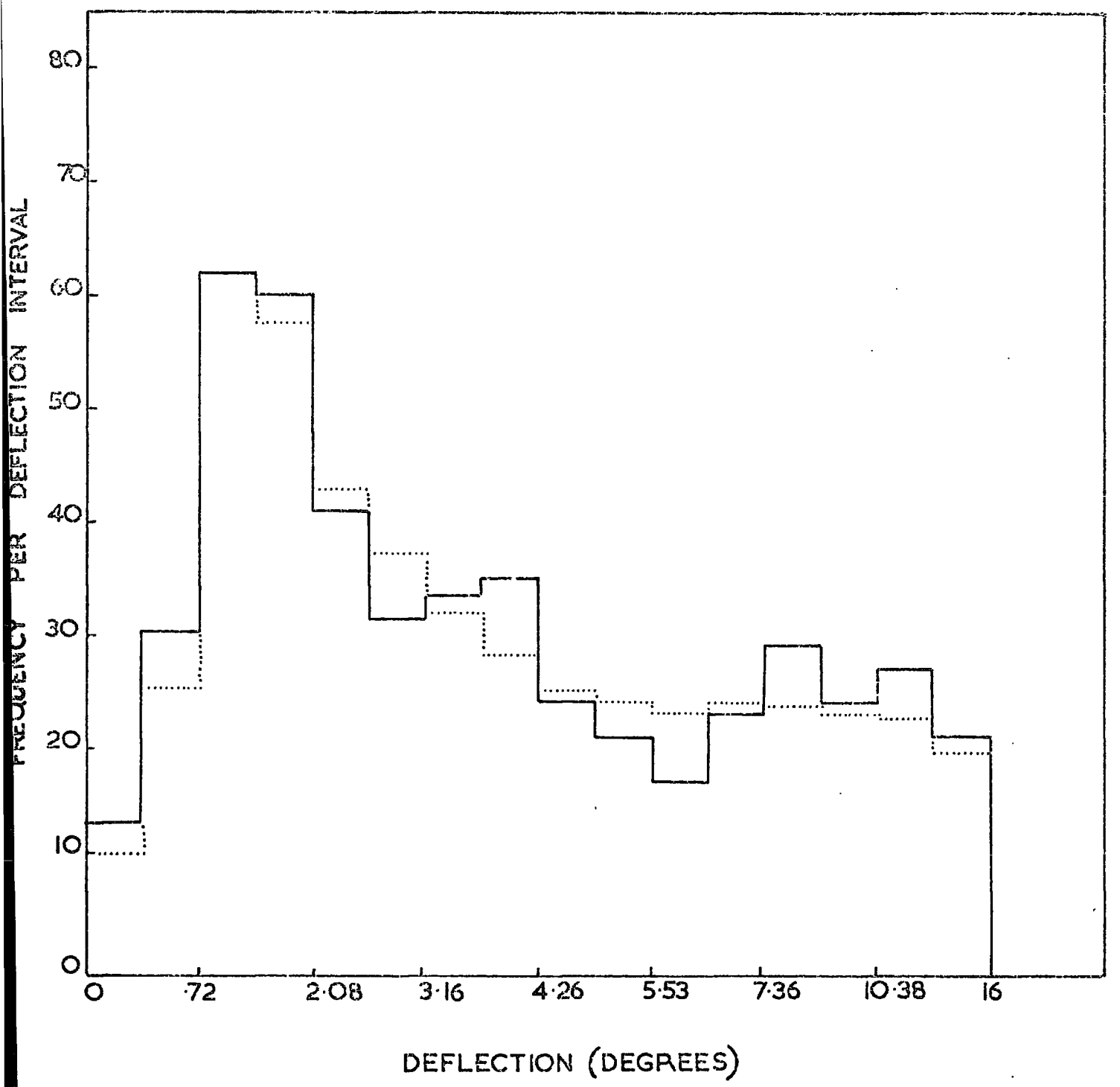
FREQUENCY PER DEFLECTION INTERVAL
80
70
60
50
40
30
20
10
0
0
·72
2·08
3·16
4·26
5·53
7·36
10·38
16
DEFLECTION (DEGREES)

Figure 4.10 The distribution of acceptable muons in the Mk. II spectrograph as a function of core distance. The (normalised) distribution for the Mk. I spectrograph is shown by the dotted line.

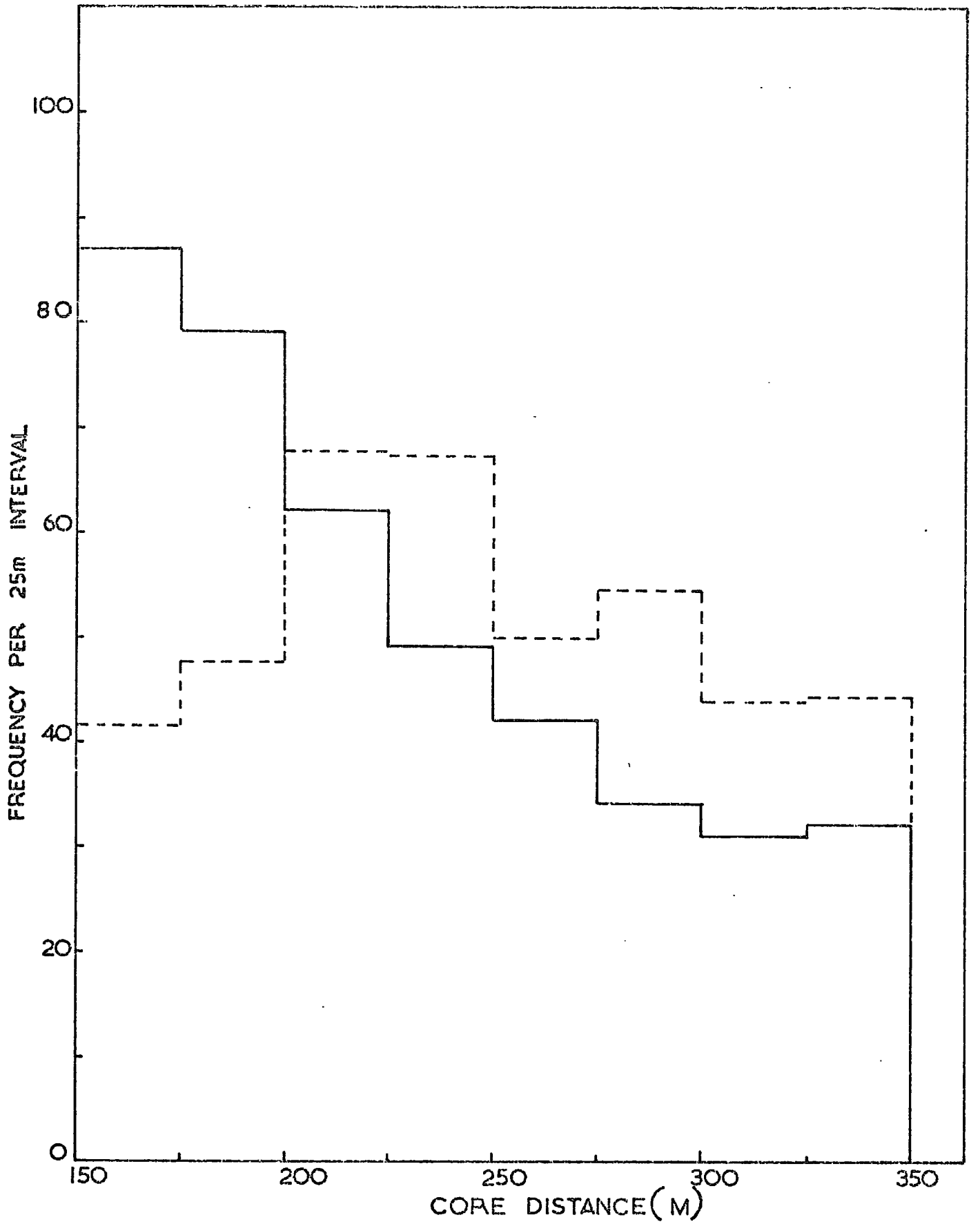
100
80
60
40
20
0
FREQUENCY PER 25m INTERVAL
150
200
250
300
350
CORE DISTANCE (M)

data of fig. 4.10). Good agreement may be observed, but it is important to note that the Mk. II sample contains some fairly dense showers which could not have been resolved using the earlier instrument. The greatest effect of these is on the highest momentum interval, as shown in the following table.

$N_\mu (\Delta\psi \leq 0.36^\circ)$ $150 < r < 250$ m.

| Mk. I Size / Core distance | $10^6 - 1.1\ 10^7$ | $1.1 - 1.8\ 10^7$ | $1.8 - 2.8\ 10^7$ | $2.8\ 10^7 - 10^8$ | Total |
|---|---|---|---|---|---|
| 150 - 175m | 4 | 3 | 3 | 1 | 11 |
| 175 - 200m | 5 | 9 | 3 | 1 | 18 |
| 200 - 225m | 2.5 | 5 | 3 | 2 | 12.5 |
| 225 - 250m | 2 | 2 | 1 | 2 | 7 |
| Total | 13.5 | 19 | 10 | 6 | 48.5 |
| **Mk. II** | | | | | |
| 150 -175m | 1 | 0 | 5 | 1 | 7 |
| 175 - 200m | 0 | 1 | 0 | 1 | 2 |
| 200 - 225m | 0 | 0 | 1 | 0 | 1 |
| 225 - 250m | 0 | 1 | 0 | 0 | 1 |
| Total | 1 | 2 | 6 | 2 | 11 |

For the Mk. I sample of "fast" events (ie. $p \gtrsim 50$ GeV/c), the value of $\bar{N} = 1.8\ 10^7$, and $\bar{r} = 196$ metre, while for the Mk. II sample $\bar{N} = 2.2\ 10^7$ and $\bar{r} = 178$ metres. Taking these figures into account, the variation in apparent muon density caused by the above changes in N and r is almost a factor of two. This means that the Mk. II sample is yielding almost twice as many high energy muons in this core distance range, simply due to the changes in the mean shower size and core distance for analysable events (the increase in number of energetic muons arises because of the steepness of the 50 GeV/c lateral distribution curve). Unfortunately, the very small number of events in the $250 < r < 350$ m. region ($\sim 150$, with two

$\Delta\psi \leq 0.36^{o}$ events) means that no firm conclusions can be drawn at present about the accuracy of the Mk. I spectra in this region of specific interest.

4.3 Conclusions.

No firm results concerning the accuracy of the original Mk. I spectra can yet be given. However, the Mk. II instrument has been shown to be capable of producing high accuracy, and to be less prone to saturation by virtue of extra shielding and improved track resolution. The inclusion of a further six to nine months data in the sample should permit fairly detailed conclusions to be drawn on the validity of the earlier data, but the points raised in the previous section should be investigated further. Special care must be taken in the core distance distribution, particularly for high energy events, and this will be made difficult by the changes to the analysis programme currently being undertaken by Leeds University. The showers comprising Mk. I data were all analysed using a single exponent structure function, and this has now been changed in favour of a two-parameter fit. The overall effect of this on the core distance ascribed to a particular shower is not clear, but any systematic difference from the original values could cause great difficulty in interpretation of the muon spectra. Likewise, the change from N, via $E_{100}$ to $\rho_{500}$ as a measure of shower size or primary energy must be investigated in relation to the recorded muon content of the shower, and re-analysis of much of the EAS data for the period 1965-9 may be necessary before completely satisfactory comparisons can be made.

# CHAPTER FIVE

# AIR SHOWER MODELS

## 5.1. Introduction

The major role of those extensive air shower experiments presently in progress is one of finding the maximum amount of information possible about the nature and energy of the primary particle together with details of its interaction with air nuclei. The development of an air shower in the atmosphere is very complex, and many different mechanisms operate at all stages of the shower. However, it is necessary to employ some form of model of the shower, so that measurements taken at the observation level may be related to those early stages of shower development which are important in muon studies. The greatest limitation of such models is the very large number of possibly relevant parameters, and the almost total lack of direct experimental evidence on cross-sections, transverse momentum distributions and on the very nature of ultra-high energy interactions. Many of the appropriate parameter values and interaction models must be extrapolated over several orders of magnitude in energy from the available accelerator data, but these values represent the only possible starting point for the necessary calcualtions. With the advent of larger and faster computers, it is becoming feasible to take account of more parameters, and, perhaps more important, to investigate the consequence of small variations of several parameters upon particular measurable quantities of EAS.

There are two main categories into which EAS model calculations may be divided; firstly, the analytic approach, which reduces the problem to sets of complex equations which may be either solved or evaluated numerically in the so called "step-by-step" method and secondly, the Monte-Carlo approach, as employed by Bradt and Rappaport (1967). This latter method utilises a random-number method to approximate the statistical nature of the processes occuring during development of the shower. There is no doubt that the latter method gives a clearer picture of the "life" of each individual particle,

but when the problem to be investigated requires data on very large numbers of individual particles (e.g. the momentum spectra of muons), there seems to be very little to choose between the two methods in terms of overall accuracy. The main drawback with a pure Monte-Carlo calculation is the time taken to simulate fully each shower. Further investigation may show where a compromise between the two methods, including the best features of both approaches, may be obtained. While the step-by-step method appears to cover the overall features of muon spectra adequately, an improved method allowing for statistical fluctuations in production may yield more information on the distribution of high energy muons in samples of limited size, which may not be obvious in the analytic method. Further, a clear picture of the longitudinal development of the muon component and its associated fluctuations (and the dependence of the fluctuations on varying parameter values) would be of great value in the studies of the height of origin of muons to be described in Chapter 6.

## 5.2. Description of the Models

### 5.2.1 Introduction

A full description of the models employed is given by Orford (1968) and Orford and Turver (1968), but a summary is given here particularly on the aspects which will receive further comment. The present model calculations are biassed strongly towards the muon component of EAS, in particular the distributions in momentum of muons distant from the shower core.

### 5.2.2 The "900" Series of Models

These models were originally designed to give a rigorous mathematical solution to the equations representing the development of showers of primary energy $10^{17}$eV from 50 KM to 10 KM above sea level. This region covers the most important production levels of muons of energy in excess of 100 GeV occurring at core distances of greater than 100m. and termination of this rigorous treatment at 10 KM above sea level introduces a very small error in the predicted densities of such high energy muons

(Orford (1968)). The method employed is one of successive collisions, similar to that used extensively in the simulation of electromagnetic cascades. The interaction model assumed is one in which secondary particles are produced with energies distributed according to the suggestion of Cocconi, Koerster and Perkins (1961), and no isobar or strange particle formation is included. The results from this model may be added directly to those derived by the method described in the following section, to build up the total predicted density of muons at each momentum and core distance.

5.2.3 The "1000" Series of Models

These models cover the lower region of the atmosphere below an altitude of 10 KM and employ a method of fixed interaction heights (ie. the separation between interactions of a particle is equal to its interaction length). This method allows the overall longitudinal development of the shower to be calculated first, and then the appropriate lateral spread due to the chosen transverse momentum distribution is applied to the particles originating from each fixed height. This calculation has the advantage of simplicity, and is also relatively quick to perform. The results from this part of the overall model alone give a sufficiently accurate representation of the shower for muon momenta up to about 30 GeV/c (except for very large core distances), and have so been used extensively in the work to be described in Chapter 6. An approximation to the number of electrons at a given observation level has also been derived from this model.

5.3. Sensitivity of the Model Predictions to Basic Parameters

5.3.1 Introduction

The models described in the previous section may be expected to predict the overall shape of muon momentum spectra well for core distances greater than 100 metres. However, the integral muon densities greater than 1 GeV/c predicted for core distances 100-500m. for a primary proton and a conservative interaction model are considerably (about 100%) lower than that obtained from the lateral distributions measured (Orford and Turver (1969). For this

reason, a series of calculations to check the effect of various basic parameters was undertaken, in an attempt to resolve the apparent discrepancy. The primary particle was assumed to be a proton of energy $2 \times 10^{17}$eV in all cases.

5.3.2 The Effect of Pion and Proton Interaction Lenghts

The chosen pion interaction length for the models described in section 5.2 was 120 gm $cm^{-2}$, whereas some workers favour a figure of 100 gm $cm^{-2}$ (Hillas (1971)). A check on the effect of a change of some 20% in this value yielded changes of less than 10% in the integral muon density at the core distances of interest here, so that small variations in the value chosen for this parameter have little overall effect. A similar check has been carried out on the effect of changing the proton interaction length from its assumed value of 80 gm $cm^{-2}$ to 75 gm $cm^{-2}$ (as used e.g. by Grieder (1969)) The effect on the muon densities at 300m. from the core was between 2-3% and it is concluded from these checks that the observed discrepancies between models and data are unlikely to be caused by incorrect assumptions of the value of either pion or proton interaction lengths.

5.3.3 The Effect of the Inelasticity of Nucleon-Nucleon Collisions

Small changes ($\sim \pm$ 10%) in the value of the n-n inelasticity about a preferred value of 0.5 in the present model have a fairly marked effect on the muon density predicted with the present model (e.g. the change from 0.5 to 0.44 gives a change of between 30-40% in the muon density above 1 GeV/c at 300m. from the core). It is very difficult to choose a "best" value for this parameter, since the data available cover the range 0.2 to 0.9, with a mean of 0.54 (Winn et al (1965)). Further conclusions about this value must await precise accelerator data, which should soon be available for energies greater than 50 GeV.

5.3.4 The Energy Distribution of Particles produced in Interactions.

The models described in section 5.2 assume that the pions produced in high energy nucleon interactions have equal probabilities of moving forward or backwards in the centre-of-mass system, and have energies represented by two exponential distributions in the laboratory system. Because of the

Figure 5.1 Differential momentum spectra at core distances of 300m in showers of primary energy $2.10^8$GeV when the primary particle is a proton.

(1) Spectrum from the model of Orford (1968)

(2) As above, but with the backward cone contribution in $\pi$-n collisions set to zero.

(3) 900 + 1000 series spectrum with the latest form of $\pi$-n backward cone.

(4) Scaled spectrum from A.M. Hillas model E.

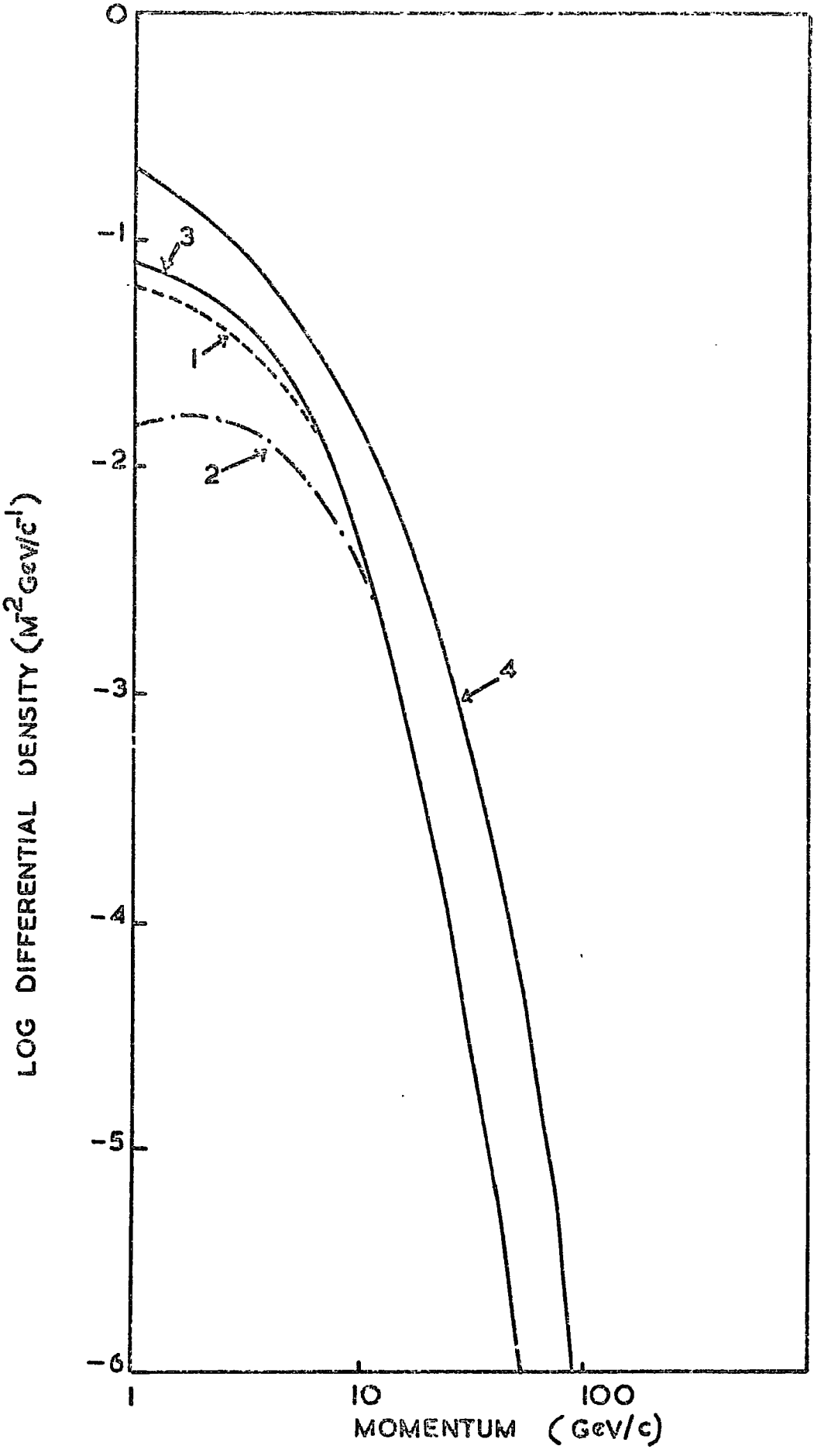
0
-1
-2
-3
-4
-5
-6
1
10
100
MOMENTUM (GeV/c)
LOG DIFFERENTIAL DENSITY (M²GeV/c⁻¹)
1
2
3
4

form of the relativistic transformation, the pions in the "forward" cone (ie. those moving forward in the C.M. system) have, in general, a far higher mean energy than those in the backward core. The form of the energy distribution in the laboratory system is assumed to be

$$f(E)\,dE \propto \left\{ \frac{e}{T}^{-E/T} + \frac{e}{G}^{-E/G} \right\} dE \quad \ldots\ldots \quad 5.1$$

following Cocconi, Koester and Perkins (1962). Here T and G are the mean energies of the pions in the forward and backward cones respectively. Many earlier models have either ignored the backward cone pions, or treated them in an approximate fashion, and in order to assess the relative importance of the backward core pions, a calculation was performed with the backward cone contribution in pion-nucleon collisions set to zero. The resulting muon momentum spectra at core distances of 300m. are shown in figure 5.1, and it is evident that there is a large effect below muon momentum of 5 GeV/c. A more detailed study of the effect of different forms of backward cone energy distributions was undertaken.

The form used by Orford (1968) for the models described in section 5.2 was an approximation only, providing a value of G dependent on $E_p$. The calculation was improved to take account of the correct kinematical consideration of the $\pi^-$ - n interaction using a centre-of-mass system (see e.g. Hayakawa 1969). This give the relation of mean backward cone energy against energy radiated as shown in fig. 5.2 where the approximation used by Orford (1968) is also shown.

From a comparison with the results of the Leeds group (Dr. A.M. Hillas, private communication), it became apparent that the use of a centre-of-mass system in $\pi^-$ n collisions was inaccurate if the forward and backward cones were supposed to contain equal numbers of particles. The use of a centre-of-symmetry system in which the incident pion is considered to be accompanied by a virtual nucleon (as first suggested by Salzman and Salzman (1960)) overcomes this objection, and results in a form of G(E) shown also in fig. 5.2. This function is very similar in shape to that given by

Figure 5.2 The variation of mean backward cone energy with radiated energy in $\pi^-$ n collisions. The upper solid curve is due to Hillas (private communication), the lower from kinematical considerations employing a centre - of - mass system. The broken line is the approximation used by Orford (1968).

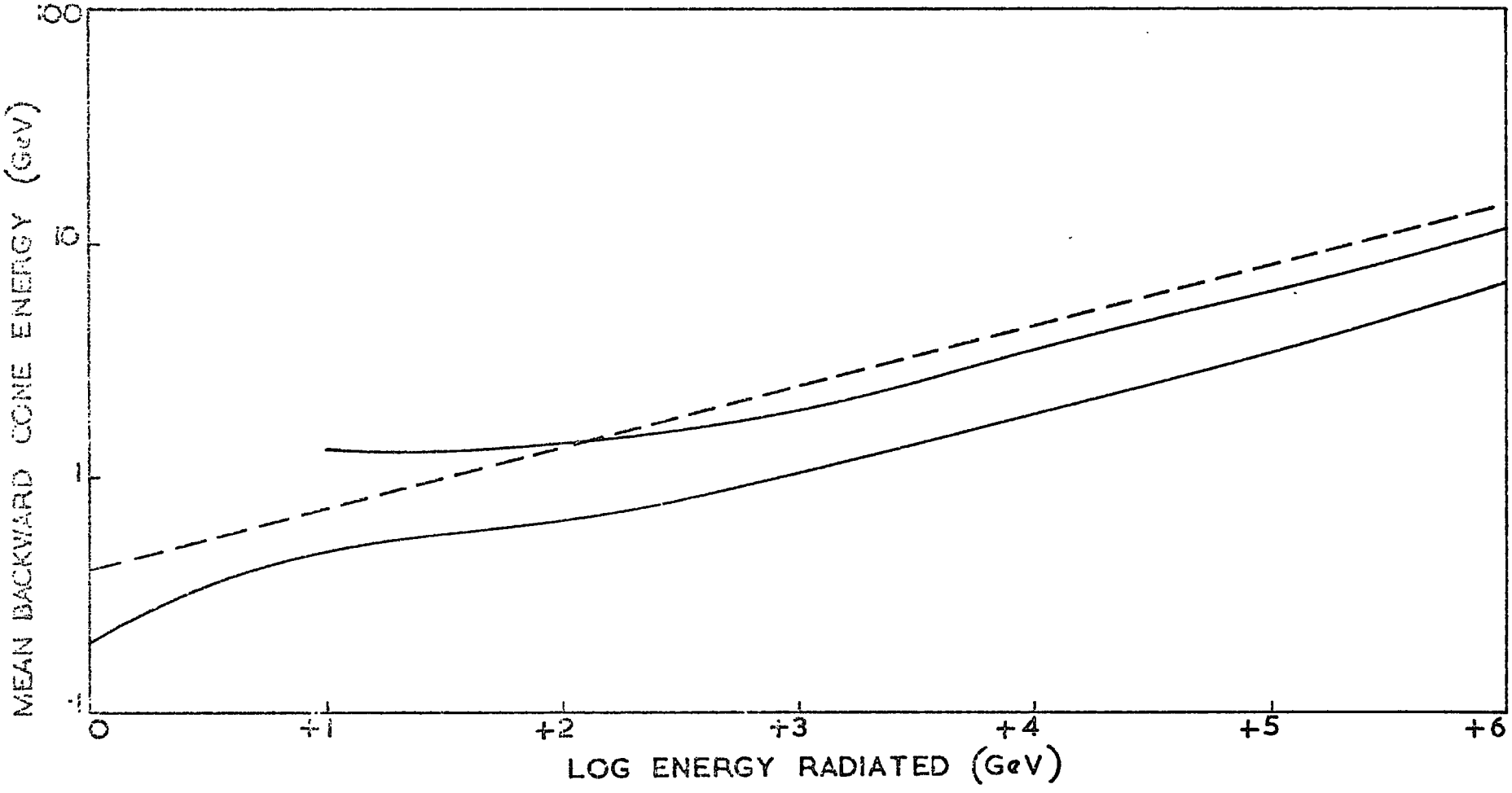
100
50
0
+1
+2
+3
+4
+5
+6
MEAN BACKWARD CONE ENERGY (GeV)
LOG ENERGY RADIATED (GeV)

pure kinematics in a C.M. system, but is almost a factor of two greater in magnitude at all energies. Accordingly, a simple check on the difference caused by the various forms was carred out as follows:

Firstly, the mean energy of the secondaries $\bar{E}$ is found

$$\bar{E} = \frac{\int E\, f(E)\, dE}{\int f(E)\, dE} \qquad 5.2$$

where $f(E)$ is given in equation 5.1

hence $$E_{rad} = n_s \bar{E} = \frac{n_s}{2} (T + G) \qquad 5.3$$

The value of G is deduced from kinematic relations in the C.M. system, adjusted to fit the relation used by Hillas, and the energy balanced by equation 5.3. The results of this calculation are also shown in fig 5.1. The general trend arising from the inclusion of the improvements in the values of $G(E)$ is to bring the values of $A_\mu (>1\text{GeV})$ closer to the experimentally measured points, and it appears that the relation for G used by Hillas (1971) gives results which fit fairly well over this energy range.

5.3.5 Summary

The series of checks described above indicated that the most likely cause of discrepancies between model predictions and experimental data lies in the treatment of the energy distribution of secondary particles (the effect of many other parameters, such as the shape of the transverse momentum distribution, are treated fully by Orford (1968)). The approximations used in the early versions of the models of section 5.2 appear to cause an underestimate of the low-energy end of the muon spectrum (compared with the results of Hillas et al (1971)), and this results in a considerable underestimation of the integral muon densities at large core distances.

## 5.4. The Comparison of Model Predictions with Experimental Results

### 5.4.1 Muon Momentum Spectra at large core distances

Orford and Turver (1969) and Pickersgill (1972) describe the method used to convert a muon momentum spectrum predicted from a model into a

deflection spectrum expected in the spectrograph, and also described a form of $\chi^2$ testing against the experimental data. It is intended that this method be used to compare model predictions with the data collected from the Mk.II spectrograph, when sufficient data has been processed. This method is less prone to bias than one requiring the production of a momentum spectrum from the basic angular deflection data, and so is more desirable in terms of accuracy when attempting to define preferred model parameter values.

5.4.2 Distributions in the Height of Origin of Muons in EAS

The 1000 series models provide data on the height of production distributions for muons of known momenta at prescribed core distances (strictly, these are only accurate when the contributions from the 900 series is small: this has been estimated conservatively to be so when muon momenta are less than 30 GeV/c). The procedure adopted requires the use of some form of interpolation of energies, as the effect of energy loss means that muons of the same energy at production but originating from different heights retain different proportions of their energy at sea level. Hence the predicted sea level spectrum of muons originating from a particular height is interpolated at convenient steps from 1 to 100 GeV/c. The process is repeated for all other production heights, and the total sea level spectrum obtained. The relative contribution of each production height to the total spectrum may then be obtained. Since it is the distributions in height of origin of muons which is of interest rather than absolute numbers the effect of variations in $\Delta_\mu$ (>1 GeV) due to changes described in section 5.3 are relatively unimportant in this section. The height distributions obtained from the model have been used directly in the work to be described in Chapter 6 and also by evaluating the relation

$$\bar{H} = \frac{\int_1^{30} H(p)\, S(p)\, dp}{\int_1^{30} S(p)\, dp} \qquad 5.4$$

where H(p) is the height distribution of muons of momentum p, S(p) is the differental muon momentum spectrum, the mean production heights of muons in the momentum range 1 to 30 GeV/c have been determined. The results of this calculation are shown in fig. 5.3 where the sensitivity of the mean production height to model parameters is shown. The four lines refer to primary protons and iron nuclei, with two possible exponents in the multiplicity law for $n_s$ charged secondary particles produced in interactions at energies higher than 3000 GeV. A change in the multiplicity exponent from 0.25 to 0.50 shows a greater change in mean height than does a change in primary particle mass from A=1 to A=56. The tendency of the experimental points (from the work to be described in Chapter 6) is to favour the exponent 0.25, but the errors involved do not rule out a larger figure. An extension of this calculation to give $\bar{H}$ for energies between 1 and 100 GeV would be an improvement, but this is very difficult with the two models used here.

5.4.3 The Longitudinal Development of the Electron Component of EAS

The distribution in height of the electron component of EAS is important e.g for the prediction of the form of radio emission resulting from geomagnetic distortion of the shower front (Allan, 1971). Since the models of section 5.2 are primarily concerned with the muon component, accurate predictions on the electron-photon component have not been undertaken. However, it is important that any model should predict reasonable electron sizes for a given primary energy, and this has been checked by a simple method.

In order to perform the muon calculations, the energy spectra of charged pions at various heights must be obtained. If it is assumed that the number of neutral pions is equal to half of that of the charged pions, and that each neutral pion decays into two $\gamma$-rays of equal energy, then a $\gamma$-ray energy spectrum can be obtained for each production height. The spectra so obtained are used in conjunction with the results of Ivanenko and Samusŏdov (1967) to predict the number of electrons produced as a function of depth below each of the fixed production heights. The development through the atmosphere and the sea level size are in good

Figure 5.3

The height of production of muons between 1 GeV/c and 30 GeV/c (at sea level) evaluated using the 1000 series model, for four primary mass and multiplicity combinations. Two experimental points are shown (from Chapter 6). The effects of variations of $\langle p_t \rangle$ and K (see text) are too small to show clearly.

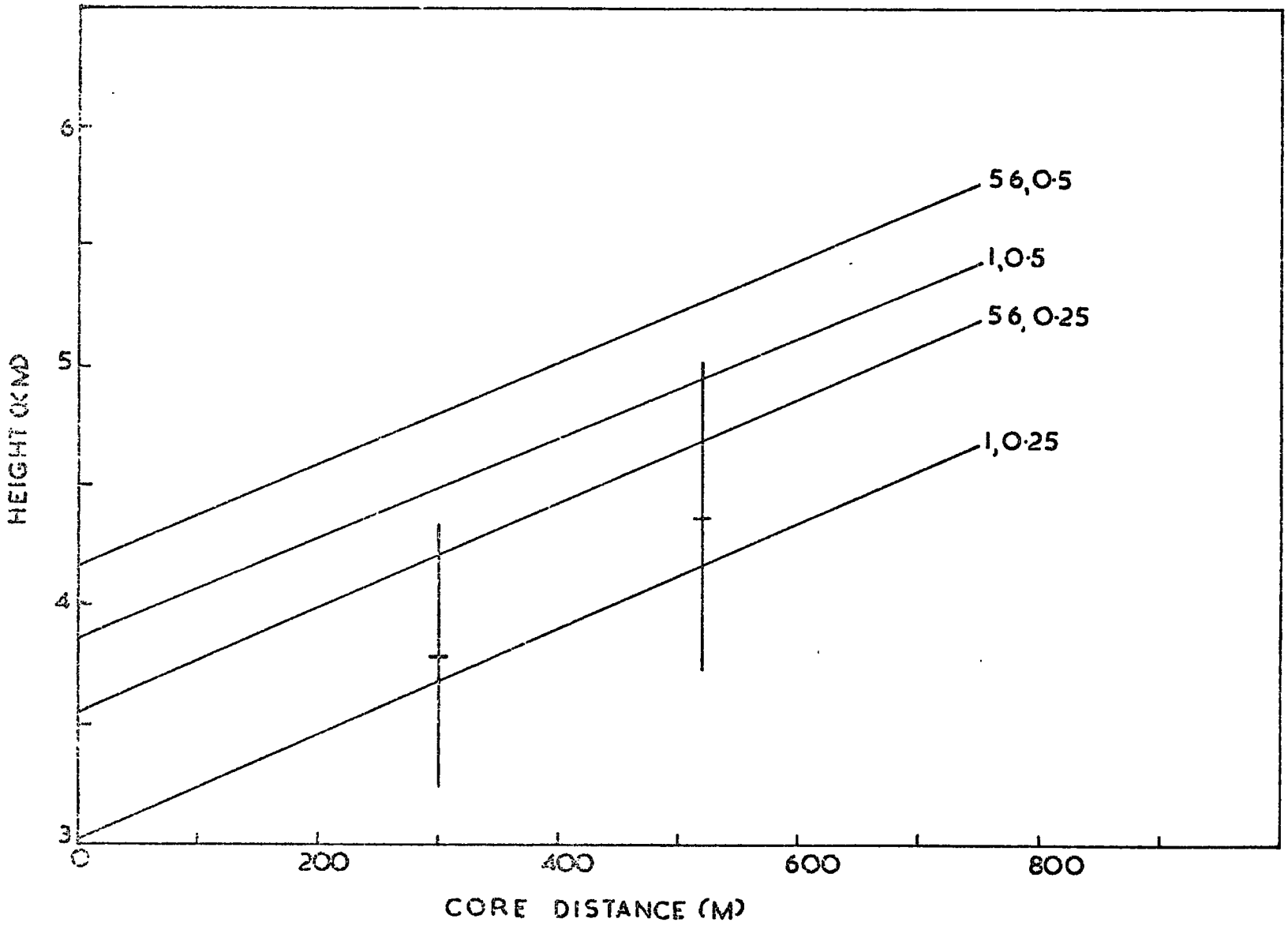
HEIGHT OKMD
6
5
4
3
0
200
400
600
800
CORE DISTANCE (M)
56,0·5
1,0·5
56,0·25
1,0·25

agreement with the results of other models.

## 5.5 The Use of Model Calculations to Indicate Useful Future Experiments

### 5.5.1 Introduction

The accuracy of model calculations now available should permit the determination of basic EAS parameters, such as primary particle mass, the multiplicity of secondary particles, mean pion transverse momentum etc., by comparison with precise experimental results. It is therefore important to design experiments to investigate the most sensitive aspects of the shower, in order to obtain firm results on a reasonable time-scale. This section deals only with such studies of the muon component, and the emphasis of the investigation is mainly upon the possible sensitivity of features of this component to the primary particle mass.

### 5.5.2 The Lateral Distribution of Muons

The lateral distribution of muons above a given threshold energy is affected by changes in the primary mass and in the form of the variation of secondary particle multiplicity with interaction energy. However, the change due to multiplicity is almost independent of core distance, whereas the variation with primary mass is most marked at larger core distances and energies above 10 GeV. The experimental considerations of an absorber experiment to measure lateral distribution are relatively straight forward (e.g. Blake et al (1971), Allan et al (1967). However, very large areas ($\sim$50 $m^2$) and considerable absorber depths are required for reasonable data rates at such large distances (typical densities of muons of greater than 1 GeV/c being less than 0.1 $m^{-2}$ at 1 Km.) The lateral distributions for various threshold energies are shown in figs. 5.4 to 5.6.

### 5.5.3 Muon Momentum Spectra at High Momenta

The shape of the muon momentum spectrum at momenta above 10 GeV/c is fairly strongly dependent on primary mass and secondary multiplicity (as shown in fig. 5.8) and also on mean transverse momentum (e.g. Orford, (1968)). It may therefore be possible to discount several combinations of these parameters using data acquired using magnet spectrograph

Figure 5.4 The lateral distribution of muons of momenta greater than 1 GeV/c for two primary masses. The ratio as a function of distance is inset. The primary particle energy was $2 \times 10^{17}$eV.

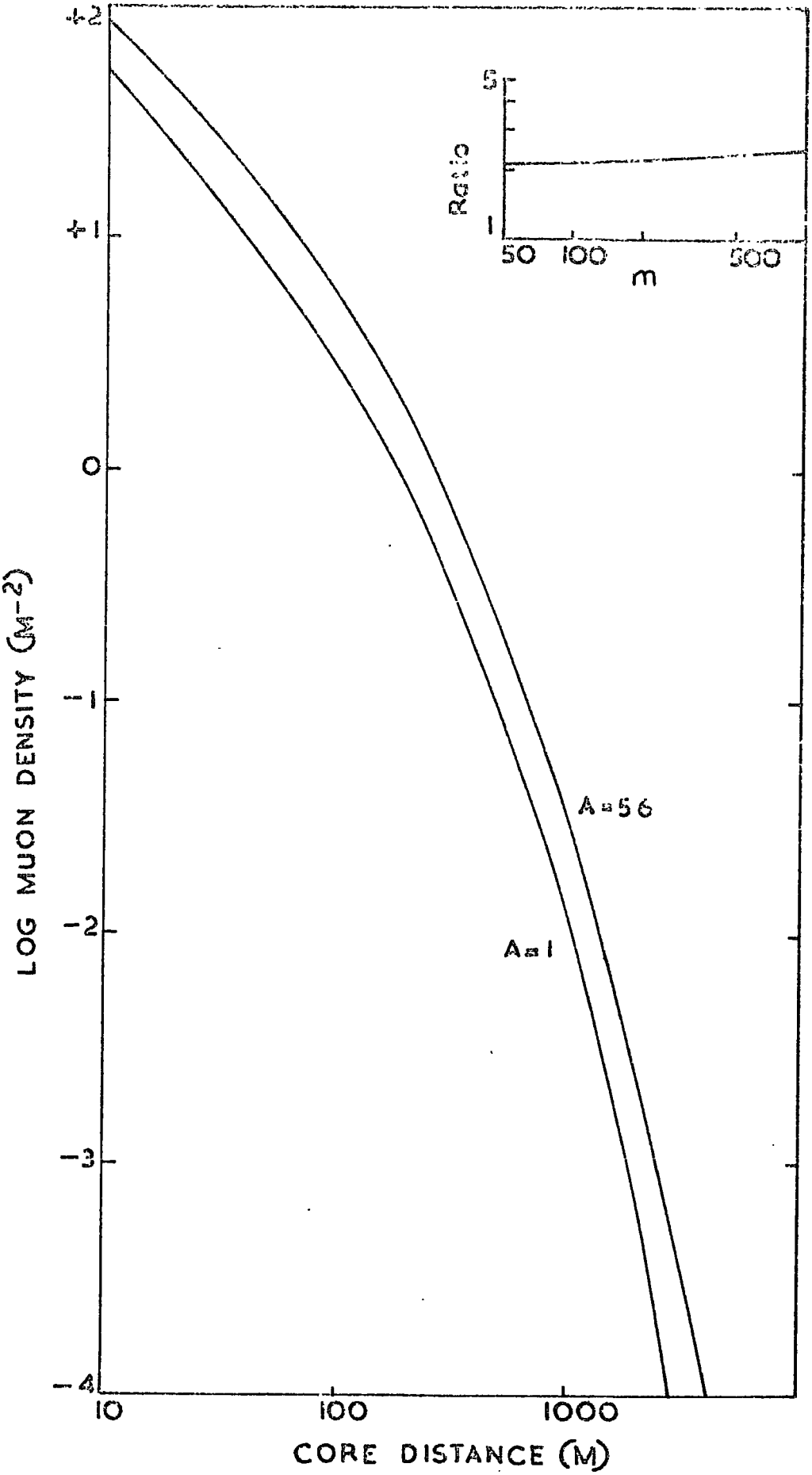
+2
+1
0
-1
-2
-3
-4
LOG MUON DENSITY (M⁻²)
10
100
1000
CORE DISTANCE (M)
A=56
A=1
Ratio
5
1
50
100
500
m

Figure 5.5 As figure 5.4 but for $>$ 10 GeV/c.

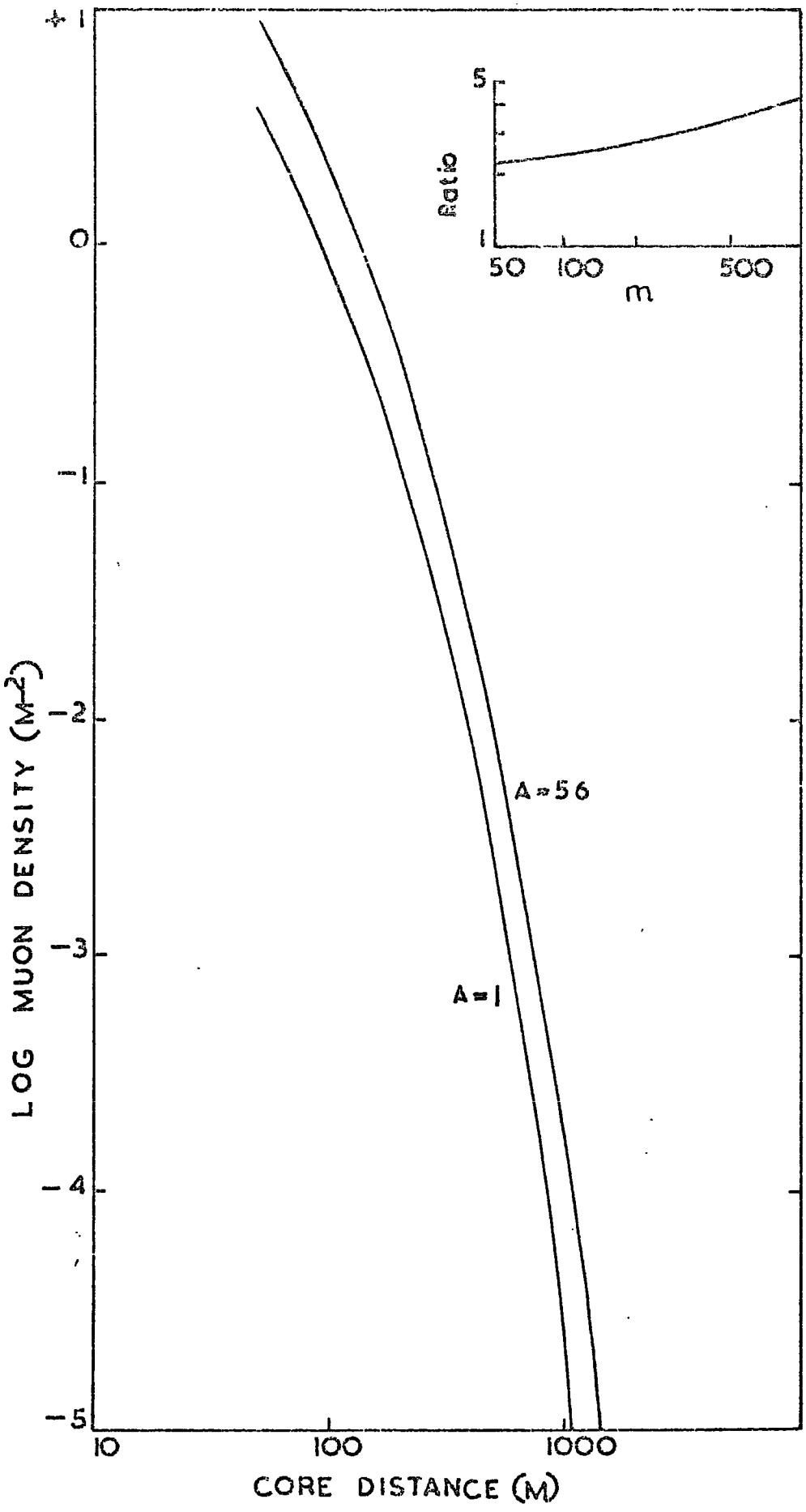
+1
0
-1
-2
-3
-4
-5
LOG MUON DENSITY (M⁻²)
10
100
1000
CORE DISTANCE (M)
A=56
A=1
Ratio
5
1
50
100
500
m

Figure 5.6 As figure 5.4 but for $\geq$ 30 GeV/c.

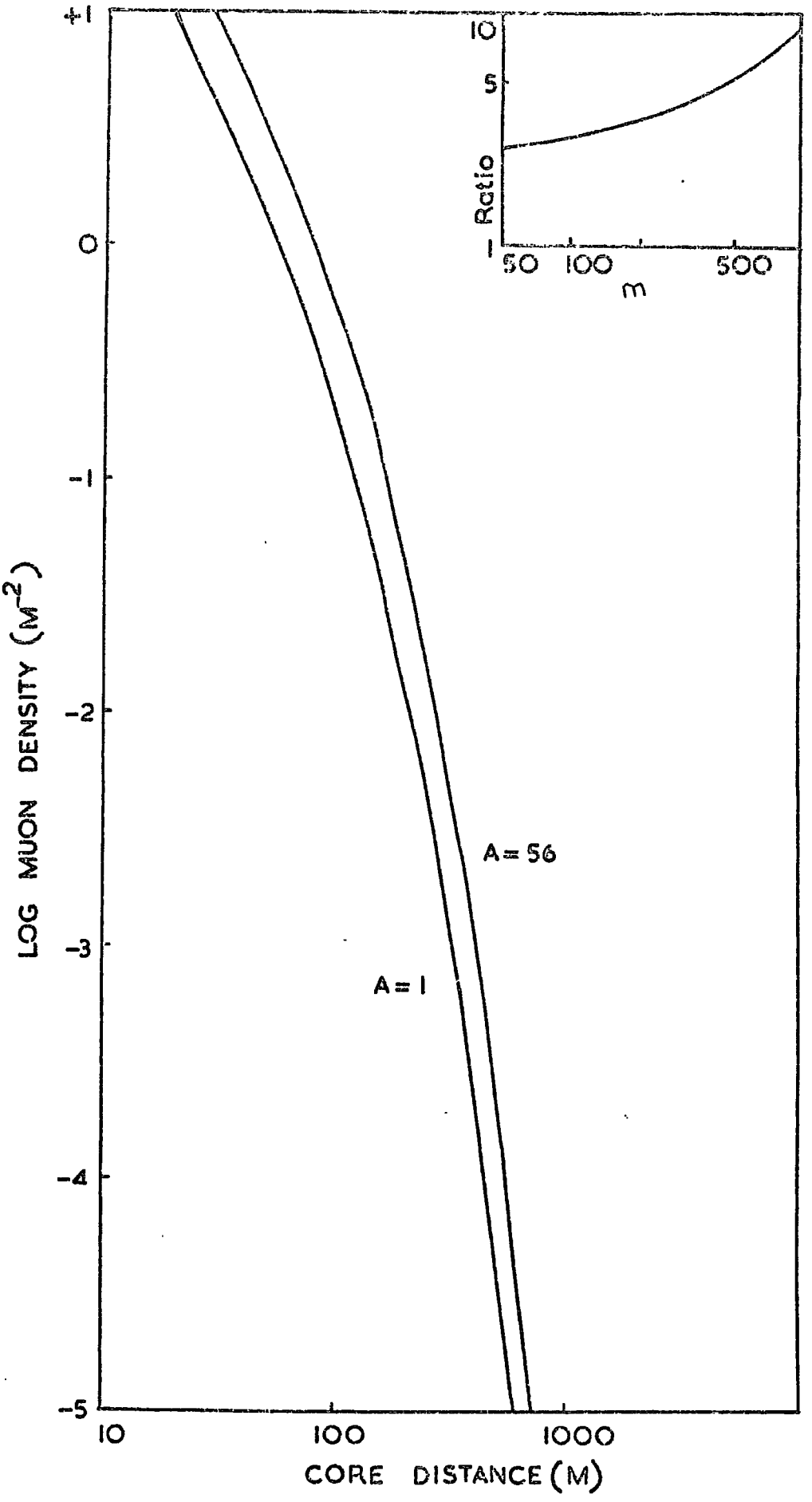
+1
0
-1
-2
-3
-4
-5
LOG MUON DENSITY ($M^{-2}$)
10
100
1000
CORE DISTANCE (M)
A = 56
A = 1
10
5
1
Ratio
50
100
500
m

techniques. The high momentum resolution of the Mk. II spectrograph will alleviate the problems of noise and Coulomb scattering which limit the usefulness of the earlier measurement. The relatively small acceptance area of magnet spectrographs means that the acquisition rate of high energy particles is low (about 25 per year greater than 50 GeV with the Mk. I spectrograph). This technique also yields considerable advantages in lateral distribution measurements - the information is direct and it is fairly simple to correct for acceptance effects, which render some absorber experiments inaccurate.

5.5.4 Muon Momentum Spectra at Large Core Distances

Figure 5.7 shows the mass sensitivity of the integral muon momentum spectrum at a core distance of 850m. The difference in shape is far more marked than at 300 m. Further, a core distance of 850m., even in showers of primary energy $> 10^{18}$eV, implies a lower soft component contamination than at 300m., which makes processing of data simpler. Large area spectrographs are required for such measurements, but the momentum resolution need only be modest, say 50 GeV/c. Most important, however, is that the core location uncertainty must be small ($\pm$ 20-30m.) for a very large range of core distances. This may be achieved with a spectrograph situated in a carefully chosen location well outside the present 500m. array, and sampling well measured showers falling inside the array having good core location accuracy, would overcome the objection raised above.

5.5.5 Muon Momentum Spectra at Small Core Distances

Fig. 5.8 shows the sensitivity of muon momentum spectra at a core distance of 100m. for a shower of $5.10^6$ particles. In order to differentiate adequately in terms of primary mass, measurements at momenta in excess of 100 GeV/c are necessary. Such measurements may be possible with the Mk. II spectrograph, but the difficulties of obscuration by the soft component of high momentum muons at such small core distances must be considered. The

Figure 5.7 The mass dependence of the integral muon momentum spectrum at a core distance of 850 m. The ratio of mass A=56 to proton primary as a function of momentum is inset.

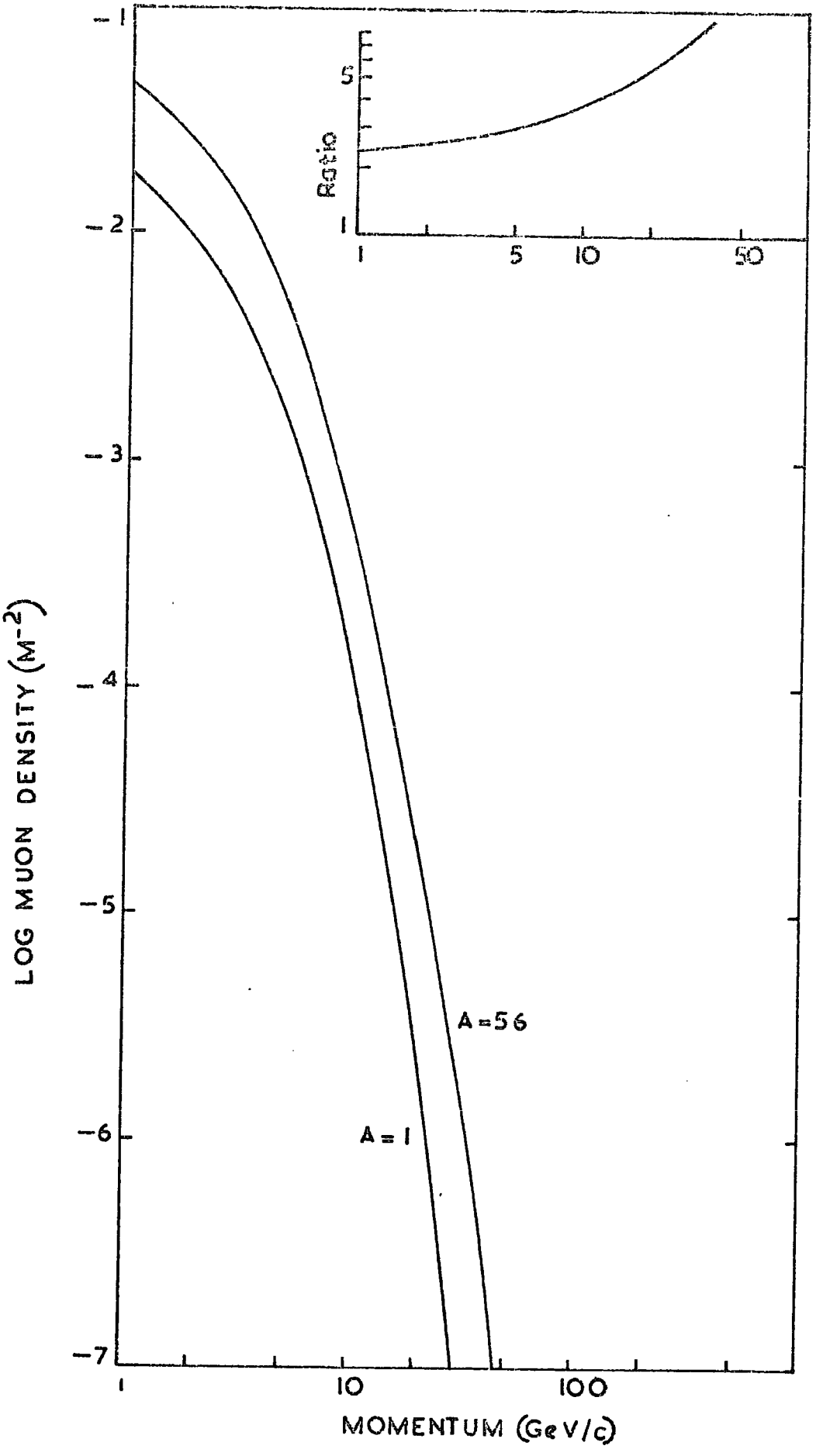
LOG MUON DENSITY ($M^{-2}$)
MOMENTUM (GeV/c)
A=56
A=1
Ratio
-1
-2
-3
-4
-5
-6
-7
1
10
100
5
50

Figure 5.8 The mass dependence of the integral muon momentum spectrum at a core distance of 100 m. in a shower of size $5.10^6$ particles. The ratio as a function of momentum is inset.

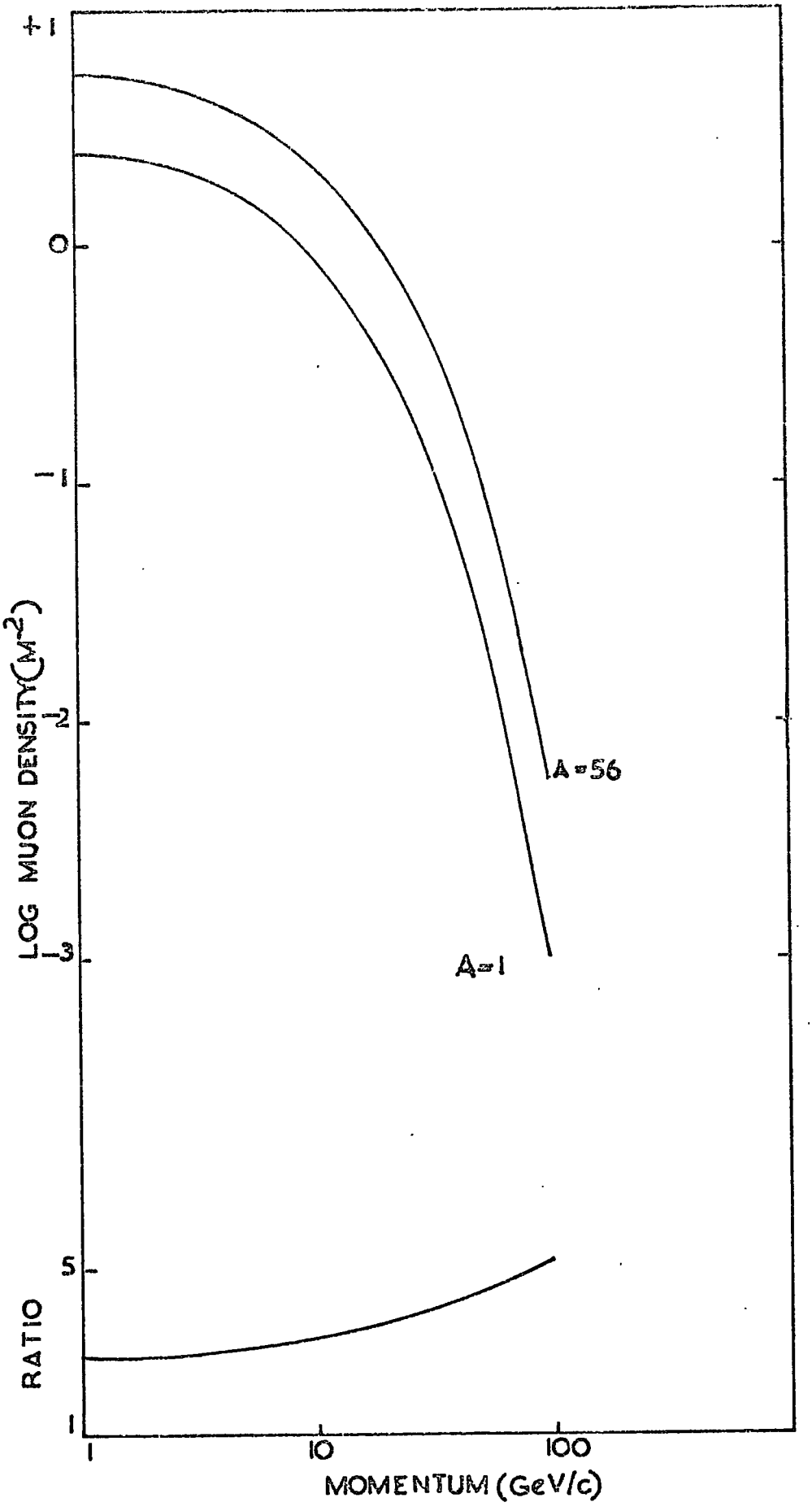
+1
0
-1
-2
-3
LOG MUON DENSITY($M^{-2}$)
A=56
A=1
5
1
RATIO
1
10
100
MOMENTUM (GeV/c)

Figure 5.9

The variation of the density of 100 GeV/c muons 100 m. from the core of a $5.10^6$ shower, as a function of mass, multiplicity and mean transverse momentum. The solid lines refer to a secondary particle multiplicity $\propto E^{0.25}$, and the broken lines $\propto E^{0.5}$.

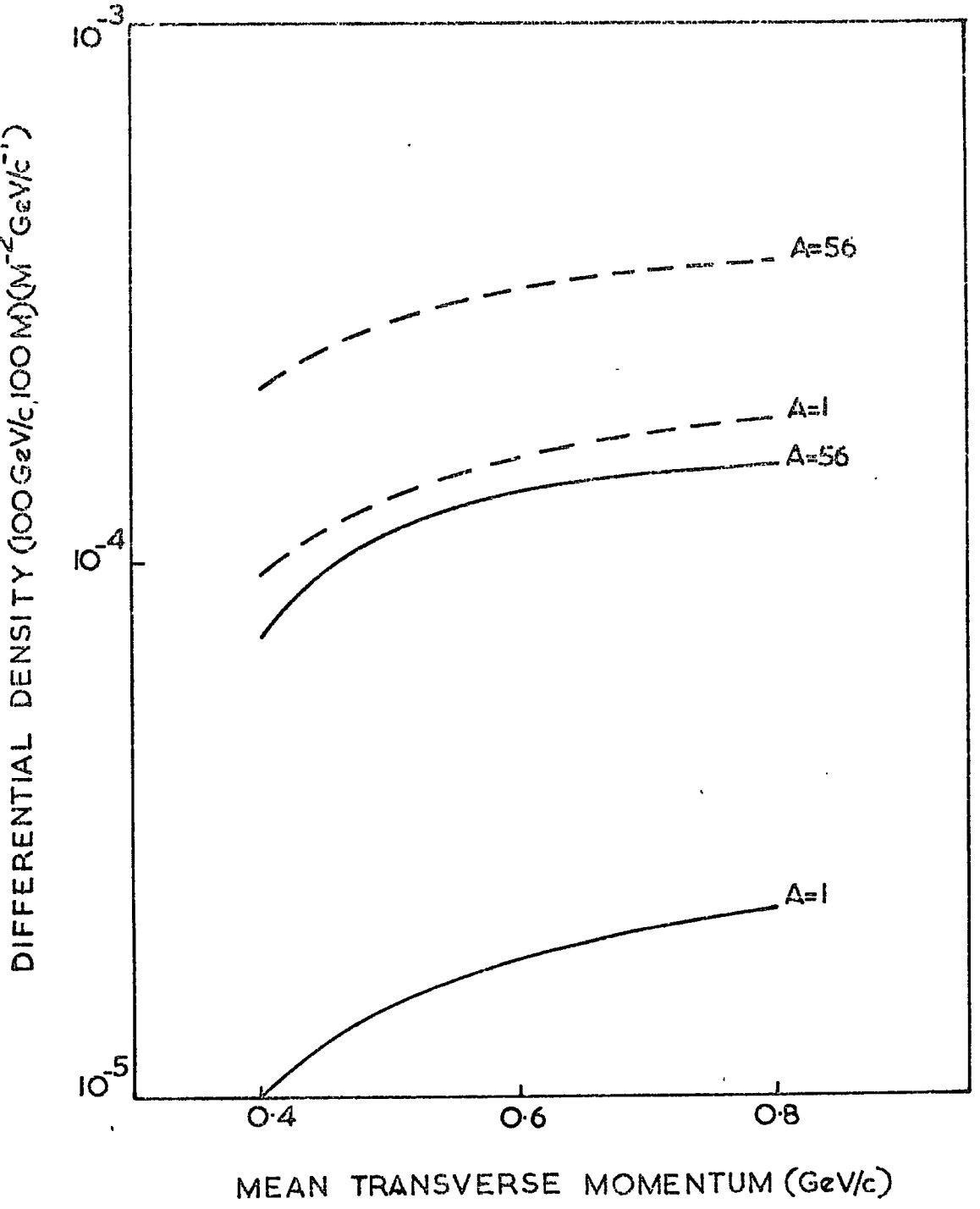
$10^{-3}$
$10^{-4}$
$10^{-5}$
A=56
A=1
A=56
A=1
0·4
0·6
0·8
DIFFERENTIAL DENSITY (100 GeV/c, 100 M)($M^{-2}$ GeV/$c^{-1}$)
MEAN TRANSVERSE MOMENTUM (GeV/c)

integral muon density close to the core of such smaller showers also depends quite strongly on mean transverse momentum, as shown in fig. 5.9

5.5.6 Discussion

Four possible categories of muon experiments have been considered In almost all the cases, the change produced by a variation in primary mass from 1 to 56 can also be produced by a change in multiplicity law exponent from 0.25 to 0.5, except perhaps at very large core distances. The suggestions in section 5.5.2 are already in progress, and data should be available within one year. The most likely field for a sensitive test may be in the large core distance region, and either large area, low resolution spectrographs (for momentum spectra and lateral distributions) or a large area shielded muon detector (for lateral distributions) should yield interesting results. If the multiplicity law exponent could be reliably restricted to less than 0.5 (say 0.25), the task would be considerably easier. Such restriction may be possible from study of other aspects of EAS. Furthermore, data on the secondary particle multiplicity at fairly high energies should be available soon from the latest high energy accelerator experiments.

# CHAPTER SIX

# THE HEIGHT OF ORIGIN OF MUONS IN EAS

## 6.1 Introduction

The model calculations described in the previous chapter indicate that the longitudinal development of an EAS is sensitive to both the primary particle mass and the nature of the fundamental nuclear collisions of the cascade. Direct measurements on the electron-photon component do not allow firm conclusions to be drawn about the development heights of electrons in the shower, because of the large fluctuations associated with the e-$\gamma$ components (but Allan (1971) and Marsden et al (1971) succeed in outlining possible indirect methods). Muons, however, relate more directly to the nuclear interactions and the longitudinal development than the e-$\gamma$ component, and so they may retain some indication of the nature of the primary particle and the nuclear interactions. The method used in the work described in this chapter is basically trigonometric - the arrival direction of the shower core, the distance of the core from the muon momentum spectrograph, and the muon arrival angle at the spectrograph are required to give a production height estimate for the measured muon.

## 6.2 General Description of Method

### 6.2.1 Basic Trigonometrical Relations

The fundamental relation used in this method may be represented diagrammatically, as in fig. 6.1. A muon of momentum P arriving at the spectrograph, a distance r from the shower core, must originate from a height h such that

$$\frac{P_t}{P} = \frac{r}{h} \quad \ldots\ldots\ldots\ldots\ldots 6.1$$

where $P_t$ is the transverse momentum possessed by the muon. This relation holds fairly well for momenta above 10 GeV/c; below this the muon does not travel in "straight" lines due to scattering, but the relation is still broadly correct. Equation 6.1 contains two unknowns, $P_t$ and h; the form of the $P_t$ distribution appears to be well represented by the CKP

Figure 6.1 (i) The relation between muon momentum, core distance, height of origin and transverse momentum.

(ii) The basic relation used to determine height of origin after projecting the shower arrival direction into the spectrograph measuring plane.

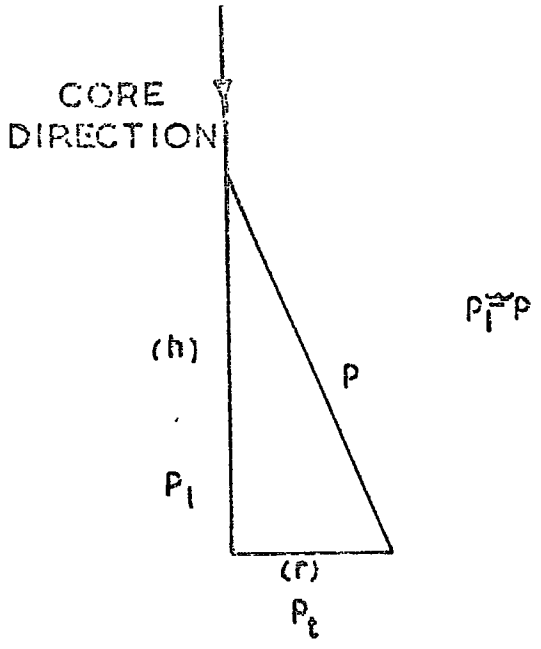


$P_1 \simeq P$

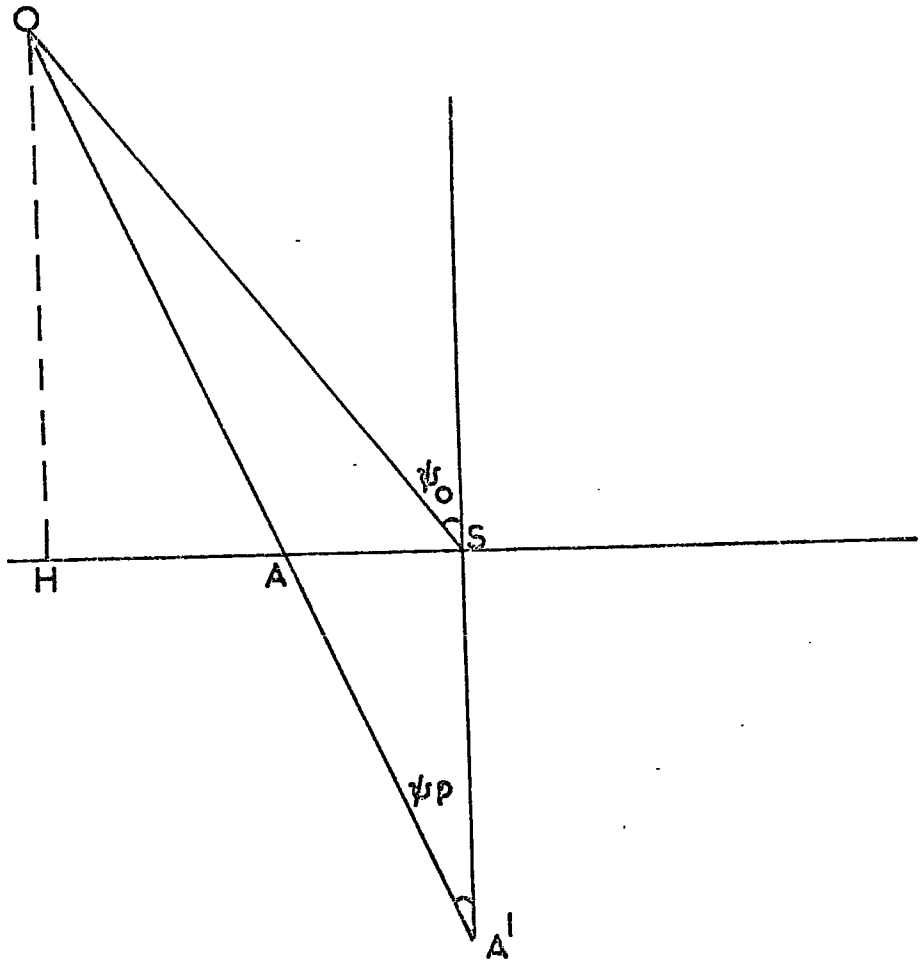

distribution used in the previous chapter. Making this assumption, a value for h may be derived by turning equation 6.1 into a form more directly comparable with experimental measurements.

6.2.2 Relative Arrival Directions of Muon to the Shower Core Direction

The main constraint on the studies of the angular properties of muons is the spectrograph itself. Because of the design of the instrument, the incident angle of the muon may only be recorded in one plane, so that the core arrival direction must also be projected on to the spectrograph measurement plane. The projected core direction angle $\psi_p$, is given by:

$$\tan(\psi_p) = \tan(\theta)\cos(\phi + 34.5^\circ) \quad \ldots\ldots\ldots \quad 6.2$$

where $\theta$, $\phi$ are the zenith and azimuth angles respectively. The projected core distance is also required, and is found by rotation of axes:

$$r_\perp = Y\cos(34.5) - X\sin(34.5) \quad \ldots\ldots\ldots \quad 6.3$$

where X,Y are the cartesian coordinates of the core impact point. The common figure of $34.5^\circ$ arising in equations 6.2 and 6.3 occurs because of the orientation of the spectrograph measuring plane with respect to the chosen cartesian axes, and this orientation has some useful effects, as shown later.

Fig. 6.1 (ii) shows the effect of projecting the core direction into the spectrograph plane. OS is the (projected) muon, OAA' the (projected) core, and OH the height required. Since AS is defined as $r_\perp$, the following may be obtained:

$$H = \frac{r_\perp \cos(\psi_p)\cos(\psi_o)}{\sin(\psi_p - \psi_o)} \quad \ldots\ldots\ldots \quad 6.4$$

or

$$\frac{r_\perp}{H} = \tan(\psi_p) - \tan(\psi_o) \quad \ldots\ldots\ldots \quad 6.5$$

Since the angle $(\psi_p - \psi_o)$ is generally small (typically less than $10^\circ$), errors in the value of H arise mainly from errors in $(\psi_p - \psi_o)$. The form of equation 6.4 shows that it is more useful to work in terms of $1/H$, for the errors then relate more directly to those in $(\psi_p - \psi_o)$. Errors in $r_\perp$ are less important and are similar to the errors in core

Figure 6.2 Contours of equal numbers of showers (2497 in all) containing acceptable muons per 100m. x 100m. bins of X and Y.

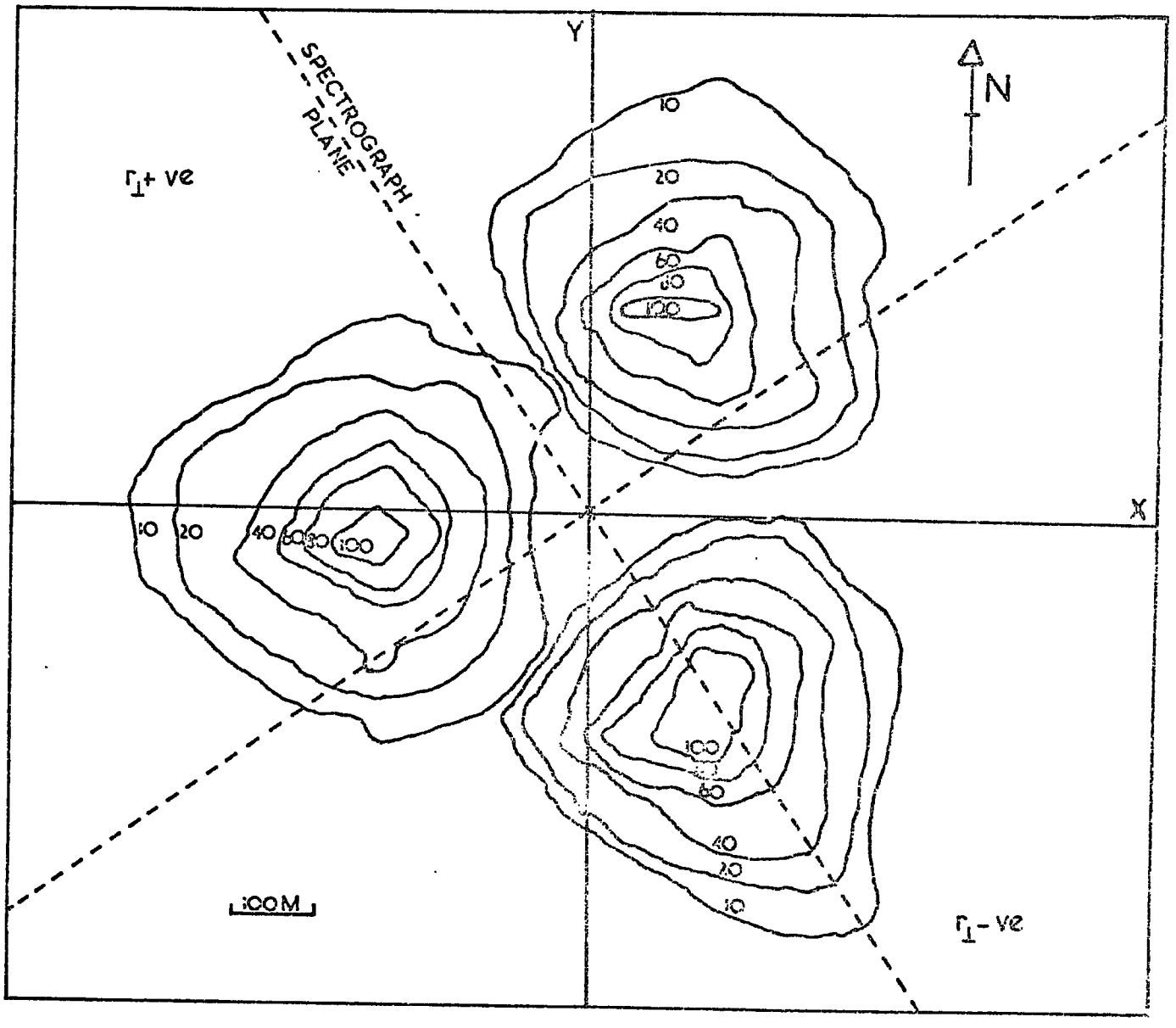
SPECTROGRAPH PLANE
Y
X
N
$\Gamma_{\perp}$ + ve
$\Gamma_{\perp}$ - ve
10
20
40
60
80
100
100 M

location described in Chapter 4. Care is necessary when using very small values of $r_\perp$ and it has been customary to exclude showers falling such that $r_\perp$ is less than 10 metres.

6.2.3 Effect of the "lobes" of the 500 m Array Collecting Area

(a) The effect on $r_\perp$

The symmetrical layout of the 500m. array, and the triggering criterion of (centre and two outer) stations, causes the most frequent, smaller showers to be detected preferentially when their cores fall away from the lines joining the outer stations to the centre (e.g. Suri (1966)). The data comprising the Mk. I data sample has been subdivided into intervals of X and Y, and fig. 6.2 shows the distribution of showers in the form of contours of equal shower numbers in 100m. x 100 m. bins of X and Y. The spectrograph plane is rotated through the above mentioned $34.5^\circ$ with respect to the XY system, and it is apparent that more showers fall in the "$r_\perp$ + ve" region than the "$r_\perp$ - ve" region because of this effect, the ratio being about 1.5:1. However, the value of $\langle r_\perp \text{ - ve} \rangle$ is larger than $\langle r_\perp \text{ + ve} \rangle$, an effect taken into account in later sections.

(b) The Effect on the observed angle $(\psi_p - \psi_o)$

The heights of origin predicted by equation 6.4 would be in the absence of scattering, positive. Inspection of this relation shows that if $\psi_p$ and $\psi_o$ are of the same sign (usually so except for near vertical showers), then $(\psi_p - \psi_o)$ must be of the same sign as $r_\perp$ in order to give a positive value of H. Since $r_\perp$ may be divided into two populations, it is to be expected that there will be two broad populations of $(\psi_p - \psi_o)$, one positive, and one negative. The effect is used later as a measure of the mean production height. Fig. 6.3 shows the broadly negative tendency of a typical $r_\perp$ - ve $(\psi_p - \psi_o)$ distribution.

6.2.4 Determination of the Measurement Error on $(\psi_p - \psi_o)$

In Chapter 2 the overall noise on $\theta$, $\phi$ was estimated at about $2.2^\circ$ in $\theta$ and $7^\circ$ in $\phi$. This, transformed into a noise on the core direction $\psi_p$ yields 2 - $2.5^\circ$. The error on the muon direction $\psi_o$ is some $0.3^\circ$

Figure 6.3 Distribution in the angle $(\psi_p - \psi_o)$ for core distances between 250 and 350 m. for 1-3 GeV/c muons. The distribution derived from projected shower arrival directions using corrected $\theta$, $\phi$ is shown in solid lines. Also shown is the curve predicted by the model described in Chapter 6.

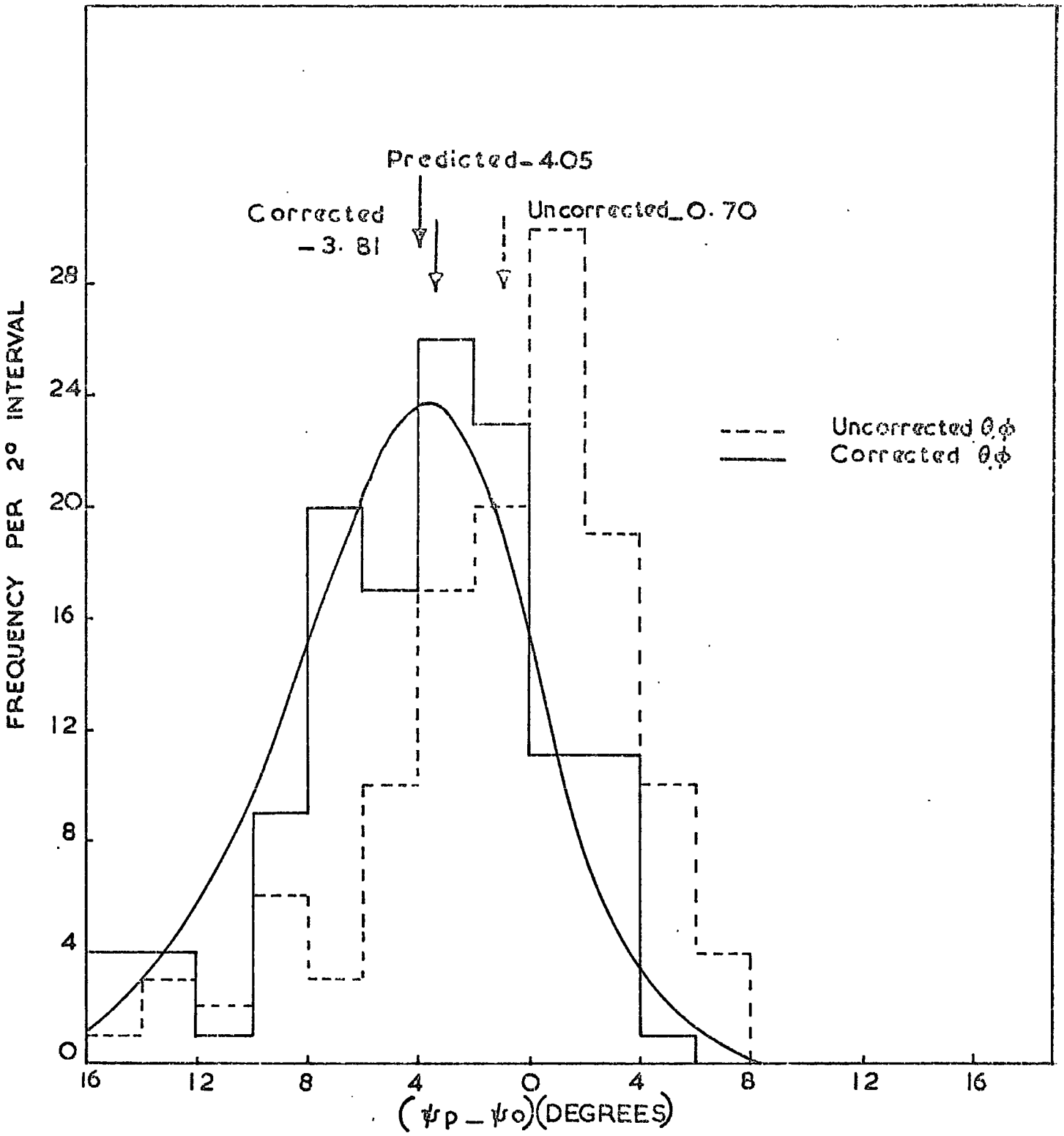
Predicted-4.05
Corrected
-3.81
Uncorrected_0.70
Uncorrected θ,φ
Corrected θ,φ
FREQUENCY PER 2° INTERVAL
28
24
20
16
12
8
4
0
16
12
8
4
0
4
8
12
16
(ψp_ψo)(DEGREES)

Figure 6.4

The distribution in $(\psi_p - \psi_o)$ for muons of momenta greater than 30 GeV/c, at all core distances from 150-600m. The broader distribution resulting from the use of corrected $\theta$, $\phi$ is evident. A similar distribution for momenta greater than 45 GeV/c has been used to determine the overall noise on $(\psi_p - \psi_o)$.

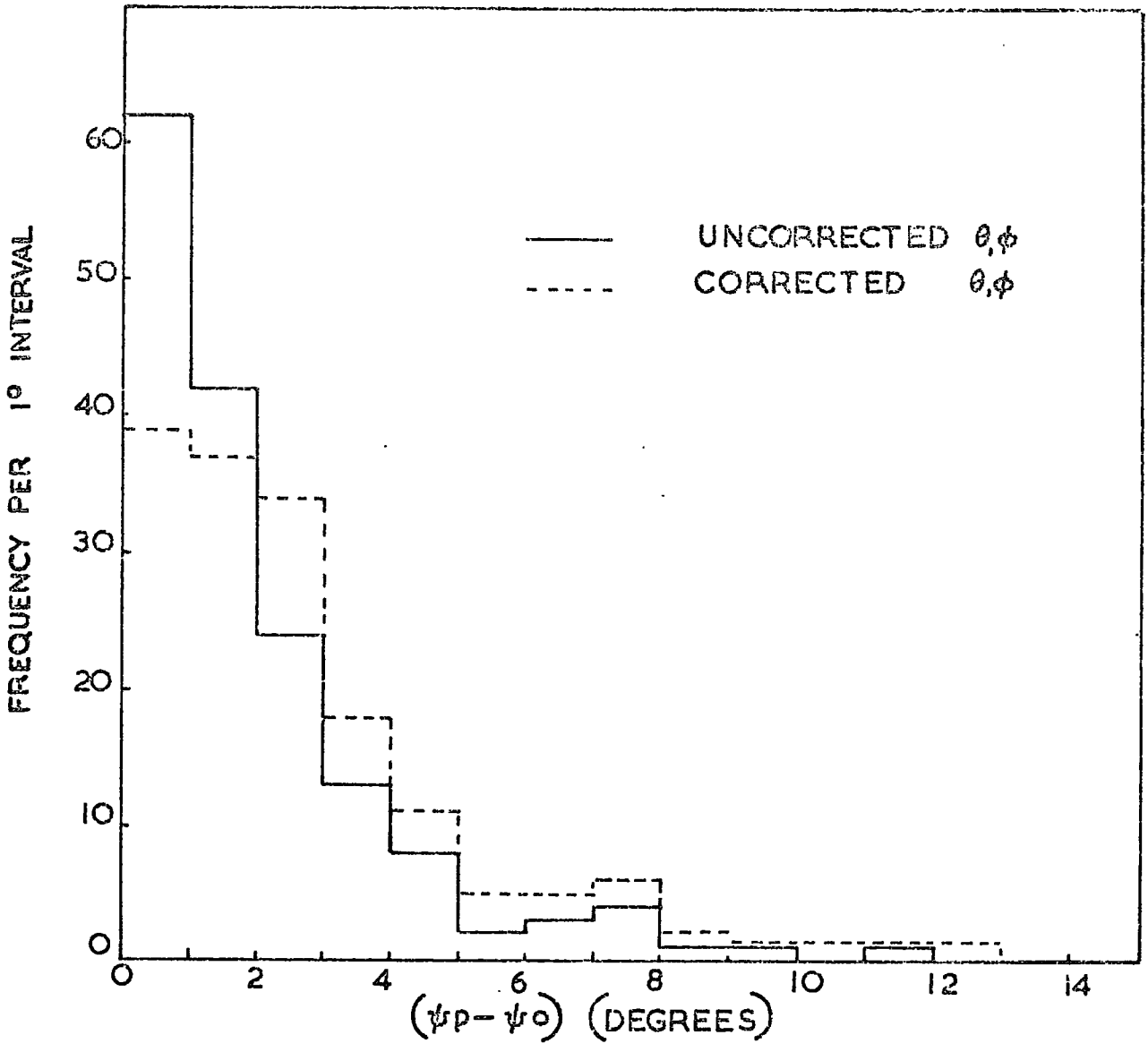
FREQUENCY PER 1° INTERVAL
60
50
40
30
20
10
0
UNCORRECTED θ,φ
CORRECTED θ,φ
0
2
4
6
8
10
12
14
(ψp−ψo) (DEGREES)

so that the greatest contribution to the overall noise figure comes from the errors in $\theta$ and $\phi$. Application of equation 6.1 to muons of momentum $p > 30$ GeV/c and height H = 10 Km (as discussed in Chapter 5), for a typical core distance of 300m., shows that the angle $(\psi_p - \psi_b)$ is less than $1^o$, so that the distribution in $(\psi_p - \psi_b)$ of high momentum muons should give a good estimate of the overall noise (including the effects of scattering). The distribution has been derived from values of $(\theta,\phi)$ uncorrected and $(\theta,\phi)$ corrected, and the results are shown in fig. 6.4. The narrower distribution of $(\psi_p - \psi_b)$ derived from values of $\theta$, $\phi$ uncorrected for curvature effects led initially to the assumption that such uncorrected $\theta,\phi$ values yield a better estimate of the core direction. Subsequent investigation showed, however that the distributions in $(\psi_p - \psi_b)$ derived from uncorrected core arrival direction did not exhibit the correct shape, or show the correct tendencies as muons were selected which had a higher origin. The conclusions drawn from this indicate that the "uncorrected" $\theta,\phi$ perhaps yield a close estimate of the shower particle direction in the vicinity of the centre detector, and so would show a smaller noise figure because of the proximity of the spectrograph to the centre of the array. This point is discussed further in section 6.4.

6.3 The Average Production Height of Muons by a Direct Method

The mean reciprocal height of origin has been determined for 16 intervals of muon momentum and core distance for the Mk. I data sample, by direct application of equation 6.4. The ranges concerned are 1-3, 3-8, 8-15, 15-30 GeV/c, for 150-250, 250-350, 350-450, 450-600 metres. The results, found by calculating the mean value of 1/H and its standard deviation, then converting the values to heights of production, are shown in fig. 6.5 to 6.8. Also shown are model predictions obtained from the calculations described in Chapter 5. The experimental results appear to favour the predictions for a proton primary, and, as a check on these results, an alternative method was used, as described in the following sections.

Figures 6.5 - 6.8 The height of production as a function of muon momentum for four bands of core distance. ~~Model predictions for two~~ primary masses are also shown. The primary particle energy was $2 \times 10^{17}$ eV. The dotted line shows the effect of a change in n-n inelasticity from 0.5 to 0.44 with a proton primary.

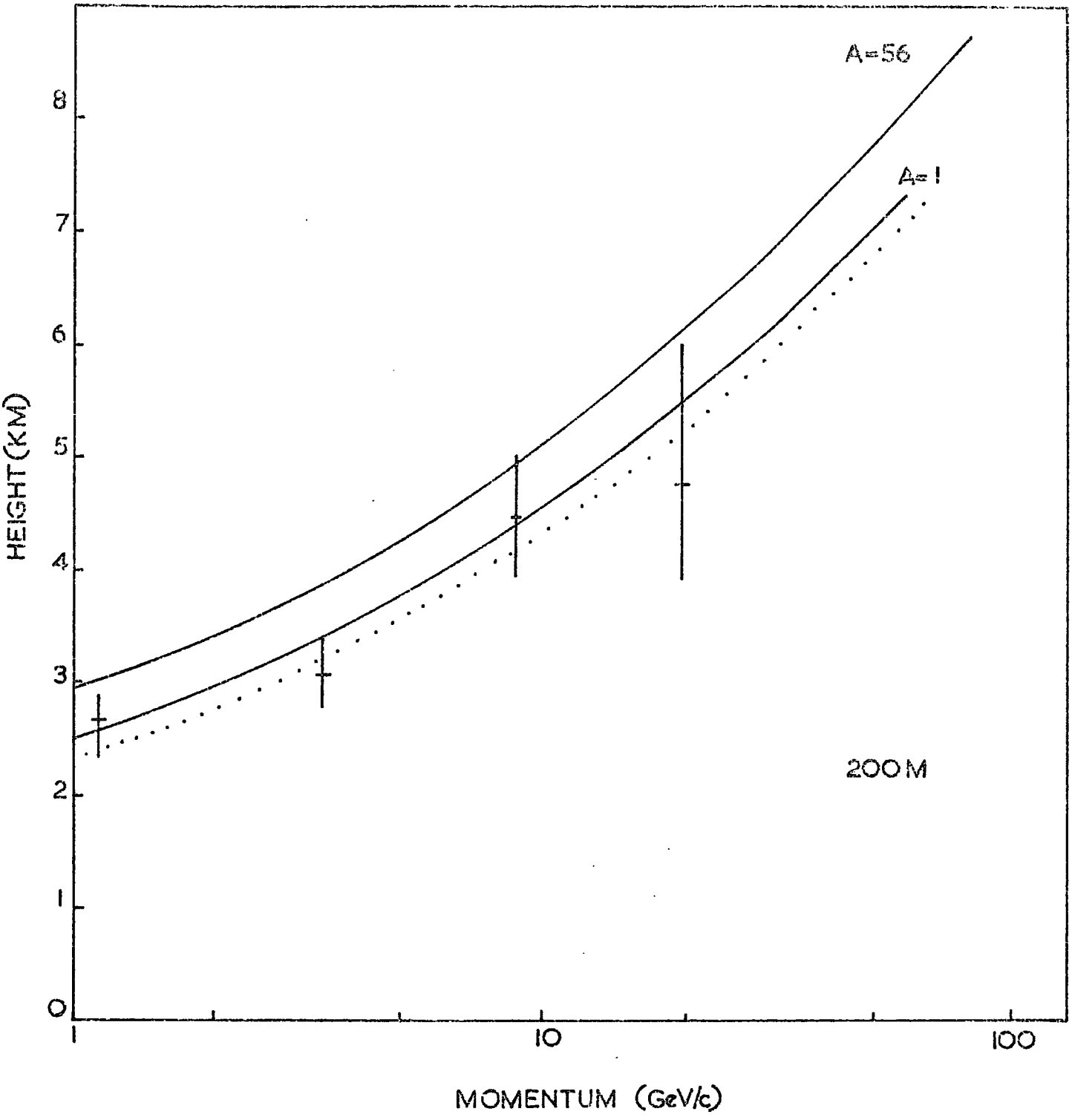
A=56
A=1
200 M
HEIGHT (KM)
0
1
2
3
4
5
6
7
8
1
10
100
MOMENTUM (GeV/c)

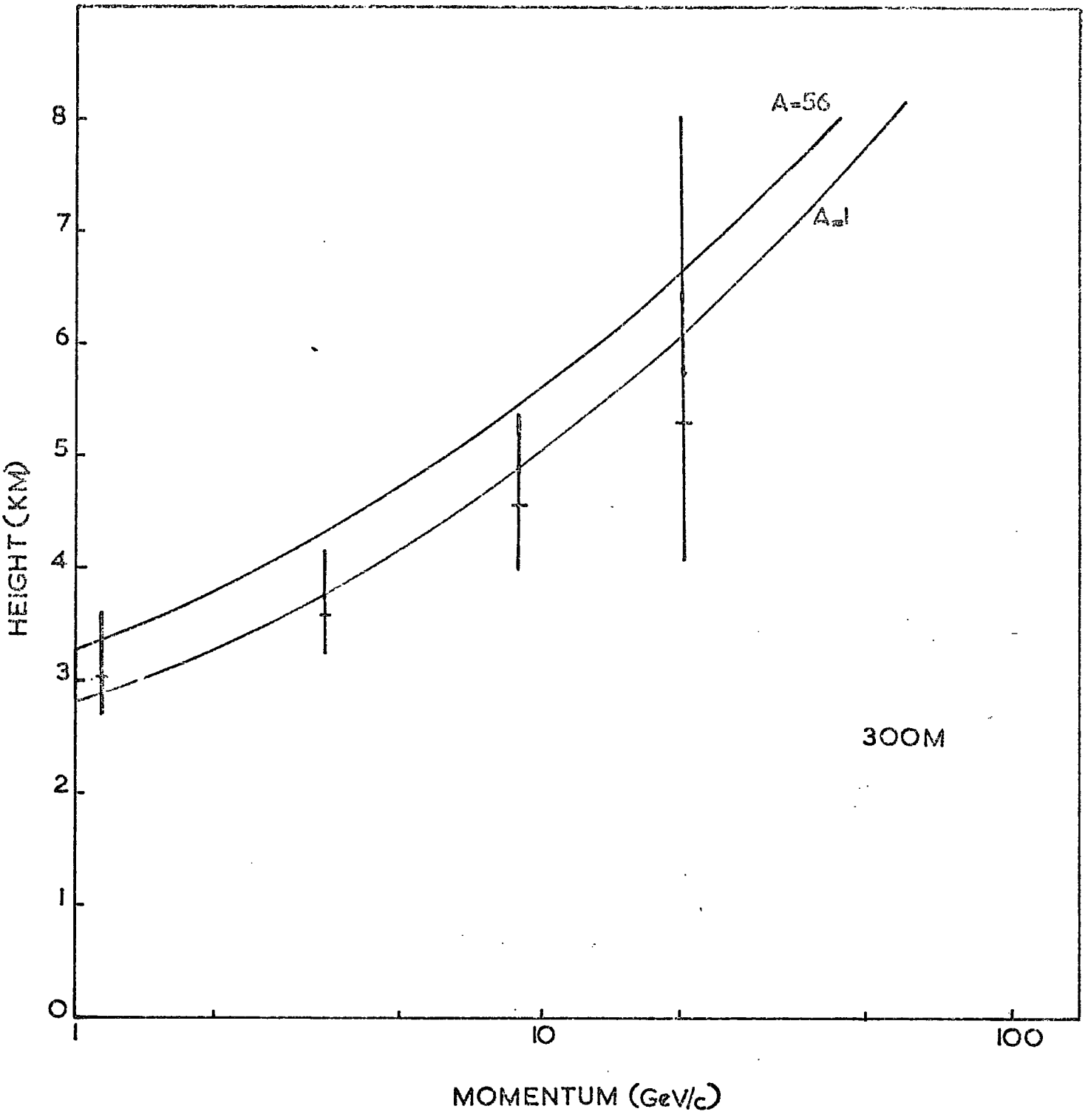
A=56
A=1
300M
HEIGHT (KM)
MOMENTUM (GeV/c)
0
1
2
3
4
5
6
7
8
1
10
100

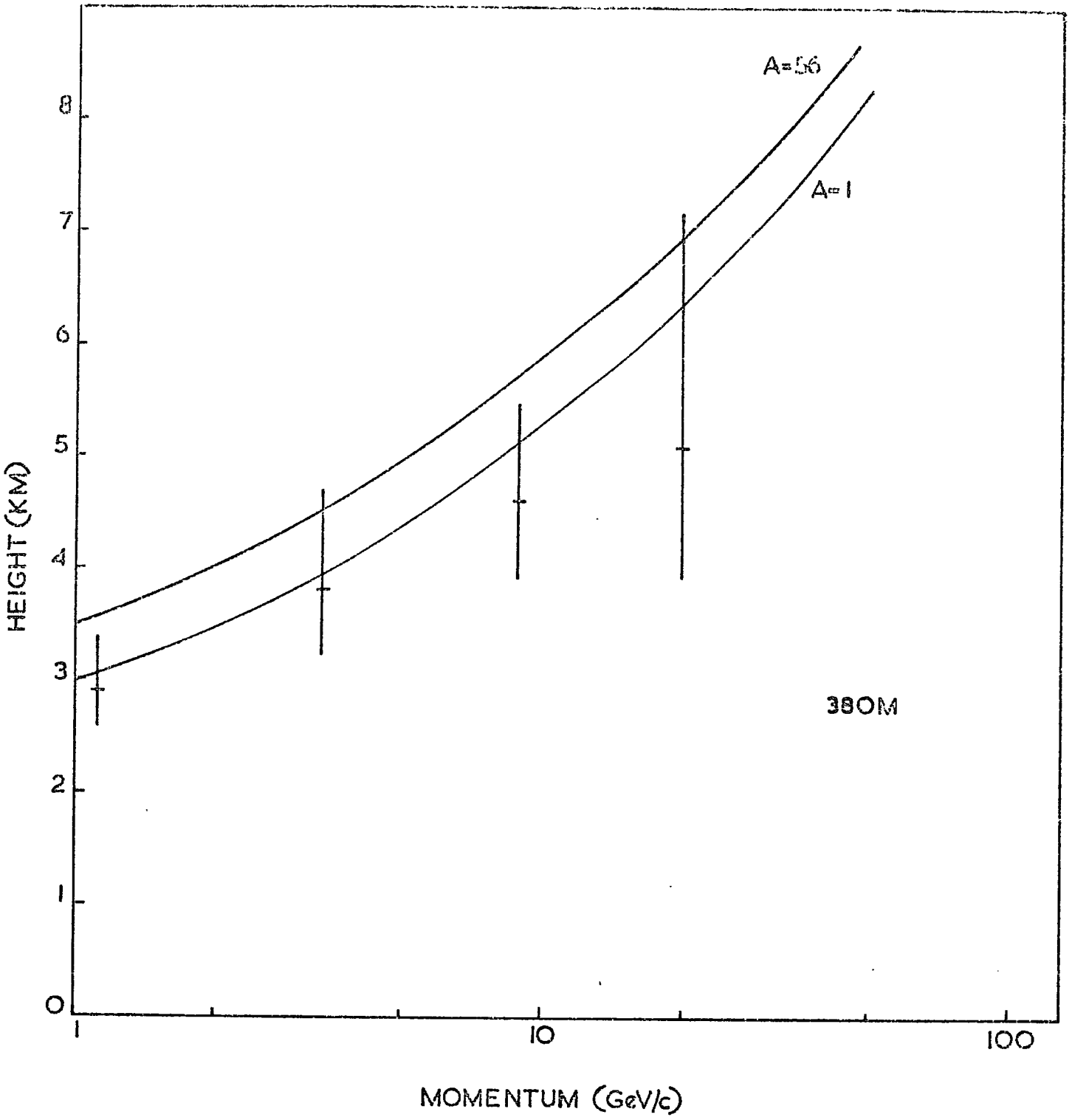
A=56
A=1
380M
HEIGHT (KM)
0
1
2
3
4
5
6
7
8
1
10
100
MOMENTUM (GeV/c)

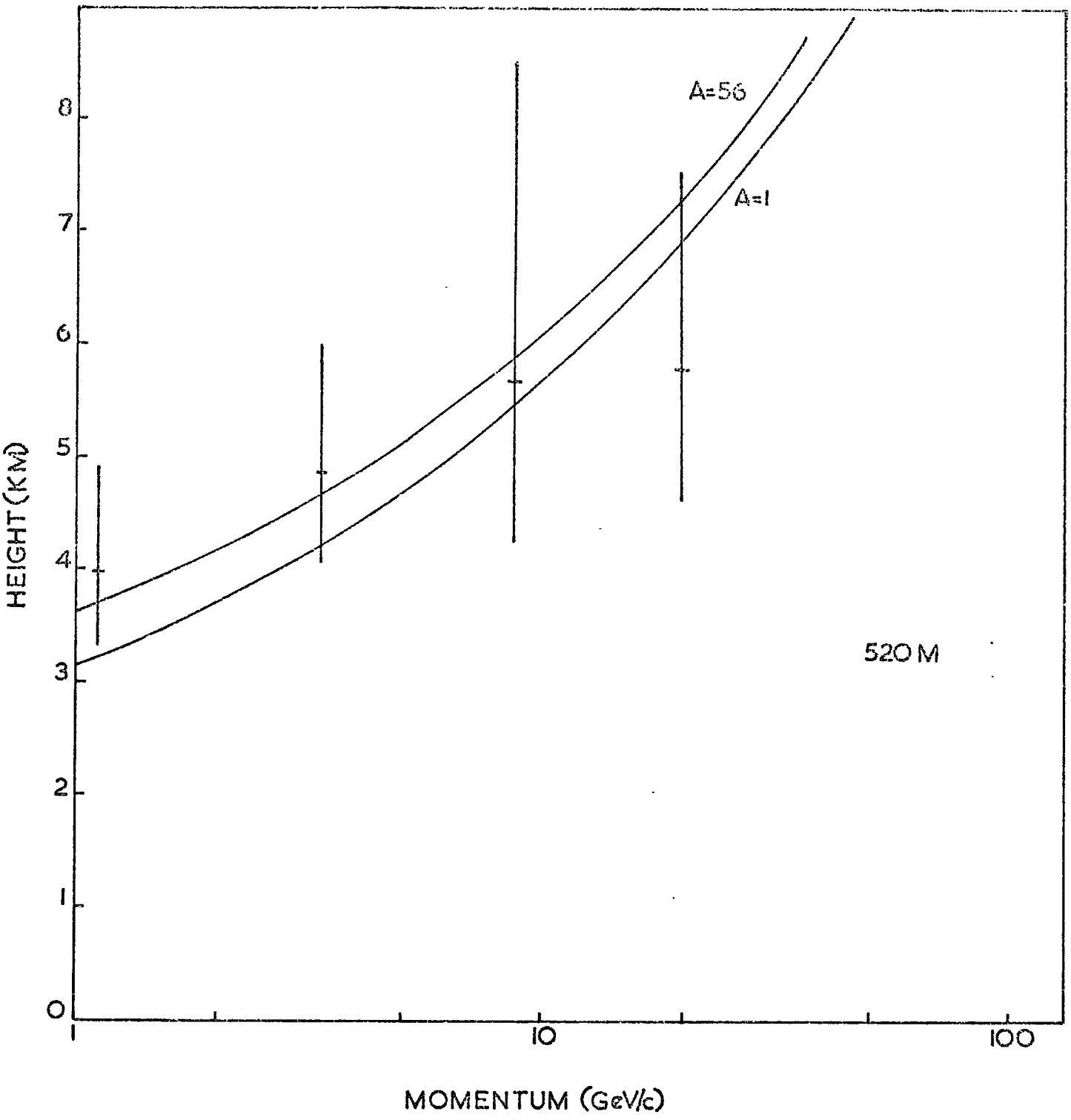
A=56
A=1
520 M
HEIGHT (KM)
0
1
2
3
4
5
6
7
8
10
100
MOMENTUM (GeV/c)

## 6.4 The Use of $(\psi_p - \psi_o)$ Distributions and Theoretical Predictions to Obtain the Production Height

### 6.4.1 Introduction

The direct method of determining the production height relies on the accuracy of equation 6.4, and also on the applicability of a simple analysis. The forms of equation 6.3 and 6.4 imply that regions of $\theta$, $\phi$, X,Y exist where small changes in any of the given values result in large changes in $1/H$. Accordingly, it was decided to predict the $(\psi_p - \psi_o)$ distribution expected at various core distances for different shower models, and to compare the predictions with the observed distributions. Such a method makes possible the correct inclusion of the angular effects of coulomb scattering and geomagnetic deflection, instead of including them in a "noise" term.

### 6.4.2 The Prediction of a Distribution in $(\psi_p - \psi_o)$ from a Distribution in Height of Production of Muons

In order to predict the form of the distribution in $(\psi_p - \psi_o)$, it is necessary to account for a) the physical processes occurring in muon production and passage to sea level, and b) systematic experimental effects which modify the expected distribution. The starting point for the calculations is the observation of a muon of momentum P at sea level (arriving vertically), within a band of core distance $r_1 - r_2$. This implies that the core "landed" in an annulus of known radii about the spectrograph. For each of the height intervals in use (chosen to match those of the 1000 series programmes described in Chapter 5), the muon momentum at production is calculated assuming a constant rate of energy loss of 2.2 MeV$(\text{gm cm}^2)^{-1}$. This enables the parent pion momentum and the $\pi$-$\mu$ decay angle to be calculated. The transverse momentum distribution used is that quoted for n-n collisions by Cocconi, Koester and Perkins (1961), known as the CKP distribution, and the mean of the distribution may be varied as an input parameter. The value of transverse momentum is obtained from equation 6.1 and the probability of this value may be determined. The geomagnetic deflection of the muon is calculated, converted into an angle, and then combined with the $\pi$-$\mu$ decay angle to produce two

possible modifying delta functions in terms of muon directions at production. The opening angle (ie. the angle relative to the core direction) is varied from $-50^{\circ}$ to $+50^{\circ}$ in $0.1^{\circ}$ steps (the wide range is to allow extreme values of $(\psi_p - \psi_o)$ to be represented), modified by the delta functions described above, and then checked trigonometrically to ensure that the values used constrain the muon to fall inside the chosen distance band. If so, the probability of observing a muon of momentum P in the chosen distance band arising from the height interval in use is determined from the CKP distribution. This process is repeated for all height intervals, and is weighted by the input muon height distribution to obtain a probability distribution in angle with respect to the core direction. This distribution is then projected into the measuring plane of the spectrograph, allowing for the non-uniform acceptance of the array due to the "lobes" shown in fig. 6.9, and then spread to represent Coulomb scatter and measurement errors by a gaussian error function of width $\sigma_{tot} = \left\{ \sigma_{EAS}^2 + \sigma_A^2 + \sigma_{Pb}^2 \right\}^{\frac{1}{2}}$, where $\sigma_{EAS}$ represents the air shower direction measurement errors, $\sigma_a$ the r.m.s. value of coulomb scattering in the air, and $\sigma_{Pb}$ the r.m.s value of scattering in the lead shielding above the spectrograph. The portion of the distribution of angular deviation between $-16^{\circ}$ and $+16^{\circ}$ is normalised (arbitrarily), since these limits were imposed experimentally, and the mean deviation obtained. The cases $r_\perp$ + ve and $r_\perp$ - ve are treated separately, and the separation of the means of the two $(\psi_p - \psi_o)$ distributions is obtained directly. This treatment predicts the change in separation of the means of the two cases fully, for all values of momentum and core distance, and also shows the asymmetry introduced by the lobes of the array (ie. predicts more events in the $r_\perp$ + ve region than the $r_\perp$ - ve region and also that $\langle r_\perp \text{ -ve} \rangle$ is larger than $\langle r_\perp \text{+ve} \rangle$ for accepted events).

6.4.3 Discrepancies between $(\theta, \phi)$ corrected and $(\theta, \phi)$ uncorrected

The distributions in $(\psi_p - \psi_o)$ derived from the values of $(\theta, \phi)$ corrected for curvature effects agree with the predicted shapes, and also fairly well with the variation in separation of the means of the $r_\perp$ +ve and $r_\perp$ -ve cases.

Figure 6.9 The angular dependence of the "lobes" derived from the data of figure 6.2. The figure represents the number of showers within a $10^{o}$ band of angle $\alpha$, defined as $\tan\alpha = X/Y$.

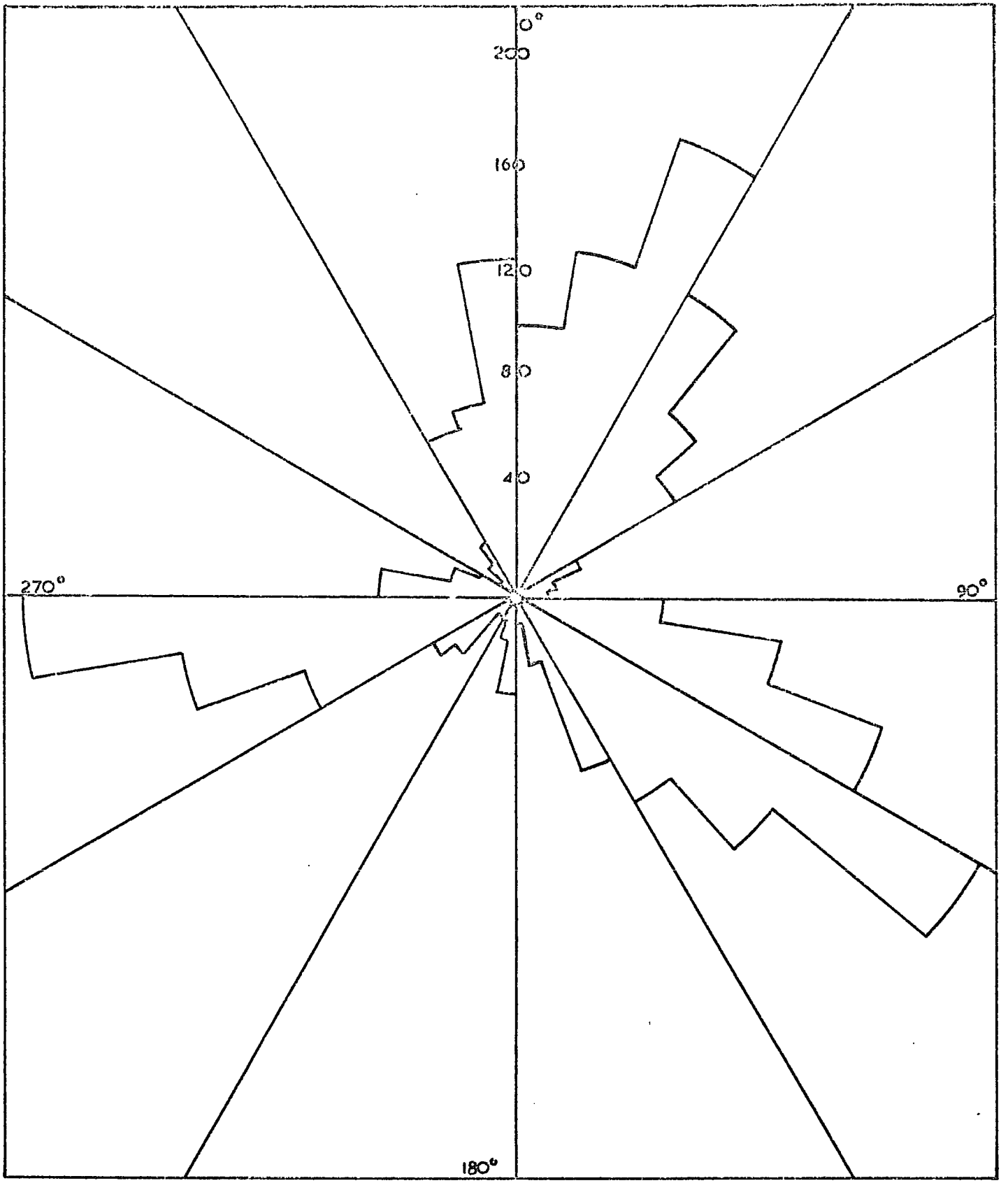
0°
200
160
120
80
40
270°
90°
180°

However, the $(\psi_p - \psi_o)$ distributions derived from the values of $(\theta, \phi)$ based on a plane shower front do not exhibit these trends, but appear to be divided almost equally about zero deflection, regardless of the sign of $r_\perp$. Figure 6.3 shows a typical example of this effect, The predicted mean (for the $r_\perp$ ve case) agrees closely with the "corrected" $(\psi_p - \psi_o)$ value, but is completely different from the "uncorrected" $(\psi_p - \psi_o)$ value. It appears therefore, that the corrections to allow for shower front curvature given by Dennis (1964) are essential if an accurate estimate of the core arrival direction is required. Typical differences between corrected and uncorrected values are $2^\circ$ in $\theta$ and $5^\circ$ in $\phi$, but some very large changes ($>50^\circ$) in $\phi$ have been observed. Evidently this effect is very important if anisotropies are to be located accurately, but for fairly large sorting bins ($>10^\circ$), the changes may be small.

6.4.4 Results and Comparison with Experiment

Fig. 6.10 to 6.13 show the comparison of the predictions described above with the experimental data for a range of core distance and momentum. The method used in predicting the distributions may be used with any muon height distribution as input data, so that comparison with other workers in this respect would be straightforward. The curves shown in the figures are obtained from the 1000 series models described in Chapter 5, for two primary particle mass numbers. The shape of the curves varies little with the overall noise $\sigma_{TOT}$, because the distributions in $(\psi_p - \psi_o)$ are closely gaussian, and as such, the separation between the means changes only slightly with the standard deviation. These curves may be used to indicate the numbers of events required to decide between primary mass of A=1 and A=56 for various ranges of momentum and core distance, in the following way:

Consider a sample of N muons in a band of momentum P and core distance r. These N muons are composed of $n_+$ and $n_-$ (the numbers in the $r_\perp$ + ve and $r_\perp$ - ve distributions respectively). Now, if $\sigma_A$ and $\sigma_{p_\perp}$ are small with respect to $\sigma_{EAS}$ (generally true above 3 GeV/c), then:

$$\sigma_{n+} \simeq \sigma_{n-} \simeq \beta(p,r)\,\sigma_{EAS} \quad \ldots\ldots\ 6.6$$

Figure 6.10 - 6.13 The variation of $\Delta$, the separation between the means of the $(\psi_p - \psi_h)$ distributions for $r_\perp$ + ve and $r_\perp$ - ve, as a function of momentum, for four core distance intervals. Model predictions for two primary masses are also shown for showers initiated by primary particles of energy $2 \times 10^{17}$ eV.

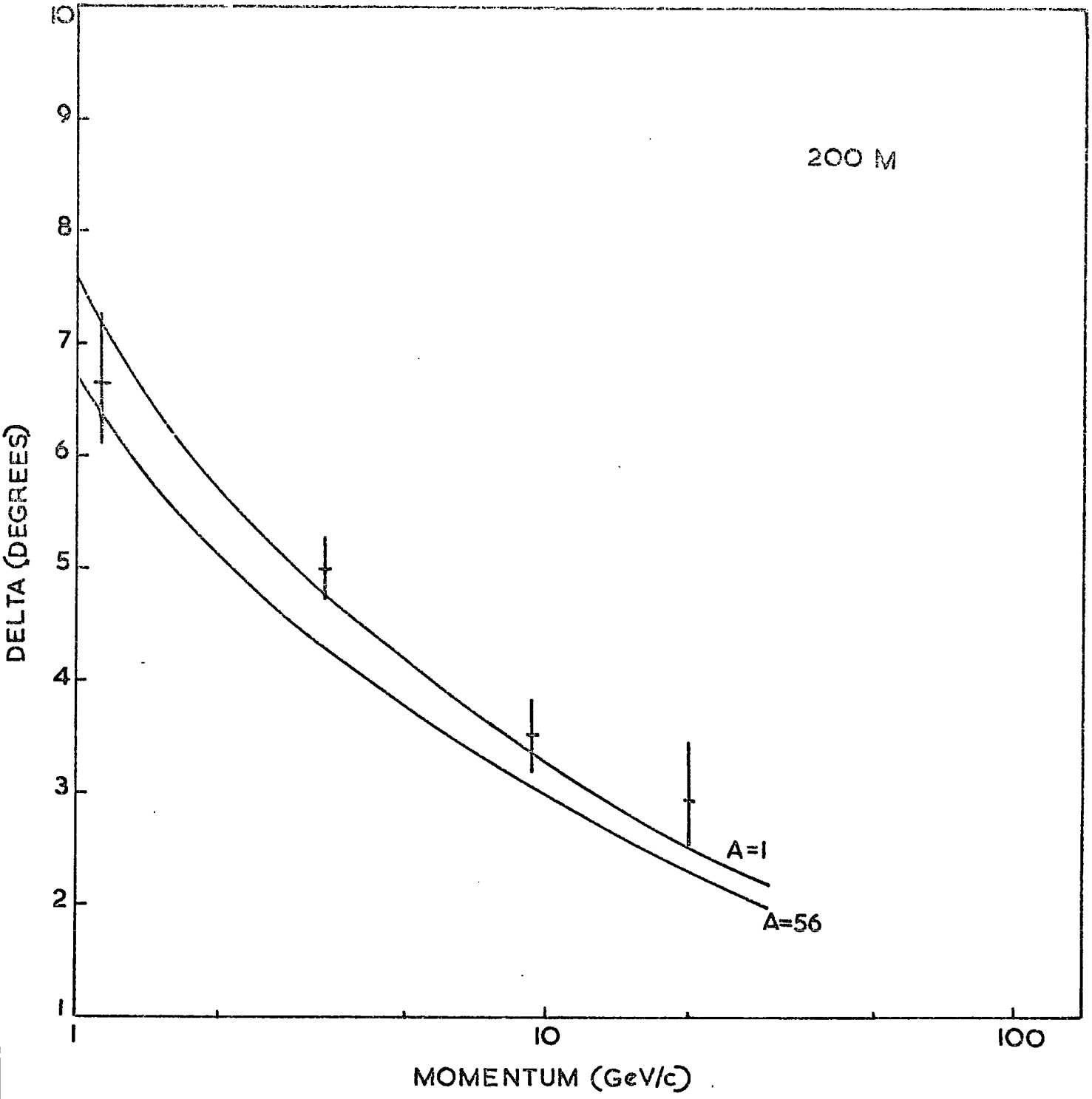
200 M
A=1
A=56
DELTA (DEGREES)
MOMENTUM (GeV/c)
10
9
8
7
6
5
4
3
2
1
1
10
100

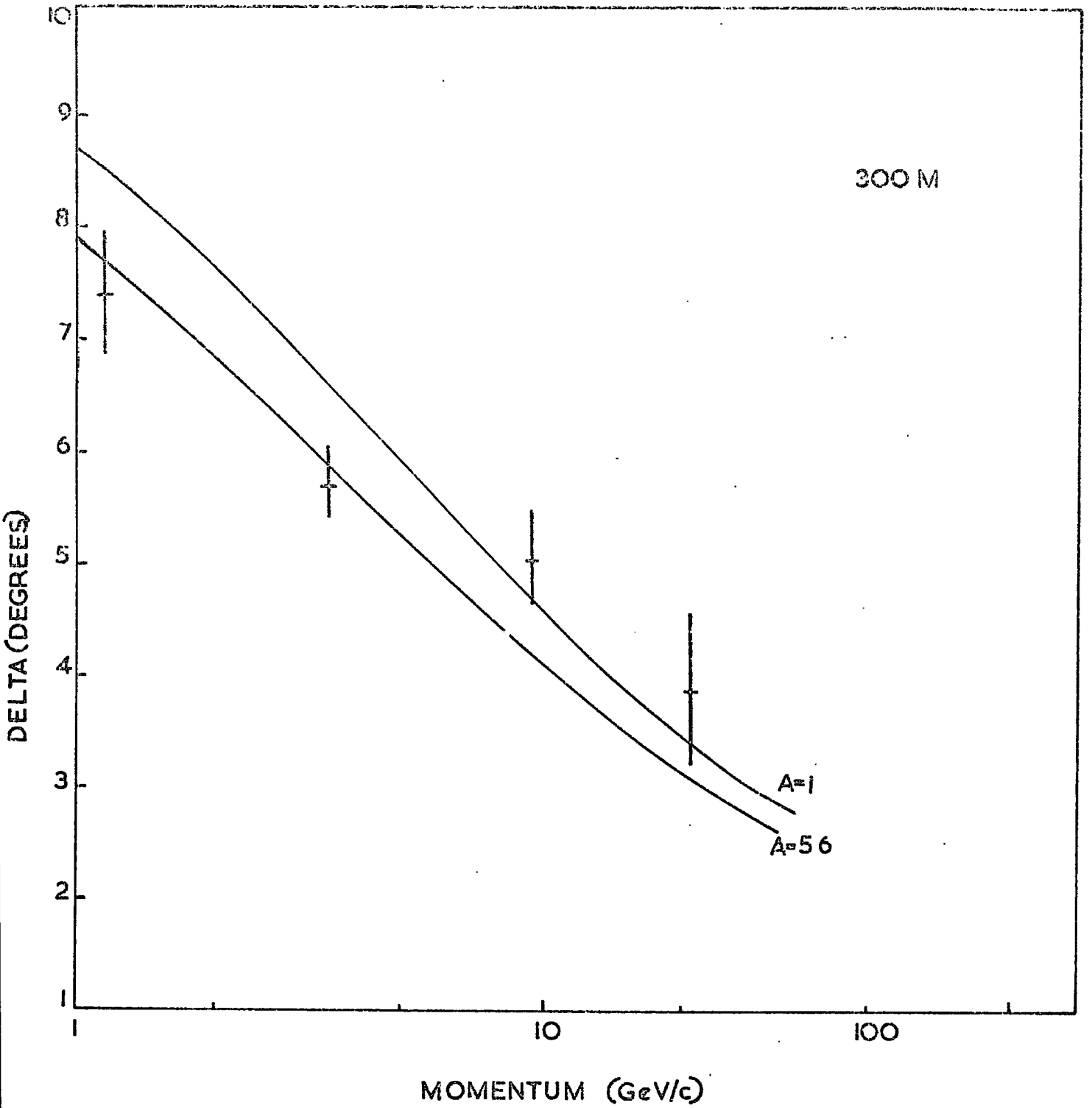
300 M
A=1
A=56
DELTA (DEGREES)
MOMENTUM (GeV/c)
10
9
8
7
6
5
4
3
2
1
1
10
100

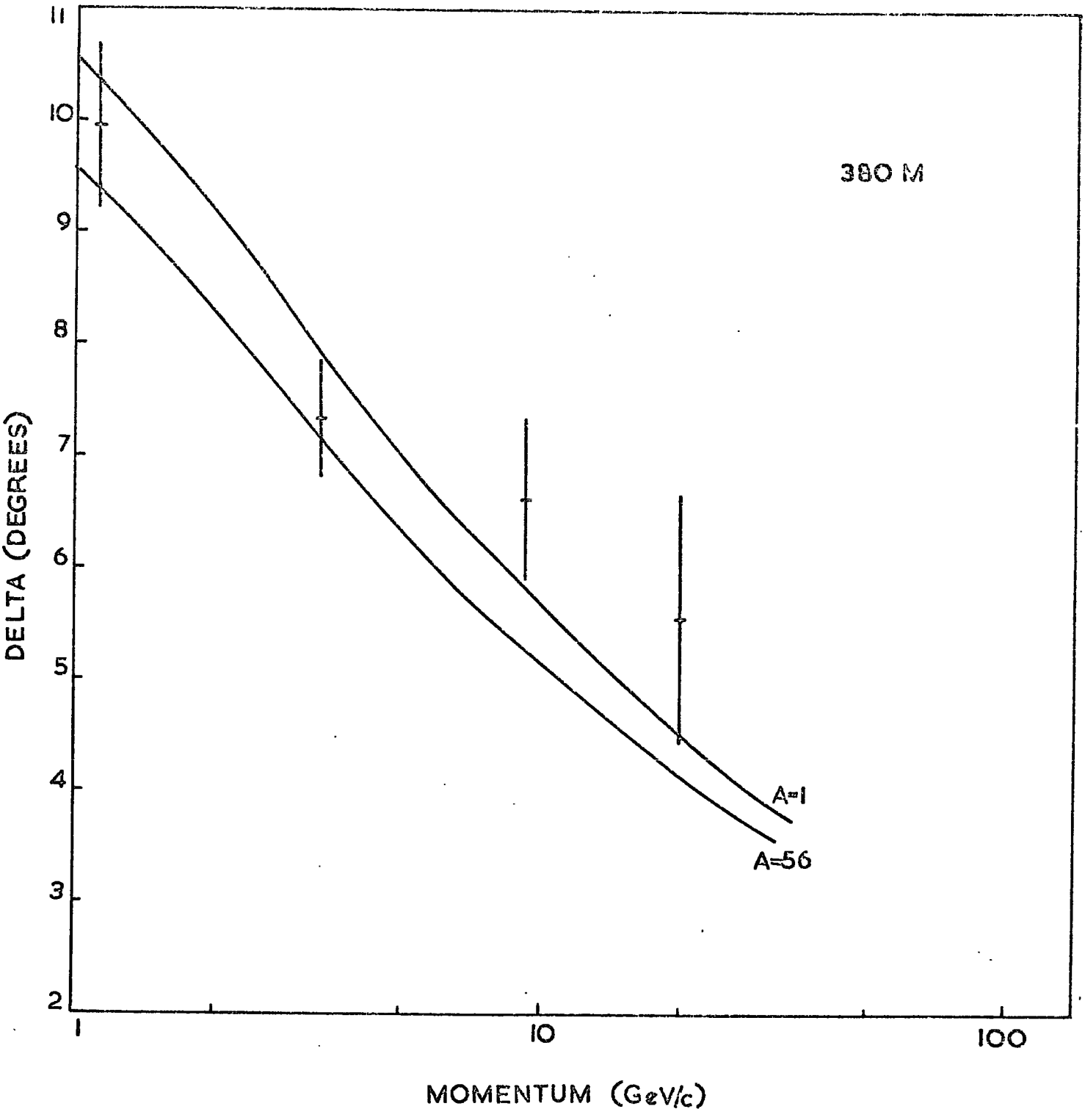
11
10
9
8
7
6
5
4
3
2
DELTA (DEGREES)
380 M
A=1
A=56
1
10
100
MOMENTUM (GeV/c)

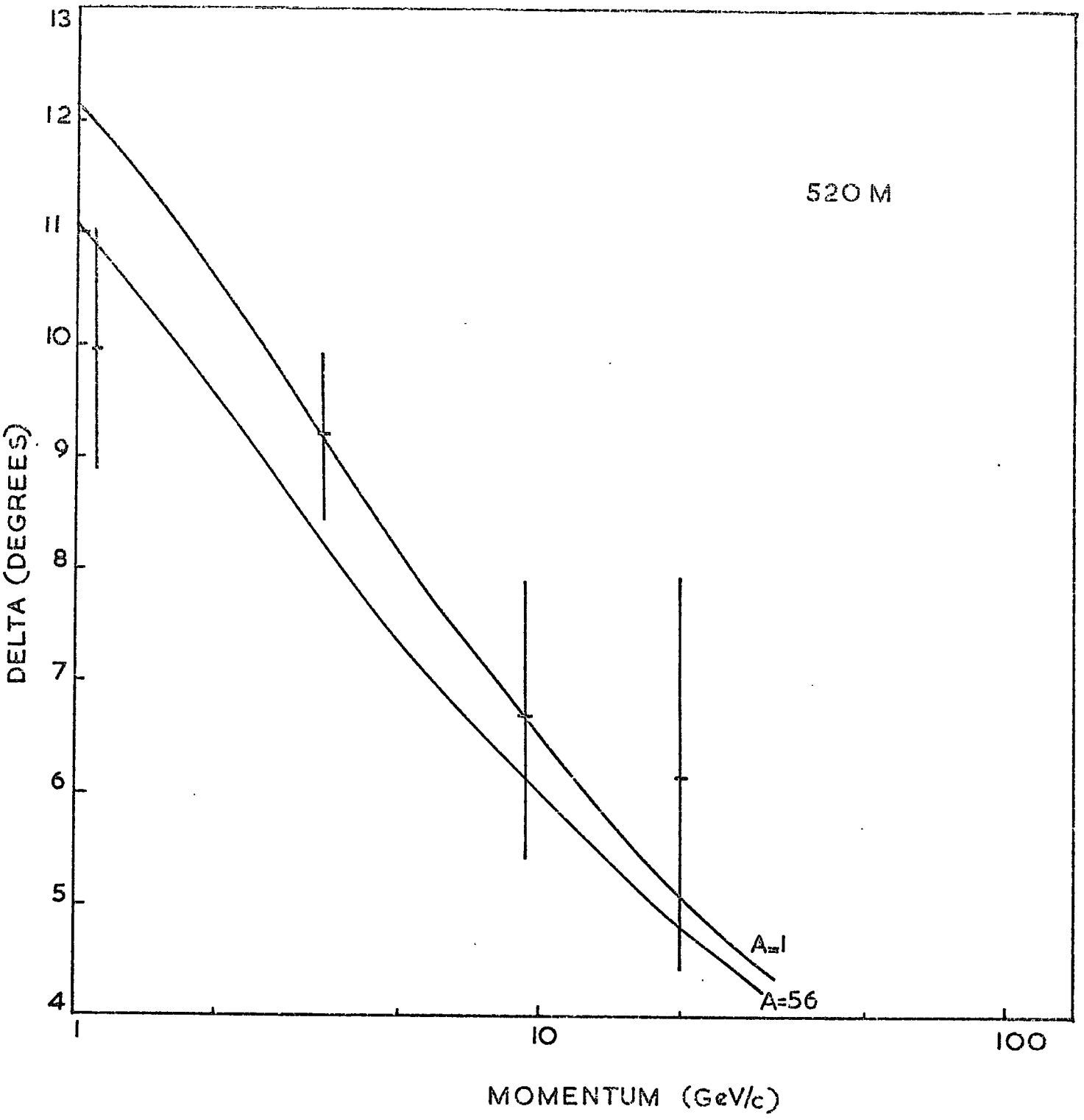
13
12
11
10
9
8
7
6
5
4
DELTA (DEGREES)
520 M
A=1
A=56
1
10
100
MOMENTUM (GeV/c)

where $\beta$ is a constant ($>$unity) for a given P,r interval.

since $n_+ + n_- = N$ (by definition)

and $n_+ : n_- \simeq 1.5:1$ (see section 6.2.3)

and the standard error on the separation of the means, $\Delta$, is given by:

$$\alpha_\Delta^2 = \alpha_{n_+}^2 + \alpha_{n_-}^2 \quad \ldots\ldots\ldots 6.7$$

where $\alpha_{n_+}$ is the standard error on the mean of the $(\psi_p - \psi_o)$ distribution for $\gamma_\perp$ ve , then

$$\alpha_\Delta(N) = 2.04\,\beta(p,r)\,\frac{\sigma_{EAS}}{\sqrt{N}} \quad \ldots\ldots\ldots 6.8$$

Hence the error on $\Delta$ for a given p,r interval for N events with an air shower measurement error $\sigma_{EAS}$ is given by equation 6.8. This means that the accuracy of the interpretation of curves such as fig. 6.10 varies linearly with EAS arrival direction errors. Values of $\beta(p,r)$ may be estimated from the Mk.I data sample, e.g.

if $\sigma_{EAS} = 2.60^\circ$ (as derived for MK.I data), $\bar{P} = 3.4$ GeV/c, r = 2.00 metres,

$\beta(3.4,200) = 1.39$ for N = 526 events

So application of equation 6.8 shows that, to obtain a standard error of $0.1^\circ$ on $\Delta(3.4, 200)$ ( a desirable figure since the separation of the curves for A=1 and A=56 is some $0.4^\circ$ at this point), either 5400 events at $\sigma_{EAS} = 2.6^\circ$, 800 events at $\sigma = 1^\circ$, or 200 events at $\sigma = 0.5^\circ$ are required. On the basis of the Mk I data, table 6.1 shows the expected errors on each P x r data point for a running time of one year with an EAS noise of $1^\circ$.

Table 6.1

| P \ r | 200 m | 300 m | 380 m | 520 m |
|---|---|---|---|---|
| 1-3 GeV/c | .38 | .37 | .48 | .73 |
| 3-8 | .19 | .21 | .34 | .90 |
| 8-15 | .22 | .28 | .47 | .87 |
| 15-30 | .33 | .45 | .76 | 1.37 |

Other values of running time and $\sigma_{EAS}$ will yield values of $\alpha_A$ in accordance with equation 6.8.

## 6.5 Discussion

### 6.5.1 Experimental Aspects of Measurements of Angular Deviation of Muons

Both methods of presentation of the height of origin, either the direct method, or via model calculations, contain the same overall limitations that arise from air shower arrival direction errors. The errors are such that no firm conclusions can be made about the value of primary particles mass at primary energies $\sim 10^{17}$eV although both methods tend to favour the A≠1 case on the whole. The implications of equation 6.8 and table 6.1 are that the necessary running time to give significant results is too great with the present noise of $2.6^{\circ}$, and some experimental improvements are necessary for a successful measurement.

Hollows (1968) quotes a time resolution of approximately 80nsec for each of the four channels, using simulated shower pulses. If it is assumed that the resulting $\sigma_{EAS}$ is roughly proportional to the resolution $\Delta t$, it is evident that a noise of $\sigma_{EAS}=1^{\circ}$ requires a timing accuracy of 30 nsec or less. It is most unlikely that the present detector system could approach such a figure, as the resolution is not set entirely by the bandwidth of the electronics employed, but rather by the design of the detector units. The passage of a charged particle through the detectors causes Cerenkov light to be emitted in a direction which is substantially away from the photomultiplier, so that the signal reaching the photocathode is the result of the summation of a large number of reflections. This gives the detector a very uniform response over a larger range of zenith angles, but is most undesirable in terms of fast timing. The provision of a simple Cerenkov detector purely for fast timing work at each station would improve the situation markedly. Such a detector must be of large enough area to collect a reasonable signal but would be more efficient than the conventional design. Any non-uniformity of response could be accurately measured

Figure 6.14 The variation of predicted $\Delta$ from model calculations for two primary masses and two muon momenta. The shower primary energy was $2 \times 10^{17}$ eV.

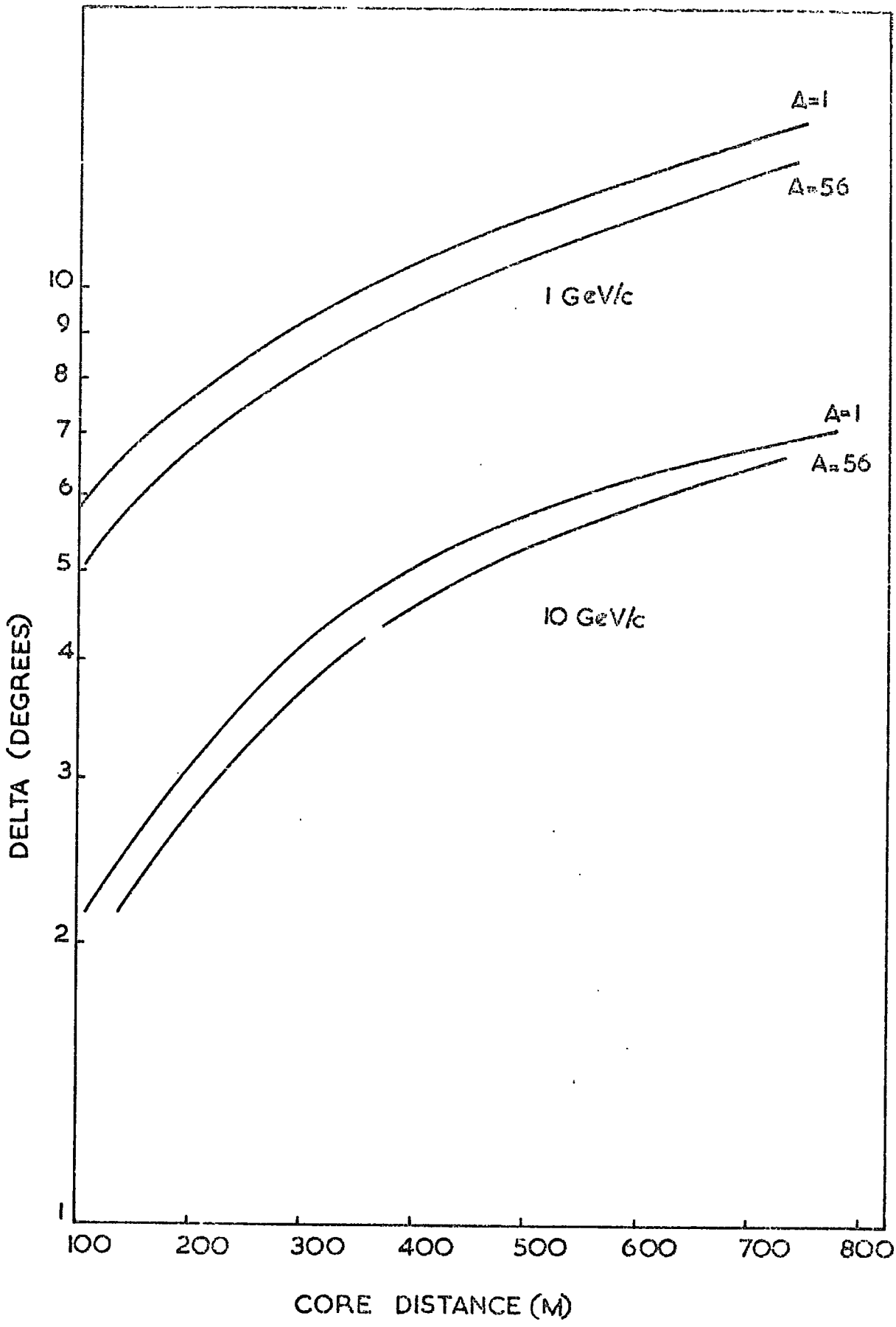
A=1
A=56
1 GeV/c
A=1
A=56
10 GeV/c
DELTA (DEGREES)
10
9
8
7
6
5
4
3
2
1
100
200
300
400
500
600
700
800
CORE DISTANCE (M)

by comparison with an adjacent conventional detector, and a restricted zenith angle range would not be important if the detectors were to be used specifically with a spectrograph (the present cutoff in zenith angle for events used in the spectrograph is $\theta = 40^{o}$, beyond which the probability of a particle fulfilling the geometrical acceptance becomes prohibitively small).

6.5.2 Longitudinal shower development

The results of the height of origin would appear to favour slightly an A=1, $n_s \propto E_p^{\frac{1}{4}}$ model. The effect of a primary particle of mass 56 is to raise the overall heights of origin of most muons by some 500m. while the effect of a multiplicity law of the form $n_s \propto E_p^{\frac{1}{2}}$ is slightly larger. The A=56, $E_p^{\frac{1}{2}}$ combination appears unlikely, as the heights predicted are generally over 1 Km too large, using both methods. However, further conclusions on the choice of model must await better statistics or improved experimental work. Fig. 6.14 indicates that the sensitivity of the separation of the means ($\Delta$) to a mass change is almost independent of core distance (ie. the ratio is almost constant), which means that virtually all the data collected in "angular" experiments may be used for investigations aimed at identifying the primary particle mass.

6.6 Comparison of the heights of origin with values from other experiments

6.6.1 Estimations of the height of origin based upon the interaction of the muon and the geomagnetic field.

Orford et al (1967), Earnshaw (1968), and Pickersgill (1971) give an account of a method of obtaining production heights by means of observations on the charge ratio of muons deflected by the Earth's magnetic field during their traversal of the atmosphere. The method produces heights of origin subject to rather large errors because the charge ratio observed are generally close to unity (Pickersgill, private communication). There is no experimental improvement which would yield significant results, but a very large data sample would improve the momentum and core distance resolution greatly. The height of origin for momenta and muons of all distances is included in fig. 6.15.

Figure 6.15 The overall height of production of muons greater than 0.3 GeV/c as a function of shower core distance. The results of other workers at comparable core distances are also shown. The line shown is the best fit to thepresent work.

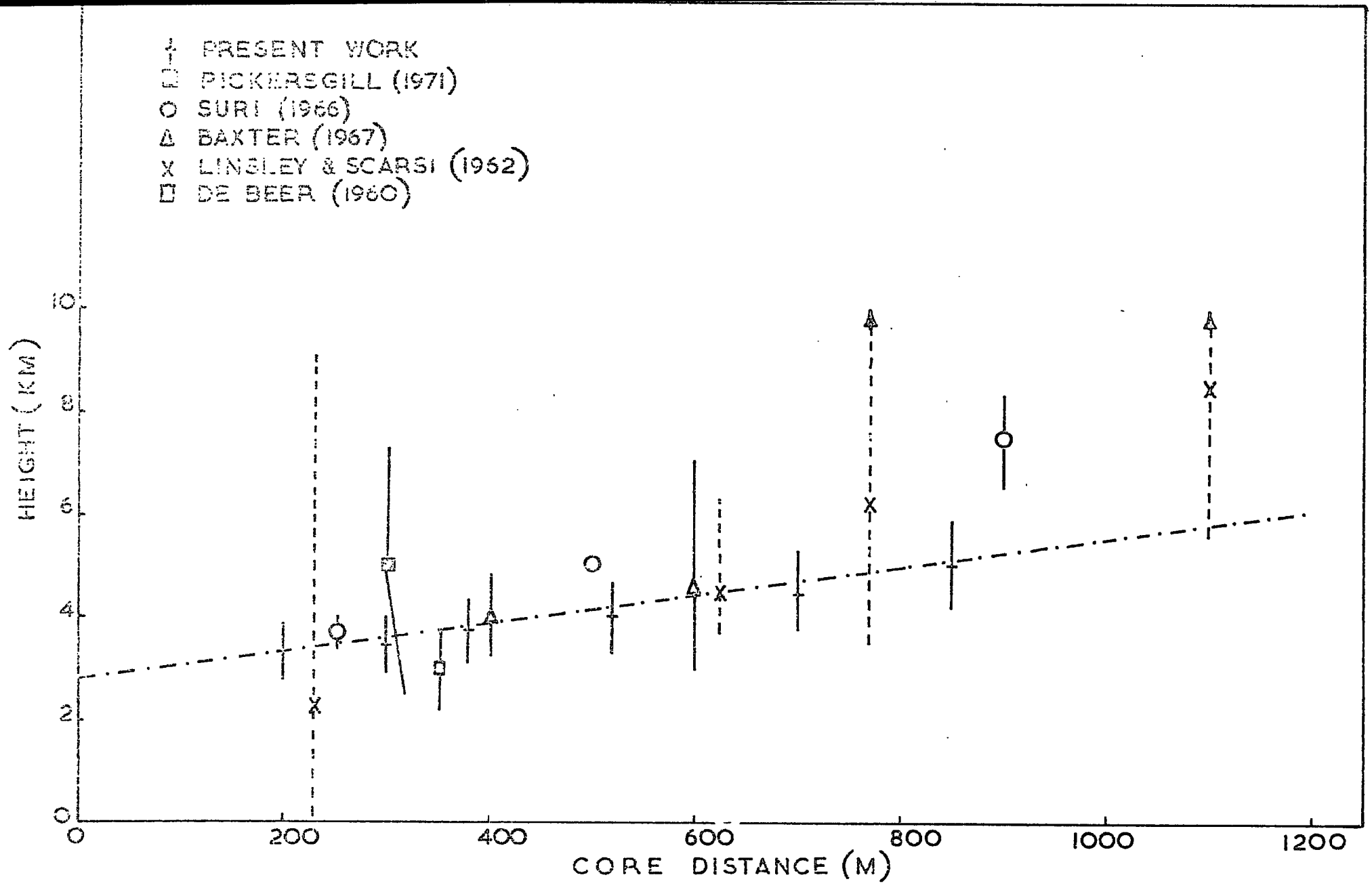
PRESENT WORK
PICKERSGILL (1971)
SURI (1966)
BAXTER (1967)
LINSLEY & SCARSI (1962)
DE BEER (1960)
HEIGHT (KM)
0
2
4
6
8
10
0
200
400
600
800
1000
1200
CORE DISTANCE (M)

6.6.2 Other measurements based upon the angular displacement of muons.

De Beer et al (1969) used a method very similar to that described in section 6.4 to predict the angular distribution of muons of momenta 1 GeV/c, and confirmed the general aspects of their calculations with spark-chamber telescopes (e.g. de Beer et al (1962). Firm conclusions were not possible because of the lack of momentum resolution in their experiment but the results for muons of all momenta were similar to those predicted from model calcultations in section 6.4. Fig. 6.15 includes a point computed by the present author from the data of de Beer (1960).

6.6.3 Alternative Methods of Obtaining the Production Height of Muons

Suri (1966) measured the mean radius of curvature of the shower front by a timing method, and Baxter (1967) determined the mean height by studies of the Cerenkov pulse profile. Both these workers used a lower cut-off energy of 0.3 GeV, and the necessary adjustments to the data shown in this chapterare described in Appendix 3. The results, shown in fig. 6.15, are in quite good agreement with those of Baxter (1967). Also shown in fig. 6.15 are the results of Linsley and Scarsi (1962), obtained by timing the delay of each muon with respect to the shower front (these measurements have been adjusted to account for the change in observation altitude).

6.7. Summary

The heights of production of muons derived from the data from the Mk I spectrograph agree well with the results of other workers, where ever suitable comparisions may be made. However, the advantage of the present method is that a clear picture of the variation of production height with both muon momentum and core distance is available. It is correspondingly simpler to compare the present experimental results with model predictions. The suggested modifications to the arrival direction measuring equipment at Haverah Park may allow a feature of shower development sensitive to the primary particle mass to be fully exploited.

# CHAPTER SEVEN

# CONCLUSION AND SUGGESTIONS FOR FUTURE WORK

## 7.1. The Momentum Spectrum of Muons

The spectra quoted in Chapter 4 show little overall change from those presented by Machin et al (1969), in spite of the complete revision of the EAS data. In particular the relatively high density of muons of momentum 50 GeV/c at 300m. from the shower core is still observed and some independent confirmation of this observation has been provided by the results of Suga et al (1969). The improved spectrograph has been shown to be correctly adjusted, with an overall noise figure corresponding to a momentum resolution of better than 120 GeV/c. However, the data sample accumulated from nine months running of the new instrument is insufficiently large to enable firm conclusions to be drawn regarding the validity of the original spectra.

One change in the experiment, that of increasing the thickness of the shielding layer above the spectrograph, has caused a distinct change in the range of core distance and shower size recorded by the instrument. In order to obtain a fair comparison of the two data samples, it will be necessary to exert strict controls over the core distance intervals used in the analysis.

A further increase in experimental effort devoted to measurements of the momentum spectrum alone is not worthwhile in view of the sensitivity to the primary particle mass of the muon spectrum in the regions accessible to the Mk. II spectrograph with the data from a further two or three years' running time. An accurate 100 GeV/c muon density at large core distances will be invaluable for comparison with various predictions to help identify a preferred model, and the importance of this point must not be underestimated, since it is so closely related to the initial interaction of the primary particle.

## 7.2 Height of Production of Muons

The relatively straightforward experimental considerations make the determination of the production height of muons of known momentum and core distance an attractive prospect for comparison with model predictions. The knowledge of muon momentum is invaluable; it enables full account of scattering, energy loss and geomagnetic deflection to be made, and the momentum dependence of production height to be accurately investigated. The overall results indicate that the production heights implied by a multiplicity law of the form $\propto E_{rad}^{0.5}$ are too large for primary particles of any mass, and that $\propto E_{rad}^{0.25}$ is closer to the truth. The present results do not allow firm conclusions to be drawn about the primary composition: there is perhaps an overall tendency to favour proton primaries, but heavier nuclei cannot be ruled out. The deduction of a simple equation linking production height with muon momentum and core distance has enabled accurate comparison with other workers to be made and the results are in good agreement with those derived by several different methods.

The insensitivity of the production height of muons above 1 GeV to the inelasticity of the n-n interactions, and particularly to the mean transverse momentum, imply that the method allows closer study of other important parameters without the need for a precise knowledge of these two values. With the provision of better core direction measurements (recommended in Chapter 6), the height resolution could be improved to that necessary to distinguish between different primary particle masses. Fig. 6.14 shows that the height resolution does not depend greatly on the core distance at which measurements are made; it is to be expected that, with a smaller error in core direction measurements, the errors in the base-line $r_\perp$ will become more important, and then the larger core distances ($r_\perp > 300$m) will yield the best results.

Should an increased data rate be considered necessary, a further large area spectrograph of moderate resolution (say $\sim$50 GeV/c) would be the ideal instrument. The low yield of energetic muons make a figure for momentum resolution much greater than 50 GeV/c unnecessary, so that

the larger, more easily operated 17mm. flash tubes could be employed as visual detectors. It would be advisable to orientate such a second spectrograph so that its measuring planes intereects another "lobe" of the array so exploiting the separation effects described in section 6.2.3.

## 7.3. Model Predictions

In view of the current interest in the primary mass composition at energies about $10^{17}$eV, the further exploration by model simulation of the aspects of the muon component which reflect the nature of the primary particle is desirable. The results of Chapter 5 indicate that one of the most sensitive measures of primary mass is the shape of the lateral distribution of muons, particularly at large core distances (>500m) and high momentum (>10 GeV/c). The experimental drawbacks to measurements of this type are two fold; (i) the rate of useful events is low, so that several detectors are necessary, and (ii) the accuracy in core distance must be uniform over the entire range, and of the order of 30m. The choice of detector is important - the momentum resolution of a spectrograph has to be offset against its small area and fairly high cost, while a shielded scintillator array of some $100m^2$ has no momentum resolution but a much improved acquisition rate. Both types could usefully be used, especially if the spectrograph was also used for accurate height of origin determinations.

The improvements to model calculations which should be considered in the future are (i) further work on the simulation of showers due to heavy primaries, which have to data been treated by many authors as the simulation of several proton showers, (e.g. screening of portions of the heavy nucleus in the initial interactions may cause a drastic reduction in the differences expected between primary proton and heavy nuclei showers, so that an experimental result implying a very narrow mass spectrum may simply be

observing the mechanics of high energy interactions), (ii) further experimental information on the exact interaction characteristics at high energies would be invaluable, as it is possible that the present interaction models are incorrect.

# APPENDIX ONE

## A1.1 Monte Carlo Methods Applied to the Generation of Artificial Muon Tracks

The random number generator used in the work described in Chapter 3 is a machine-specific pseudo-random variable generator giving $2^{31}$ terms without repeating. Its use is described in the IBM 360 Scientific Subroutine Package Manual. For the generation of a random number belonging to a normal distribution of specified mean and standard deviation, a method devised by R.W. Hamming (Numerical Methods for Scientists and Engineers) is used. Basically, this was the relation

$$Y = \frac{\sum_{1}^{K} X_i - K/2}{\sqrt{k/12}}$$

where Y is an approximation to a set of normally distributed random numbers, X a set of uniformly distributed random numbers. Y approaches a true normal distribution asymptotically as K tends to infinity. For convenience, a figure of K = 12 is taken.

## A1.2 The Use of Artificial Tracks to Investigate the Variation of Performance of a Flash Tube Array with Incident Angle

A modification of the programme described in Chapter 3 has been used to investigate the variation of the mean number of flashed tubes as a function of incident angle within the acceptance limits of the spectrograph. Fig. A.1 shows the results of this investigation. There is an overall tendency to observe more flashed tubes at incident angles away from the vertical in agreement with a subjective check on typical events. Fig. A1.2 shows that there are some small angular regions where the array predicts very small numbers of flashed tubes (ie a "corridor" exists). These areas are very small in relation to the total acceptance, and show no dependence on the particle momentum, so that the overall effect on the momentum spectrum will be negligible. Further work on locating the "corridors" simply requires the use of smaller angular and lateral intervals in the simulation process.

Figure A1.1 The variation in the mean number of flashed tubes as a function of the incident angle $\psi_0$ of the muon.

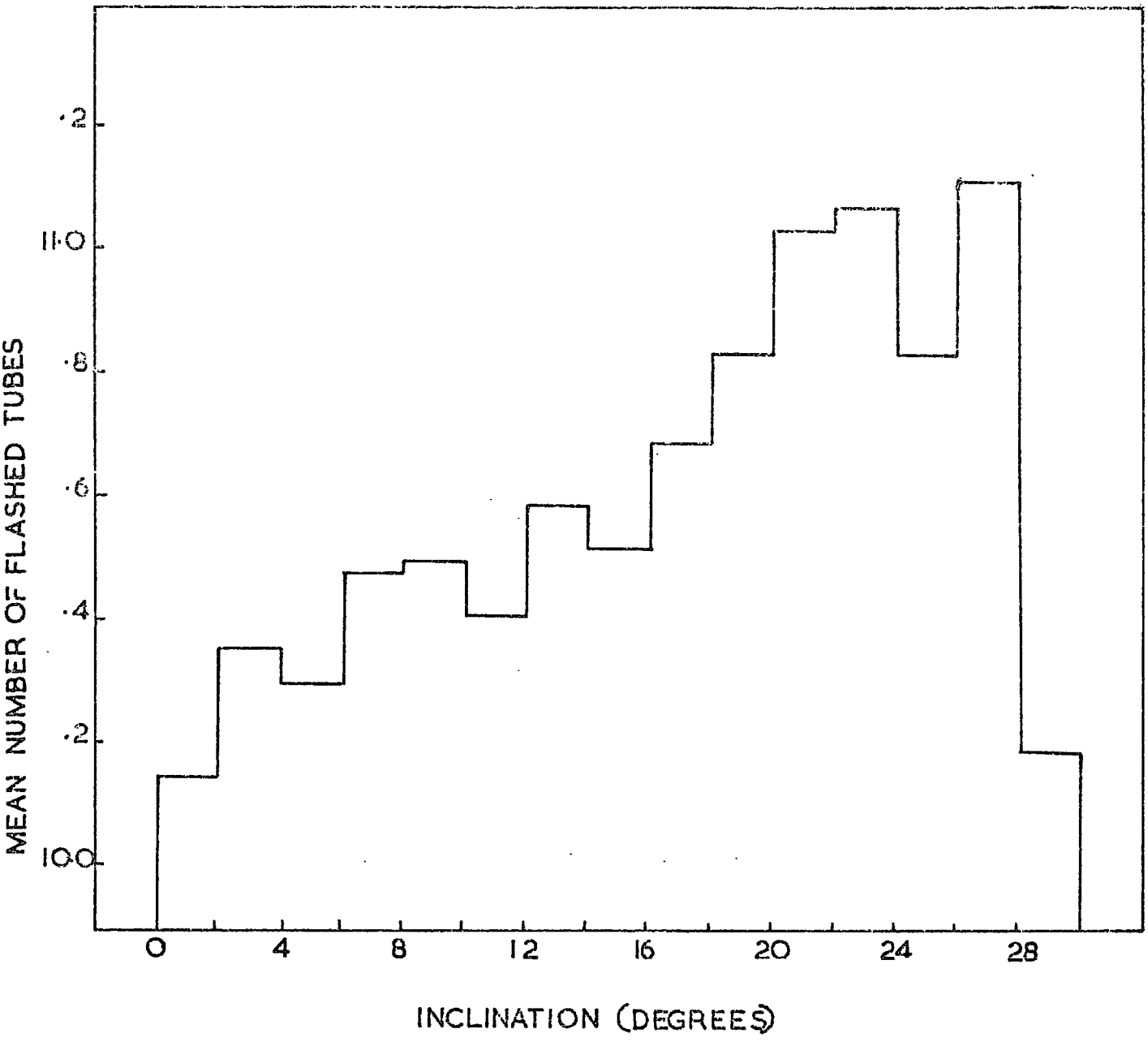
MEAN NUMBER OF FLASHED TUBES
·2
1·0
·8
·6
·4
·2
1·0
0
4
8
12
16
20
24
28
INCLINATION (DEGREES)

Figure A1.2 The percentage of all tracks containing six flashed tubes or less as a function of incident angle. The two flash tube array acceptance minima are clearly visible.

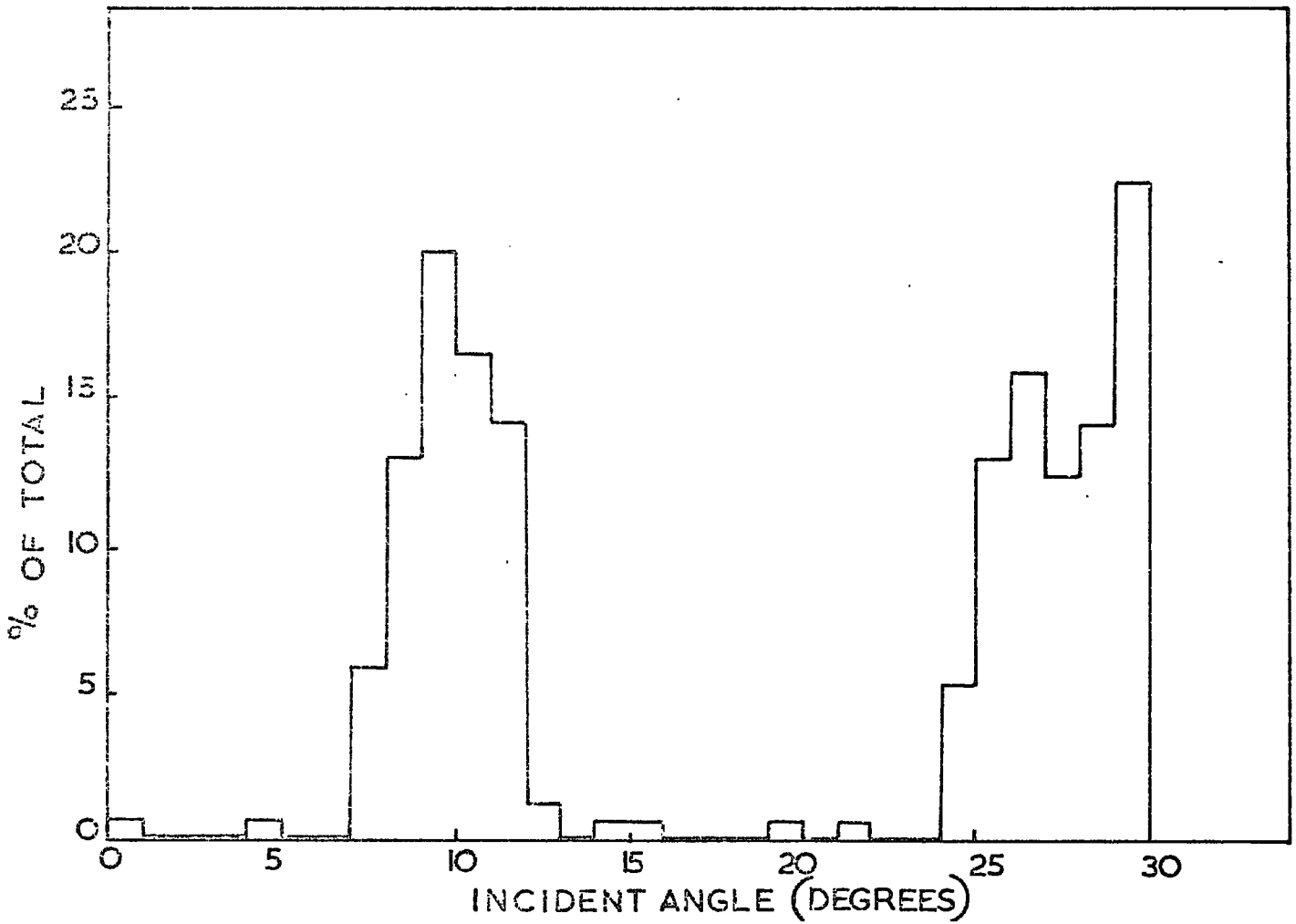
% OF TOTAL
25
20
15
10
5
0
0
5
10
15
20
25
30
INCIDENT ANGLE (DEGREES)

A2.1. Subdivision of the Muon Data into Momentum Bands

The technique used is that described by Walton (1966), and used by Earnshaw (1968) to obtain the mean true momentum for a given band of momentum derived from angular deflections in the spectrograph. The results are similar to those of Earnshaw (1968), but the sample is about a factor of two larger. The procedure for deriving the distributions has been made iterative (J.C. Earnshaw, private communication).

The mean of the distribution in each case has been determined by numerical solution of

$$\langle p \rangle = \frac{\int_1^{100} p\, s(p)\, dP}{\int_1^{100} s(p)\, dp} \qquad \text{.....A2.1}$$

No significant variation of $\langle p \rangle$ with core distance has been found.

Table A2.1

| Limits of momentum corresponding to angular deflection intervals (scattering ignored) | $\langle p \rangle$ GeV/c |
|---|---|
| 1 - 3 | 1.1 |
| 3 - 8 | 3.4 |
| 8 - 15 | 9.4 |
| 15 - 30 | 20.1 |

The distributions in momentum are shown in fig. A2.1, and the mean values in Table A2.1.

Figure A2.1 The distribution in true momentum from 1-200 GeV/c for five bands of "pure magnetic" momentum. The curve for 30 - 45 GeV/c has been ommitted for clarity,

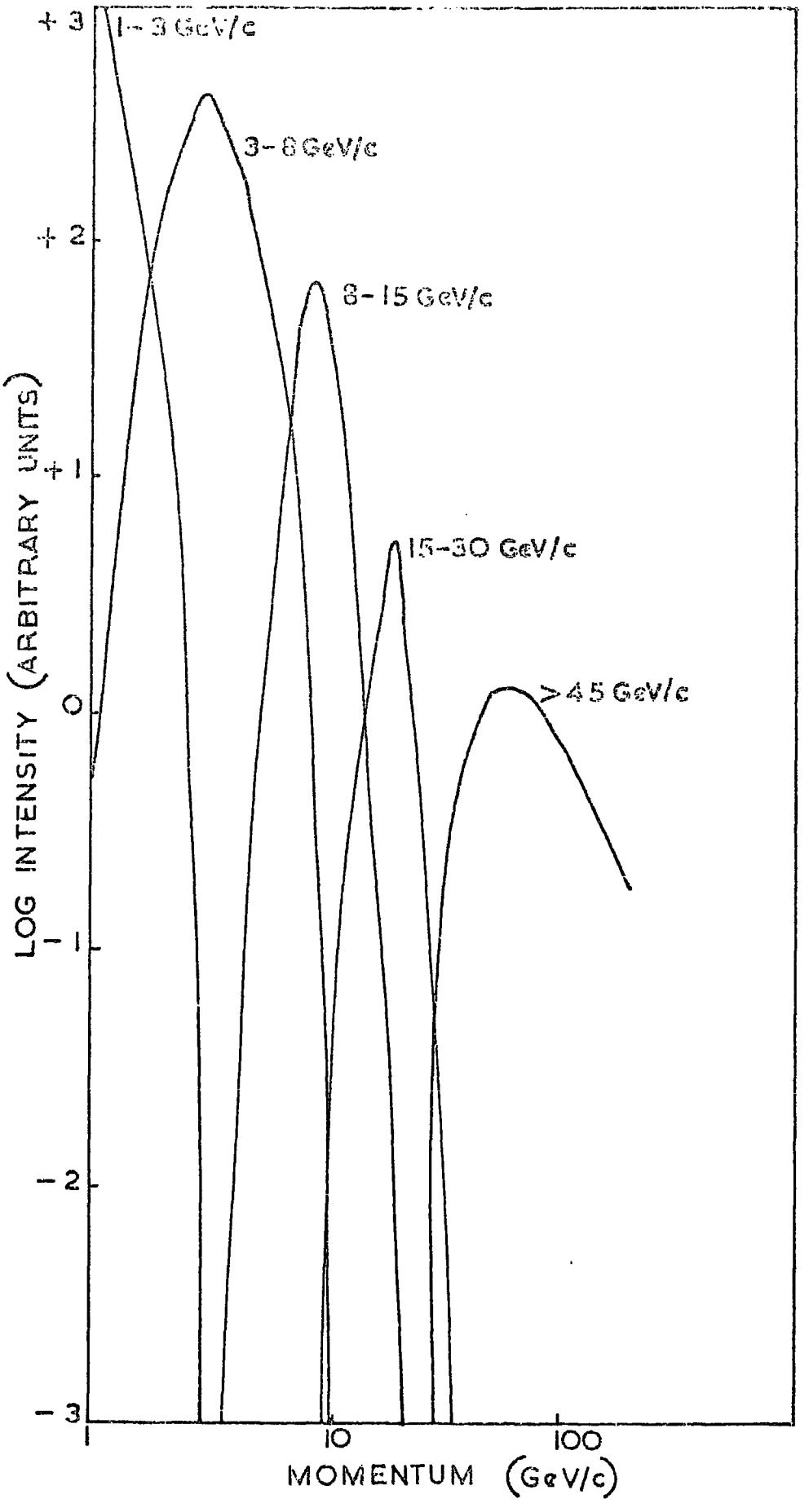
+3
+2
+1
0
-1
-2
-3
LOG INTENSITY (ARBITRARY UNITS)
1-3 GeV/c
3-8 GeV/c
8-15 GeV/c
15-30 GeV/c
>45 GeV/c
1
10
100
MOMENTUM (GeV/c)

# APPENDIX THREE

## A3.1 The Derivation of an Analytic Form for the Height of Production of Muons of Known Momentum and Core Distance

This investigation was undertaken to allow direct comparison of the experimental results with those of other workers. Fig. A3.1 shows the basic height of origin data plotted as a function of core distance for different muon momentum bands. The data were assumed to represent linear functions of r, so that fig. A3.1 may be represented by four parallel lines $L_i = Mr + c_i$, where the $c_i$ are functions only of momentum. Four least-squares fit lines were computed, and the mean and standard error calculated to find M. The four resulting values for $c_i$ were then compared with the momentum dependence of the production height for a fixed r interval and resolved into a constant term and a $\log_{10} P$ term (using the values for p taken from Appendix two). Hence the final result $H(P,r) = H_o + \alpha \log_{10} P + r/\beta$ .....A3.1 was obtained, where $H_o = 1.68 \pm 0.15$KM, $\alpha = 1.74 \pm 0.20$, $\beta = 263 \pm 33$, with all errors determined from the spread in the least-squares calculations. The resulting equation represents the production height fairly well for core distances of 150 - 600m., and for momentum from 1-30 GeV/c. At higher energies the relation underestimates the production height but an improvement involving the substitution of $P^{\gamma}$ for $\log_{10} P$ may improve the representation.

## A3.2 The Derivation of H(>p) for Intervals of Core Distance

The overall production height of muons greater than 1 GeV/c was derived from equation A3.1 and from the calculated muon momentum spectrum. If the height of origin is denoted H(P,r) and the momentum spectrum S(P), then

$$\bar{H} = \frac{\int_1^{30} H(P,r)\, s(P)\, dp}{\int_1^{30} S(P)\, dp} \qquad \text{..... A3.2}$$

The value of $\langle H \rangle$ as a function of r may be regarded as the expectation value for an experiment measuring the height of production of muons from

Figure A3.1 The mean height of production of muons as a function of core distance for the momentum bands shown. The four lines have the same gradient, equal to the mean of the least-squares fits to the four sets of data.

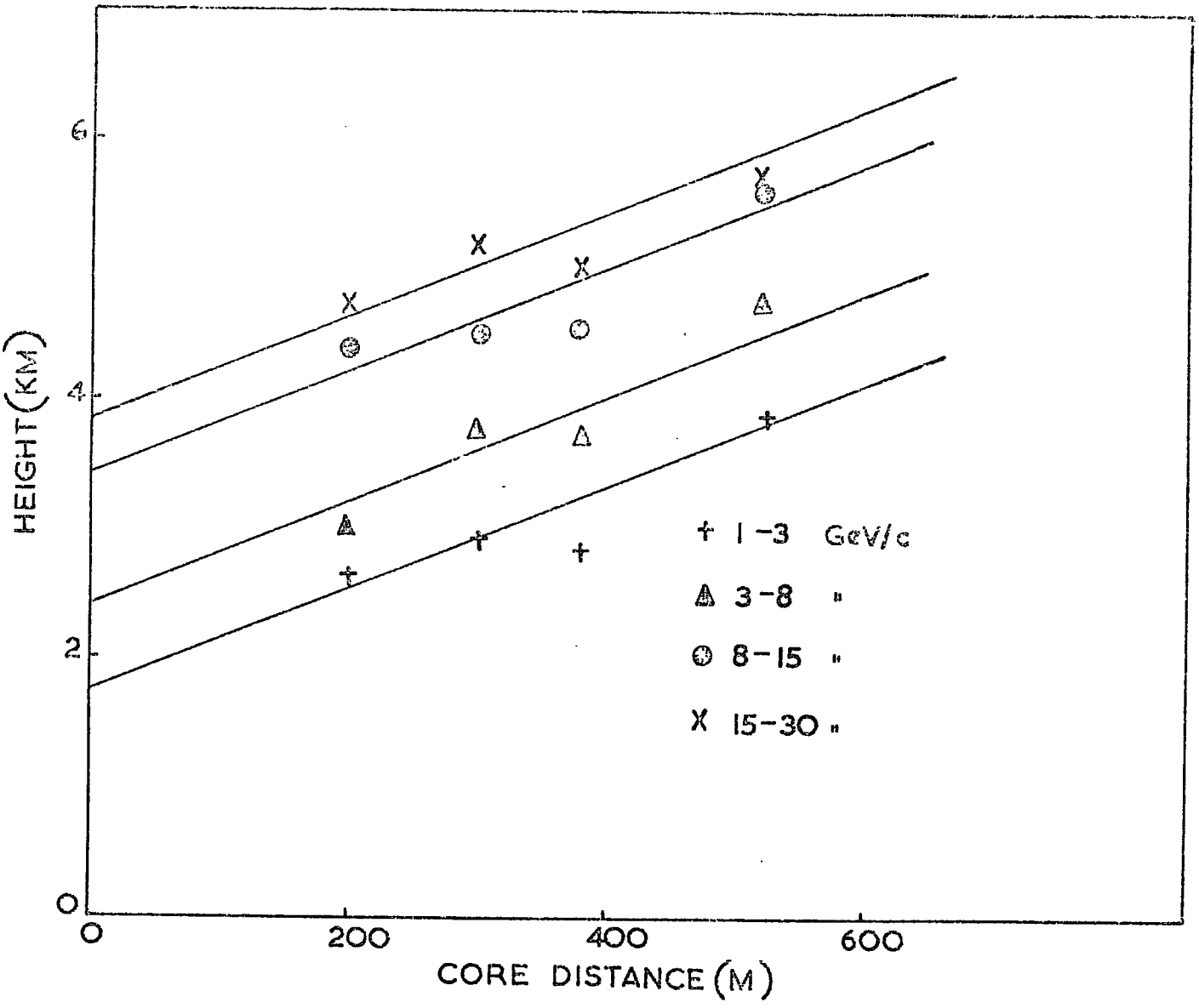
HEIGHT (KM)
6
4
2
0
0
200
400
600
CORE DISTANCE (M)
+ 1-3 GeV/c
Δ 3-8 "
⊗ 8-15 "
X 15-30 "

1 - 30 GeV/c with no momentum resolution, or as the overall production height of muons $>$ 1 GeV/c (since the contribution of muons of momentum $>$30 GeV/c is very small due to the steepness of the momentum spectrum).

In order to compare with the results of Baxter et al (1968) and Suri (1966) who both used a low-energy cut off of 300 MeV, it is necessary to extend the results below 1 GeV/c. The use of equation A3.1 is probably accurate for a momentum of 0.5 GeV/c, and this point has been taken as the mean of the momentum band 0.3 - 1 GeV/c. The relative contribution to the overall spectrum from those muons of momentum 0.3 - 1 GeV/c was obtained from the lateral distribution calculated by Hillas (private communication) for each distance interval, and a weighted mean height obtained. The results agree well with those of Baxter, and fairly well with those of Suri. Experiments yielding data at different threshold energies may be treated similarly.

# REFERENCES


ALLAN, H.R., BLAKE, P.R., NEAT, K.P. and PIDOCK, J.K., 1967, Proc. Int. Conf CALGARY, 2, 98.

ALLAN, H.R., 1971, Proc. Int. Conf. Hobart (in prep).

ANDREWS, D., EVANS, A.C., HUGHES, R.R., MARSDEN, D.J. REID, R.J.O., SMOLKO, I., TENNENT, R.M., WATSON, A.A., WILSON, J.G. and WRAY, A.M., 1969, Proc. Int. Conf. Budapest EAS-159.

ANDREWS, D., 1970, Ph.D Thesis, University of Leeds.

ANDREWS, D., EDGE, D.M., EVANS, A.C., REID, R.J.O., TENNENT, R.M., WATSON, A.A., WILSON, J.G. and WRAY, A.M., 1971, Proc. Int. Conf. Hobart (in prep)

ASKARYAN, G.A., 1965, Soviet Physics JETP, 21, 658.

BARRETT, P.H., BOLLINGER, L.M., COCCONI, G., EISENBERG, Y., and GREISEN, K., 1952, Rev. Mod. Phys. 24, 133-178.

BAXTER, A.J., WATSON, A.A., WILSON, J.G., 1968, Proc. Int. Conf. Galgary 46, 9.

de BEER, J.F., 1960, Ph.D Thesis, Potchefstroom University.

de BEER, J.F., CRANSHAW, T.E., and PARHAM A.G., 1962, Phil. Mag. 7, 499.

de BEER, J.F. de VILLIERS, E.J., REINECKE, J.P.L. and VENTER, F.A., 1969, Proc. Int. Conf. Budapest, EAS 56.

BENNETT, S. AND GREISEN, K., 1961, Phys. Rev. 124, 1982-1987.

BLAKE, P.R., FERGUSON, H and NASH, W.F., 1971, Proc. Int. Conf. Hobart (in prep).

BRADT, H. and RAPPAPORT, S.A., 1967, Phys. Rev., 164, 1567.

BRAY, A.D., CRAWFORD, D.F., JAUNCEY, D.L., McCUSKER, C.B.A., MELLY, D., NELSON, D., POOLE, P.C., RATHGEBER, M.H., SEET, S.H., ULRICHS, J., WARD, R.H. and WINN, M.M., 1965, Proc. Int. Conf. London, 2, 668.

BROWNLEE, R.G., CHAPMAN, G.J., DAVID, S.A. FISHER, A.J., HORTEN, L., GOOREVICH, L., KOHN, P.C., McCUSKER, C.B.A., OUTHRED, A., PARKINSON, A.F., PEAK. L.S., RATHGEBER, M.H., RYAN, M.J. and WINN, M.M., 1969, Proc. Int. Conf. Budapest EAS 5.

BULL, K.M. COATES, D.W., NASH, W.F., RASTIN, B.C., 1962, Nuovo, Cimento, 23, 28-38.

CHUDAKOV, A.E., NESTEROVA, N.M., ZATSEPIN, V.I. and TUKISH, E.I., 1960, Proc. Int. Conf. Moscow, II, 50-57.

CLARK, G., EARL, J. KRAUSHAAR, W., LINSLEY, J. ROSSI, B., SHERB, F., 1958, Supp. Nuovo Cimento, 8, 628-652.

CLAY, R.W., 1970, Ph.D Thesis, University of London.

COCCONI, G., KOERSTER, L.J., and PERKINS, D.H., 1961, Lawrence Radiation Laboratory, High Energy Physics Study Seminars, 28, (2), UCID-1444,1.

DENNIS, B.R., 1964, Ph.D Thesis, University of Leeds.

DOVZENKO, O.L., ZATSEPIN, G.T., MURZIN , E.A., MIKOLSKEY, S.I., and IAKOLEV, V.I., 1960, Proc. Int. Conf. Moscow, II, 134- 41.

DOVZENKO, O.L., NELEPO, B.A. and NIKOLSKII, S.J., 1957, Jor. Exp. Teor. Phiz, 32, 463-465.

EARNSHAW, J.C., 1968, Ph.D Thesis, University of Durham.

EARNSHAW, J.C., ORFORD, K.J. ROCHESTER, G.D., SOMOGYI, A.J., TURVER, K.E., and WALTON, A.B., 1967, Proc. Phys. Soc., 90, 91-108.

EARNSHAW, J.C., MACHIN, A.C., ORFORD, K.J., PICKERSGILL, D.R., and TURVER, K.E., 1971a, Proc. Int. Conf. Hobart (in prep).

EARNSHAW, J.C., MACHIN, A.C., ORFORD, K.J. PICKERSGILL, D.R. and TURVER, K.E., 1971b, Proc. Int. Conf. Hobart (in prep).

EYGES, L, 1948, Phys. Rev. 74, 1534-1535.

FOWLER, P.A., ADAMS, R.A., COWEN, V.G. and KIDD, J.M., 1967, Proc. Roy. Soc. A, 301, 39-45.

GALBRAITH, W and JELLEY, J.V., 1952, Nature, A1, 349-350.

GINSBURG, V.L. and SYROVATSKII, S.I., 1964,'The Origin of Cosmic Rays' Oxford Pergamon Press.

GLENCROSS, W.M., 1962, Ph.D Thesis, Imperial College, University of London.

GREISEN, K., 1960, Ann. Rev. Nucl. Sci. 10, 63.

GREISEN, K., 1966, Phys. Rev. Letters, 16, 748.

GRIEDER, P.K.F., 1969, Proc. Int. Conf. Budapest, EAS - 43/1.

GRIGOROV, N.L., NESTEROV, V.E., RAPORT, I.D., SAVENKO, I.A., and SKURIDIN,G.A., 1976, Proc. Calgary Conf. Part A, 512-524.

HASEGAWA, H., MATAMO, T., MUIRA, I., ODA, M., SHIBATE, S., TANAHASHI, E., and TANEKA, Y., 1962, Proc. Int. Conf. KYOTO, AIII, 86-88.

HAYAKAWA, S., 1969, 'Cosmic Ray Physics' John Wiley and Sons.

HILLAS, A.M., 1967, Proc. Int. Conf. Calgary,Can. J. Physics 46., 623

HILLAS, A.M. 1969, Proc. Int. Conf. Budapest., EAS 3.

HILLAS, A.M., HOLLOWS, J.D., HUNTER, H.W. and MARSDEN, D.J., 1971 Proc. Int. Conf. Hobart (in prep).

HOLLOWS, J.D., 1968. Ph.D Thesis, University of Leeds.

HOOK, J.R., MASLIN, G.C., ORFORD, K.J. and TURVER, K.E., 1969, Proc. Int. Conf. Budapest, EAS - 15.

IVANENKO, I.P., and SAMUSODOV, B.E., 1967, Bull. Acad. Sci. USSR, (Phys. Series), 30, 1722-1726.

JELLEY, J.V., FRUIN, J.H., PORTER, N.A., WEEKS, T.C., SMITH, F.G. AND PORTER, R.A., 1965, Nature, 205, 327.

KAHN, F.D., and LERCHE, I, 1965, Proc. Roy. Soc. A. 289, 206.

KAMATA, K., and NISHIMURA, J., 1958, Progs. Theor. Phys. Suppl. 6, 93.

KONSTANTINOV, B.P., KOCHEROV, G.E., STARBUROY, Y.U.N., and ZHURALEV, O.S., 1968, Phys. Leh, 27b, 30.

LAPIKENS, J. MARTIN, R., REID, R.J.O., ROBINSON, P.D., TENNENT, R.M., WATSON, A.A. and WILSON, J.G., 1971, Proc. Int. Conf. Hobart, (in prep).

LILLICRAP, S., 1963, Ph.D Thesis, University of Leeds.

LINSLEY, J., 1963, Proc. Int. Conf. Jaipur, 4, 77.

LINSLEY, J. and SCARSI, L., 1962a, Phys. Rev. Letters, 9, 123.

LINSLEY, J and SCARSI, L., 1962b, Phys. Rev., 128, 2384.

LLOYD, J.L., 1960, Proc. Phys. Soc. 75, 387.

McCUSKER, C.B.A., PEAK L.S., and RATHGEBER, M.H., 1968, University of Sydney, Preprint.

MACHIN, A.C., ORFORD, K.J., PICKERSGILL, D.C., and TURVER, K.E., 1969a, Proc. Int. Conf. Budapest, EAS 44/1.

MARSDEN, D.J., HILLAS, A.M., HOLLOWS, J.D., and HUNTER, H.W., 1971. Proc. Int. Conf. Hobart (in prep).

MATANO, T., NAGAMO, M., SHIBATA, S., SUGA, K., TANAHASHI, E., and HASEGAWA, H., 1967, Proc. Int. Conf. Galgary.

NISHIMURA, J. and KAMATA, K., 1950, Progs. Theor. Phys. 5, 899
1951. Progs. Theor. Phys. 6, 762, 628
1952. Progs. Theor. Phys. 7, 185.

ORFORD, K.J., 1968, Ph.D Thesis, University of Durham.

ORFORD, K.J. and TURVER, K.E., 1968, Nature, 219, 706.

ORFORD, K.J. and TURVER, K.E., 1969b, Proc. Int. Conf. Budapest, EAS 44/2

ORFORD, K.J.,TURVER, K.E. and WALTON, A.B., 1967, Proc. Int. Conf. Calgary 46, S119.

PENZIAS, A.A., and WILSON, R.W., 1965, Astrophys. J., 142, 149.

PICKERSGILL, D.R., 1971, Ph.D Thesis, University of Durham (in preparation)

PORTER, L.G., EARNSHAW, J.C., TIELSH-CASSEL, E., AHLSTROM, J., and GREISEN, K., 1970, Nucl. Inst. & Methods, 87, 87.

PORTER, N.A., LONG, C.D., McBREEN, B., MURNAGHAN, D.J.B. and WEEKES, T.C., 1965, Proc. Int. Conf. London, 2, 706.

RASTIN, B.C., 1964, Ph.D Thesis, University of Nottingham.

ROLL, P.E. and WILKINSON, D.T., 1966, Phys. Rev. Letters, 16, 405.

ROSSI, B., 1952, 'High Energy Particles', Prentice Hall Inc.

SALZMAN, F. and SALZMAN, G., 1960. Phys. Rev., 120, 599.

SAMORSKI, M., STAUBERT, R., TRUMPER, J., BOHM. E., BUSCHER, W., and FRITZE, R., 1969. Proc. Int. Conf. Budapest, EAS-13.

SHIBATA, S., NAGAMO, M., MATANO, T., SUGA, K. and HASEGAWA, H., 1965, Proc. Int. Conf. London, 2, 672-675.

SUGA, K., SHIBATA, S., MIKAMO, S., TOYODA, Y., MURAHAMI, K., LA POINTE, M., KAMATA, K and DOMINGO, V., 1969. Proc. Int. Cong. Budapest, Mu-14.

SURI, A.N., 1966, Ph.D Thesis, University of Leeds.

THIELHEIM, K.O., and KARIUS, S.,1965, Proc.Int. Conf. London, 2, 779-782.

TOYODA, Y., SUGA, K., MURAHAMI, K., HASEGAWA, H., SHIBATA, S., DOMINGO, V., ESCOBAR, I., KAMATE, K., BRADT, H.V., CLARK, E and LA POINTE, M., 1966, Proc. Int. Conf. London, 2, 708-711.

TURVER, K.E., 1963, Ph.D Thesis, University of Leeds.

WALTON, A.B., 1966, M.Sc Thesis, University of Durham.

WINN, M.M., WARD, K.H., ULRICHS.J., RATHGEBER, M.H., POOLE, P.C., NELSON, D., McCUSKER, C.B.A., JAUNCEY, D.L. CRAWFORD, D.F., and BRAY, A.D., 1965. Nuovo Cimento 36, 701-732.

ZATSEPIN, E.T., NIKOLSKII, S.I., and KHRISTIANSEN, E.B., 1963, Proc. Int. Conf. Jaipur, 4, 100-126.

## ACKNOWLEDGEMENTS

I am deeply indebted to Professor G.D. Rochester, F.R.S., for the provision of the facilities which made this study possible, and also to my supervisor, Dr. K.E. Turver, for his constant advice and encouragement.

I wish to thank Professor J.G. Wilson and his colleagues of the Department of Physics, University of Leeds for their cooperation and for the provision of the air shower analyses used in this thesis.

My colleagues Dr. J.C. Earnshaw, Dr. K.J. Orford and Mr. D.R. Pickersgill are thanked for their contribution to the collection and analysis of this data.

The assistance of the technical staff of the University of Durham, particularly Miss A.M. Bevils in track reconstruction, and Mr. W. Leslie and Mr. H. Davison in constructional work has been invaluable. The Science Research Council is thanked for the provision of a Research Studentship. I wish to thank my wife for her assistance, and for drawing the figures for this thesis. Mrs. D. Anson, who typed this thesis, is gratefully thanked.